Università degli Studi di Palermo

AREA RICERCA E TRASFERIMENTO TECNOLOGICO
SETTORE DOTTORATI E CONTRATTI PER LA RICERCA
U. O. DOTTORATI DI RICERCA

Ph.D. Course Technologies and Science for Human Health

Department of Biological, Chemical, and Pharmaceutical Sciences and Technologies

(STEBICEF)

SSD BIOS 14/A

Innovative therapeutic approaches for the recovery of protein expression in rare genetic diseases characterized by the presence of nonsense variants

Ph.D. Student

Emanuele Vitale

Coordinator

Prof. Valeria Vetri

Tutor

Prof. Laura Lentini

Co-Tutor

Prof. Maria Grazia Zizzo

XXXVIII CYCLE

2022/2025

Table of contents

1. ABSTRACT

Approximately 11% of inherited genetic diseases worldwide are caused by nonsense variants. These single-nucleotide substitutions occur within coding DNA sequences and result in the introduction of a premature termination codon (PTC) into the corresponding mRNA. As a consequence, they lead to the production of truncated, non-functional proteins or, in some cases, to their complete absence.

Several genetic disorders are associated with nonsense variants, including Choroideremia (CHM), Cystic Fibrosis (CF), Duchenne Muscular Dystrophy (DMD), and numerous other genetic diseases. Notably, nonsense variants account for approximately 34% of pathogenic mutations in Choroideremia and 15% in Cystic Fibrosis. Currently, no specific cure or therapy exists for these types of genetic defects. However, in recent decades, the field of personalized medicine has made significant progress in developing targeted treatments, particularly through nonsense suppression therapy. This pharmacological strategy employs readthrough agents to restore full-length protein synthesis.

The first aim of this Ph.D. thesis project was to evaluate the rescue of the CFTR protein in a Cystic Fibrosis G542X murine model by assessing the readthrough activity of two novel compounds, NV914 and NV930, specifically focusing on the restoration of CFTR in the lung, one of the primary organs affected by the disease.

The second objective consisted of two different aspects. The first one, was to generate a Choroideremia cellular model carrying nonsense mutations to investigate the restoration of the REP1 protein following treatment with NV molecules (NV848, NV914, and NV930), thereby evaluating their ability to induce readthrough of premature stop codons in CHM mRNA. The second aspect was focused on assessing REP1 recovery directly in primary cell cultures derived from patients harbouring nonsense variants.

Finally, the third objective of the project was to investigate the biological target of the three NV848, NV914, and NV930 molecules using the advanced cell-free experimental PURE-LITE system.

2. INTRODUCTION

2.1 Nonsense variants causing genetic diseases

A genetic mutation in the DNA sequence can lead to the development of genetic diseases. Several types of variants are described in the literature; among them, nonsense variants are single-nucleotide substitutions that occur within the DNA sequence. When the substitution occurs in coding regions of a gene, these variants result in the introduction of a stop codon (UAG, UGA, or UAA), referred to as a premature termination codon (PTC), in the mRNA sequence, leading to the production of a truncated and nonfunctional protein (Potapova NA., 2023) (**Figure 1**).

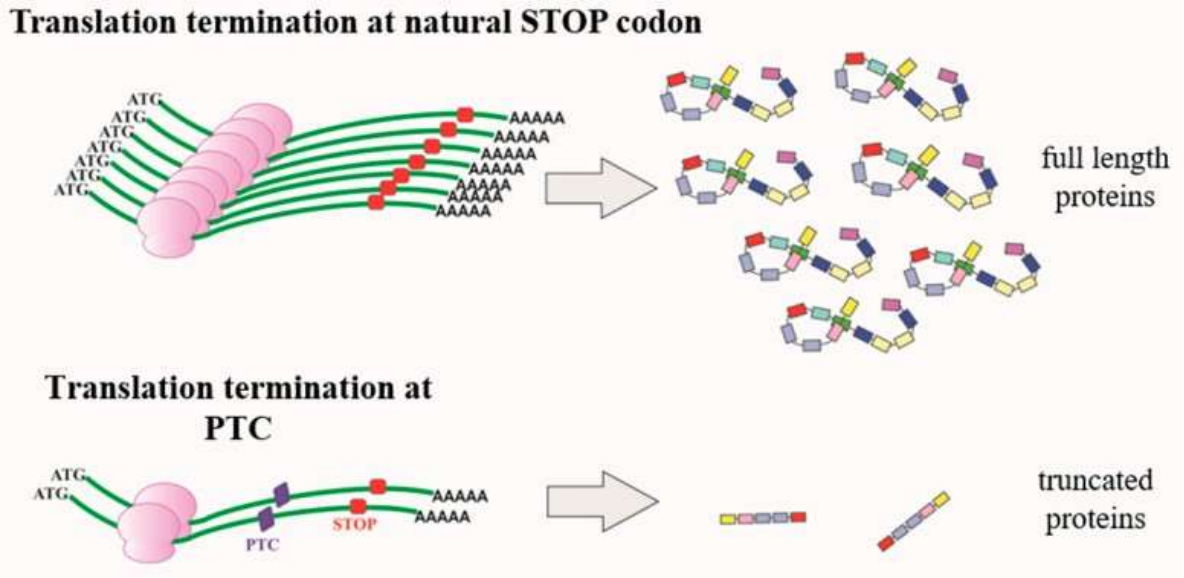

Figure 1. Natural and premature translational termination processes: *image showing the normal termination of translation that produces full-length proteins, in which ribosomes correctly translate mRNA sequences; and the translation termination when a premature termination codon (PTC) occurs in mRNA coding sequence, in which ribosomes prematurely encounter the stop codon and arrest the translation with the truncated proteins production (Borgatti M. et al., 2020).*

Recent studies, based on the human gene variant databases, including Human Gene Mutation Database (HGMD), Codon Usage Database (CUD), Database for Annotation, Visualization and Integrated Discovery (DAVID), and several others, have demonstrated that these variants are responsible for approximately 11% of all gene modifications linked with nonsense inheritable diseases (Wittenstein A. et al., 2023).

Indeed, several genetic diseases are caused by nonsense variants, with a different percentage for each one, including Cystic Fibrosis (CF), Choroideremia (CHM), Duchenne Muscular Dystrophy (DMD), Shwachman-Diamond Syndrome (SDS), Usher Syndrome (USH), β-Thalassemia and Lysosomal

Storage Diseases (LSD) (Borgatti M. et al., 2020; Pennesi ME. et al., 2019; Bezzerri V. and Cipolli M., 2019; Vitale E. et al., 2025).

2.2 Cystic Fibrosis: a "multiorgan disease"

CF is an autosomal recessive genetic disease caused by several variants in the *cystic fibrosis transmembrane regulator* (*CFTR*) gene; several variants are known in the literature (De Boeck K., 2020). In particular, more than 70,000 cases are known worldwide, with approximately 1,000 new cases added annually (Rafeeq M.M. and Murad H.A.S., 2017). The *CFTR* gene spans a region of approximately 189 kb on the long arm of chromosome 7 (position 7q31.2), comprising 27 exons (**Figure 2**). The coding sequence is approximately 4,443 nucleotides long and encodes a protein with 1,480 amino acids (Farinha C.M. and Callebaut I., 2022).

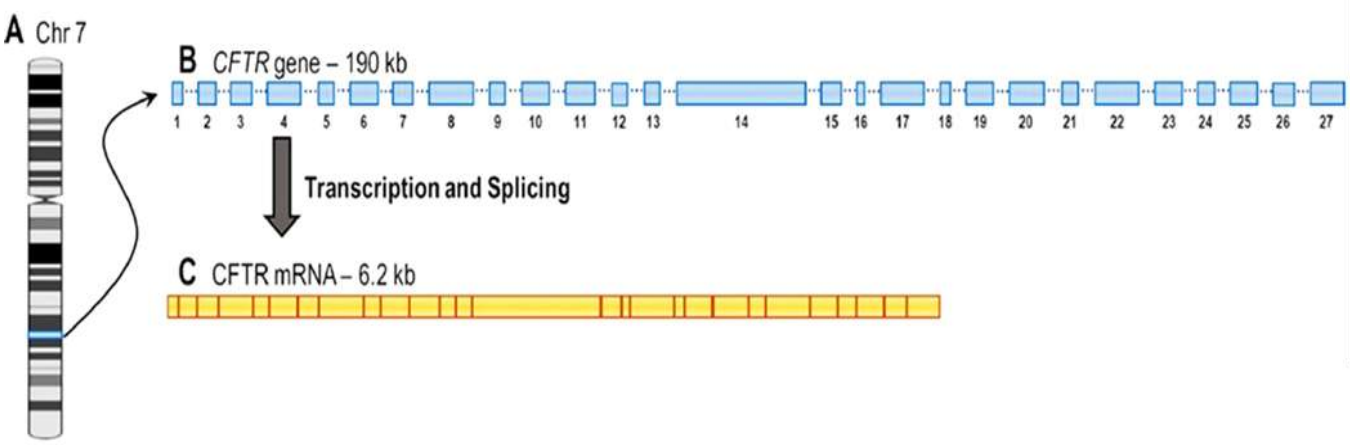

Figure 2. CFTR gene localization and structure: ***A)*** *Localization of the CFTR gene on chromosome 7;* ***B)*** *CFTR gene structure containing 27 exons and covering 190 kb of genomic human DNA;* ***C)*** *CFTR mRNA structure (Lopes-Pacheco, 2020*).

Specific variants of the *CFTR* gene cause CF, mainly known as a lung disease accompanied by chronic lung infections and inflammation, causing respiratory insufficiency and the patient's death. However, CF is also defined as a multiorgan disease because it encompasses numerous other manifestations, including pancreatic insufficiency with CF-related diabetes, intestinal obstruction in the neonatal period, male infertility, and liver manifestations, as shown in **Figure 3** (Fernandez F. E. et al., 2018).

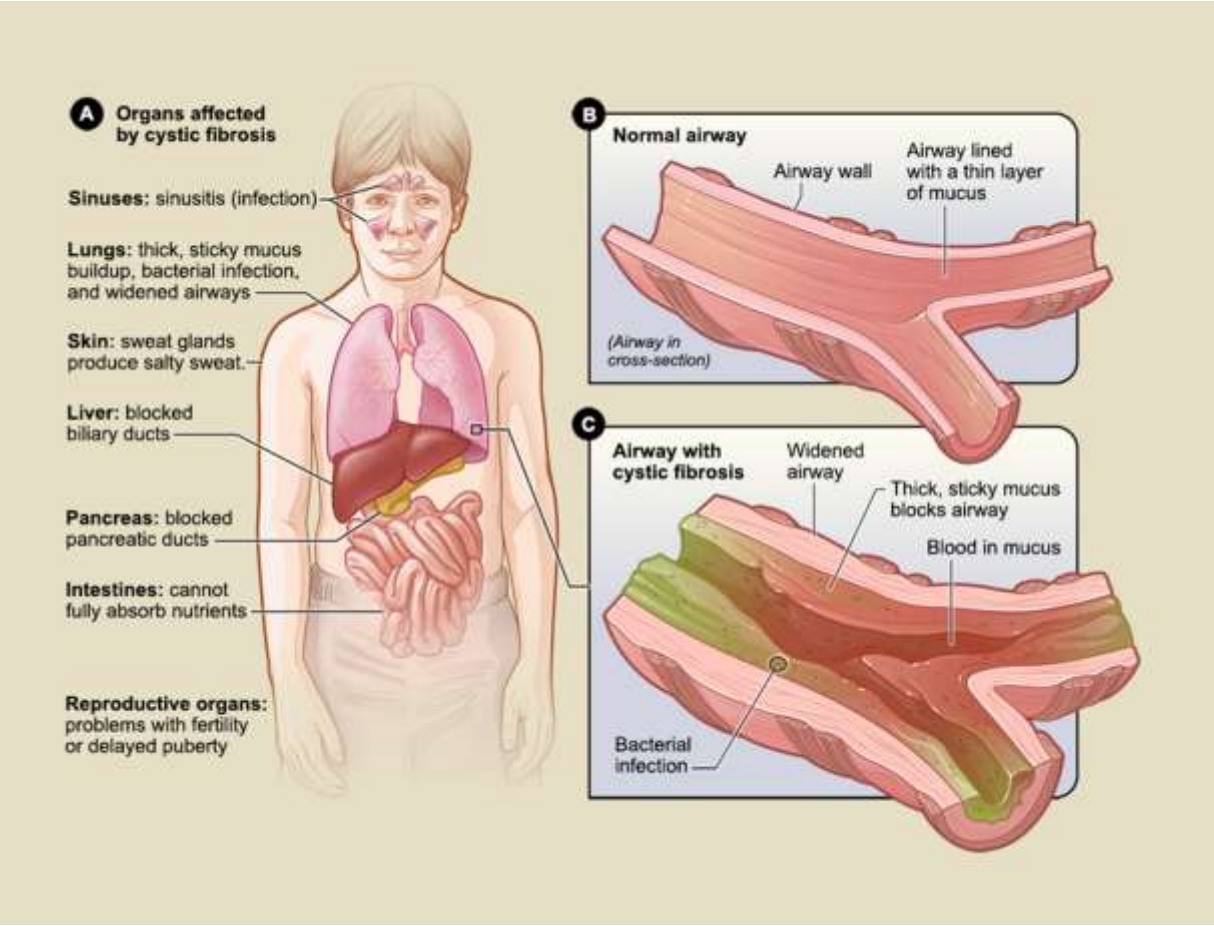

Figure 3. Cystic Fibrosis manifestations: ***A)*** *Main organs hit by CF;* ***B)*** *Healthy person airway;* ***C)*** *Cystic Fibrosis patient airway characterized by sticky mucus and widened airway with bacterial infection (NHLBI: National Heart, Lung, and Blood Institute).*

In literature, more than 2,100 variants of the *CFTR* gene have been reported, which the scientific community has divided into six classes (**Figure 4**), each one characterized by a specific phenotypic correspondence. As described by scientific guidelines, the I-II-III classes are related to CFTR complete or near-complete loss-of-function, caused also by the CFTR protein absence; instead, IV-V-VI classes are associated with a residual CFTR function (Fernandez F. E. et al., 2018; Ensinck MM. and Carlon MS., 2022; *CFTR1* database).

Class I variants are characterized by the almost total absence of a functional CFTR protein caused by the premature termination of the translation arising from splice site abnormalities, frameshifts or nonsense variants, such as G542X or R1162X. These variants are approximately presented by 22% of CF patients in almost one of their mutated alleles.

Class II variants are associated with the misfolding of the CFTR protein, which is subsequently degraded in the cytoplasm through the proteasome pathway. Notably, 88% of CF patients exhibit the ΔF508 variant in the mutated allele.

Class III variants affect the ATP-binding domains and are present in 6% of patients. Usually, they are represented by missense variants that induce the production of a protein correctly inserted in the cell membrane that shows a gating inefficiency, caused by the resistance to protein kinase A (PKA) activation. The most common example is the G551D variant.

Class IV variants are present in 6% of patients and cause the production of a protein that is properly located in the membrane, retaining the cAMP-dependent chloride channel activity, which shows a very low channel conductance.

Class V variants affect the pre-mRNA splicing process, downregulating CFTR protein production. They are harboured by 5% of CF patients and involve promoter variants that introduce incorrect amino acids in the CFTR protein sequence, causing improper protein maturation.

Class VI variants cause the instability of the CFTR protein directly in the plasma membrane and affect at least one allele of 5% of CF patients (Fernandez F. E., et al, 2018; Lee J.A., et al., 2021).

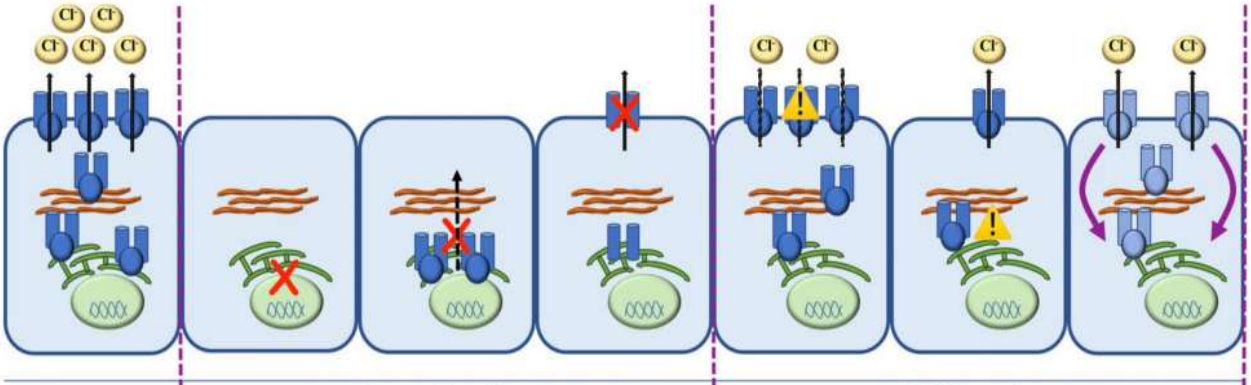

	Severe Mutations			Mild Mutations		
Wild Type	**Class I**	**Class II**	**Class III**	**Class IV**	**Class V**	**Class VI**
CFTR Defect	Defective synthesis → **No protein**	Defective traffic → **No traffic**	Impared gating → **No function**	Defective conductance → **Less function**	Reduced synthesis → **Less protein**	Reduced ½ life at the membrane → **Less stable**
Mutation example	G542X	Phe508del	G551D	R117H	3849−10kb C>T	Q1412X

Figure 4. Representation of CF variants classification: *it shows the specific CFTR defect and an example of a variant for each class (Regard L. et al, 2022).*

2.3 CFTR protein: a chloride and bicarbonate channel with gating function

The CFTR protein, a cAMP-activated, ATP-gated chloride and bicarbonate channel, is localized and predominantly expressed in the apical plasma membrane of polarized cells, enabling proper ion transport that maintains salt and water balance at the epithelial surface (Pankonien I. et al., 2022). The CFTR channel plays a crucial role in cells, and its structure, as shown in **Figure 5**, comprises a single regulatory R-domain, two transmembrane domains (TMD1 and TMD2), and two

cytosolic nucleotide-binding domains (NBD1 and NBD2). Each domain has a specific function and is fundamental to the activity of the others: TMD domains form the skeleton of the CFTR channel, while NBD domains enable the correct opening and closing of the gate when the R-domain (RD) is phosphorylated (Hanssens L.S. et al., 2021).

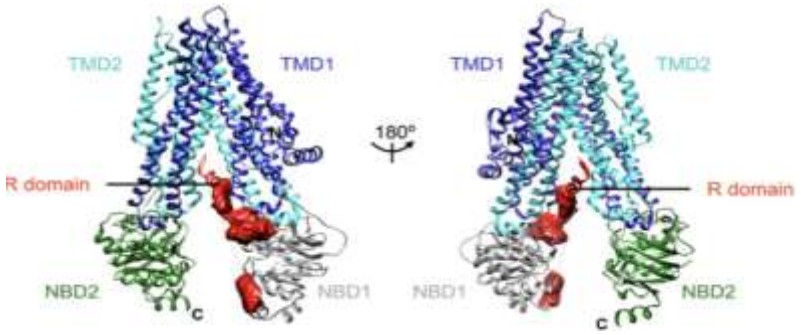

Figure 5. CFTR protein structure: *Ribbon diagram of CFTR, representing the front (left) and back (right) view (Hwang T.C. et al, 2018).*

In addition, CFTR TMD domains are composed of 12 transmembrane α-helix, and between every two helices a loop is inserted, producing six extracellular loops (ECL) and four intracellular loops (ICL), as shown in **Figure 6** (McDonald E.F. et al, 2023). Among ICL loops, ICL1 and ICL4 interact with NBD1, whereas ICL2 and ICL3 interact with NBD2. The CFTR NBD domains are characterized by three subdomains: the beta subdomain, belonging to NBD1 and covering residues 390-400 and 440−450, the alpha helical subdomain, belonging to NBD1 domain and spanning residues 500−565, and the ATPase subdomain, spanning NBD1 residues 450-500 and 566-650 (McDonald E.F. et al, 2023). Furthermore, the RD domain is highly conserved, particularly in the region defined by residues 645-845; post-translational modifications of this domain regulate CFTR gating (McDonald E.F. et al., 2023).

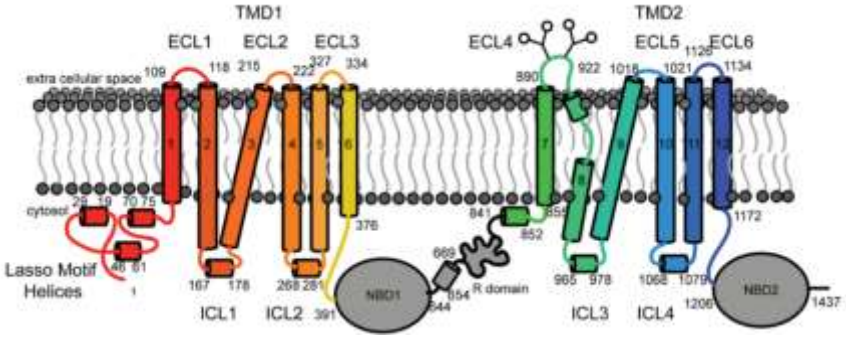

Figure 6. CFTR transmembrane topology: *CFTR protein is organized into transmembrane helices (TH) that form both intracellular loops (ICLs) and extracellular loops (ECLs). Specifically: TH2–3 form ICL1, TH4–5 form ICL2, TH8–9 form ICL3, and TH10–11 form ICL4. On the extracellular side, TH1–2 form ECL1, TH3–4 form ECL2, TH5–6 form ECL3, TH7–8 form ECL4, TH9–10 form ECL5, and TH11–12 form ECL6. Notably, TH2–3 and TH10–11 cross each other to interact with the opposite transmembrane domains (TMDs) and nucleotide-binding domains (NBDs), illustrating the complex 3D folding of the channel (McDonald E.F. et al., 2023).*

The CFTR protein plays a crucial role in hydrating airway mucus and the epithelial surfaces of different organs. It acts with the Ca^{2+}-activated Cl^- channel (CaCC), promoting chloride secretion, and regulating salt absorption by modulating the epithelial Na^+ channel (ENaC). In its mutated form, CFTR loses the ability to control ENaC activity, impairing salt absorption and disrupting fluid homeostasis. This leads to defective water transport across apical cell membranes and ultimately to improper hydration of the epithelial surface (Fernandez F. E. et al., 2018).

2.4 Nonsense variants in the *CHM* gene as a cause of Choroideremia

Choroideremia is an inherited genetic disease closely linked to chromosome X, causing degeneration of the retinal pigment epithelium (RPE), the choroid, and outer retina (Jolly JK, et al., 2015). This rare genetic disease leads to progressive vision loss during adolescence and adulthood, and finally, in the elderly, to total blindness. The first manifestations of the disease appear during childhood/adolescence, characterized by night vision loss and progressive degeneration of the peripheral vision. The vision is reduced during middle age, impairing central vision and total blindness among 66 to 72-year-olds (**Figure 7**). The eye manifestations of the disease are strictly linked to mental health, causing a diminished quality of life, followed by increased stress, anxiety, or depression, and emotional burdens, comprising loss of independence with difficulties in performing daily activities (Bozkaya D. et al., 2022).

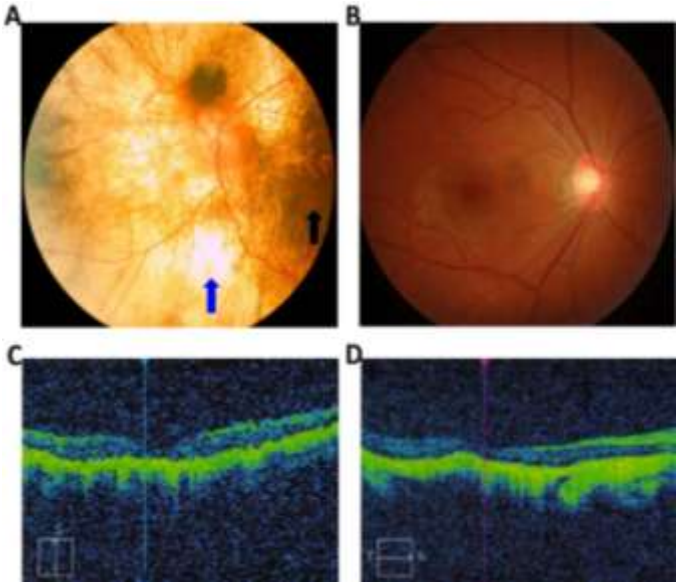

Figure 7. CHM patient phenotype: ***A-B****) fundus photograph and* ***C–D****) optical coherence tomography images;* ***A-C****) Chinese male patient with p.R267X nonsense variant;* ***B-D****) healthy Chinese male (Imani S. et al., 2018).*

Choroideremia has an incidence of approximately 1:50,000 to 1:100,000 worldwide and is caused by nullizygous deletions or hemizygous duplications of the *CHM* gene. The *CHM* gene (OMIM: 300390)

extends across 186,383 bp on the X chromosome long arm on locus 21.2-21.3. The transcription of this gene produces an mRNA composed of 15 exons, each less than 400 bp long, except for exon 15, which is 3642 bp (Imani S. et al., 2018). Nowadays, more than 280 variants have been identified in the *CHM* gene; the majority are point variants that directly introduce premature stop codons (**Figure 8**).

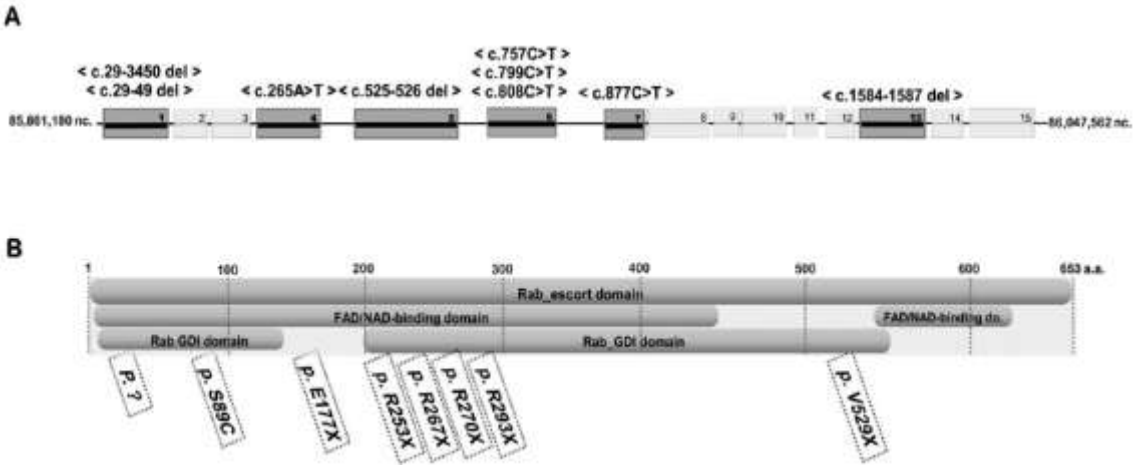

Figure 8. CHM nonsense variants: ***A****) The disease-causing variants are represented in the highlighted boxes in the exons 1, 4, 5, 6, 7, and 13.* ***B****) Pathogenic allelic variants affect the two main domains of REP1, specifically the FAD/NAD(P)-binding domain and the GDP dissociation inhibitor domain (Imani S. et al, 2018).*

In addition, the etiology and pathology of retinal degeneration caused by *CHM* variants are unknown, and no phenotype-genotype correlations have been established (Gao F.J. et al., 2020). More specifically, the diverse *CHM* gene variants are frameshift (51%), nonsense (34%), missense (8%), deletions (2%), insertions (1%), Indels (1%), other (1%) and unknown (2%) (Sarkar H. and Moosajee M., 2022) (**Figure 9**).

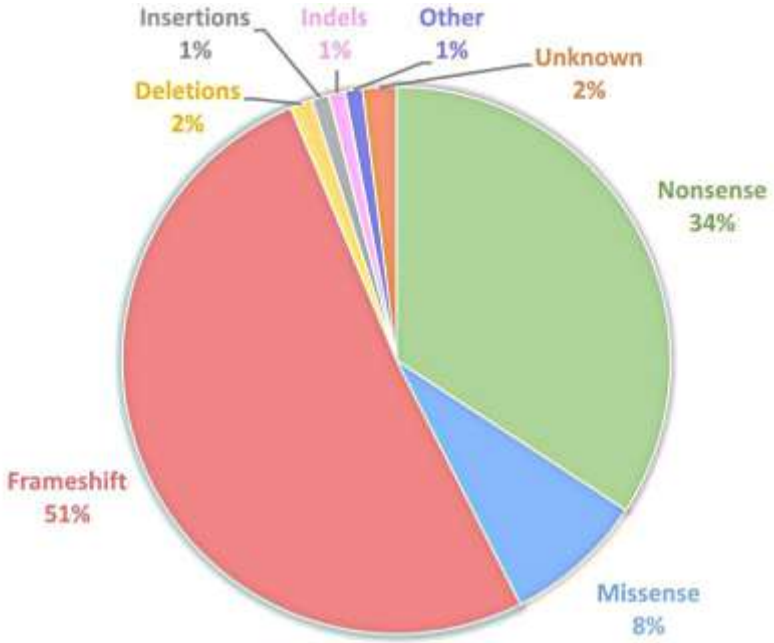

Figure 9. CHM gene variants: *diagram showing variants affecting the CHM gene (Sarkar H. and Moosajee M., 2022).*

Currently, about 116 nonsense variants have been reported in ClinVar for the CHM gene, all of which are classified as pathogenic. The most frequently occurring nonsense variants in Choroideremia are represented by p.R239X, p.R253X, p.R267X, p.R270X, and p.R293X (Sarkar H. et al, 2019). Currently, no cure or treatment is available for this genetic disease; however, various experimental approaches are showing promising results.

2.5 Molecular structure and function of REP1 protein

The *CHM* gene encodes the 95-kDa Rab Escort Protein 1 (REP1), a crucial transporter associated with vesicle traffic, which is composed of 653 amino acids. This protein is responsible for a specific post-translational modification, namely prenylation, which involves the addition of a prenyl group to the Rab GTPases, a family of G proteins belonging to the Ras superfamily, crucial for vesicle trafficking (Pylypenko O. et al, 2018). In addition to facilitating prenylation, REP1 is essential for the correct transport of Rabs through the cytoplasm, ensuring their appropriate membrane localization (De Silva S.R. et al., 2021). The Rab geranyl-geranyl-transferase II (RabGGTase II) is involved in the prenylation process; specifically, this complex can catalyze the addition of several geranyl groups to specific cysteine protein residues, namely the Rab protein (Pylypenko O. et al., 2018). However, unlike other prenyl transferase enzymes, RabGGTaseII can’t directly recognize its substrate; thus, in

this scenario, REP1 can carry out its natural function, working as a chaperone protein and introducing the Rabs protein to the RabGGTaseII complex (Pylypenko O. et al., 2003).

For instance, in the retinal pigment epithelium (RPE), the REP1 protein plays a key role in the transport of RAB27a to present it to RabGGTase II, so that the lack of REP1 causes the absence of a correct prenylated RAB27a, leading to early disease onset in the eye (Fry L.E. et al., 2021). X-Ray crystallographic studies have shown that REP1 owns several domains constituted by α-elix and β-strand, organized in a globular structure (**Figure 10-A**), which holds a hydrophobic pocket that can bind Rabs protein (Pylypenko O. et al., 2003), while immunofluorescence analyses revealed its correct cell cytoplasmatic distribution (**Figure 10-B**) (Vasireddy V. et al., 2013).

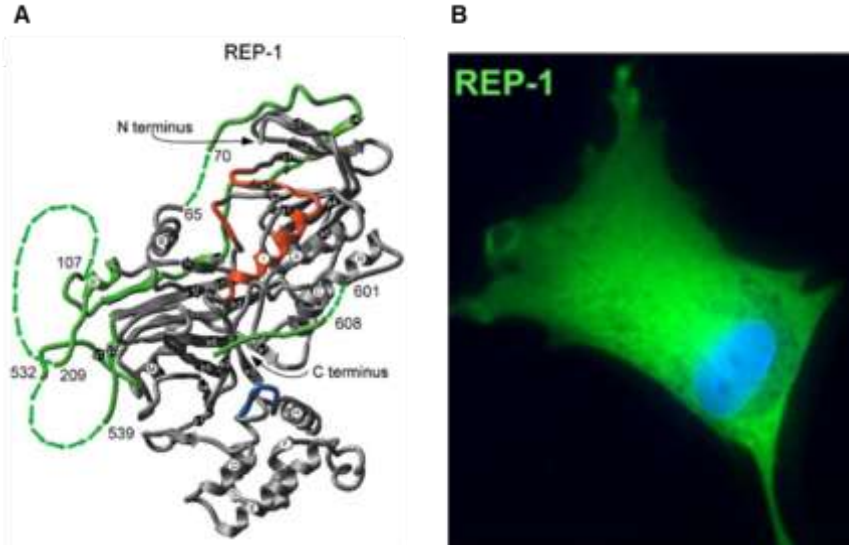

Figure 10. The REP1 protein structure and cell localization: *A) ribbon model showing REP1 structure, in green and grey structural elements, in red the hydrophobic binding platform and in blue the effector loop (Pylypenko O. et al., 2003);* ***B****) Immunofluorescence analysis revealing the REP1 correct localization inside the cells, with a cytoplasmatic distribution (Vasireddy V. et al., 2013).*

In particular, due to the REP1-Rabs cycle, REP1 binds the inactive Rab-GDP protein in the cytosol presenting them to the α-β subunits of the RabGGTaseII complex, that can add the geranyl-geranyl diphosphate (GGPP) to the C-terminus of the Rab protein, allowing now the correct transport of Rabs by REP1 to the final destination in membrane; once released, the Rab-GDP protein is activated in Rab-GTP, and REP1 can restart the cycle by binding a new inactive Rab in the cytosol, as shown in **Figure 11** (Fry L.E. et al. 2021).

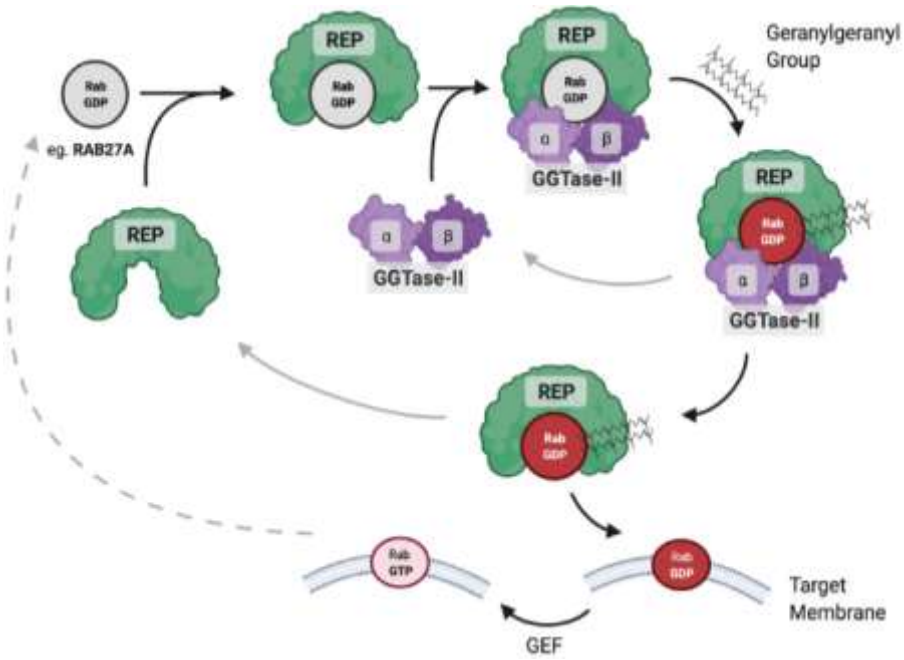

Figure 11. REP1 molecular pathway: *representation of the main intracellular REP1 trafficking pathway in RPE cells, allowed by correct geranylation of Rabs protein performed by REP1 (Fry L.E. et al., 2021).*

Therefore, the absence of this protein in the cells causes defects in intracellular vesicular trafficking, with cellular dysfunction and premature cell death. These conditions are strictly linked with the degeneration of the retinal pigment epithelium (RPE), the photoreceptors in the retina, and the choriocapillaris (Fry L.E. et al., 2021).

2.6 Emerging therapeutic approaches to the rescue of the premature stop codon effects

More than 7,000 rare genetic diseases have been recorded, and as previously discussed, 11% of all genetic variants associated with these human-inherited rare genetic diseases are nonsense variants. Today, there is no cure or treatment for nonsense-related diseases (NRDs), but in the last decades, several promising approaches have been developed (Vitale E. et al., 2025; Ricci D. et al., 2025). The first involves techniques such as CRISPR/Cas9, the second involves mRNA-based therapy, while the last involves suppression therapy based on translational readthrough-inducing drugs (TRIDs) and anticodon-engineered tRNA (ACE tRNA).

2.6.1 Gene editing for the correction of DNA nonsense variants

Different technologies are currently under development based on gene editing. Among these, interesting results have been shown by CRISPR-Cas9 (Doudna J.A., 2020; Golkar Z., 2020). Against nonsense variants, several research groups are actively investigating these gene editing tools, especially in the context of CF. The Base Editors were investigated in patient-derived organoids

carrying the R785X, W1282X, or R553X variants. Clevers' group has generated and characterized an intestinal organoid biobank representing 664 CF patients, focusing on rare variants, evaluating two different ABE (Adenine Base Editor) systems (**Figure 12**), the xCas9-ABE and the SpCas9-ABE. This study has demonstrated that a subset of organoids showed the expected A-to-G nucleotide conversion, with no detectable off-target effects in the genome, but with an editing efficiency that varies depending on the Cas9 and sgRNA used, but that does not exceed 9,3% for any of the three variants assessed (Geurts M.H. et al., 2020; Maule G. et al., 2020). In addition, these base editors can be delivered via chemically modified mRNAs, which result in more stable ones than unmodified ones, with no significant off-targets, as already evaluated *in vitro* for the correction of the W1282X nonsense variant by the Xue group (Jiang T. et al., 2020). This approach enabled the efficient rescue of the pathogenic variant, highlighting a novel and potentially effective strategy for base editor delivery (Jiang T. et al., 2020).

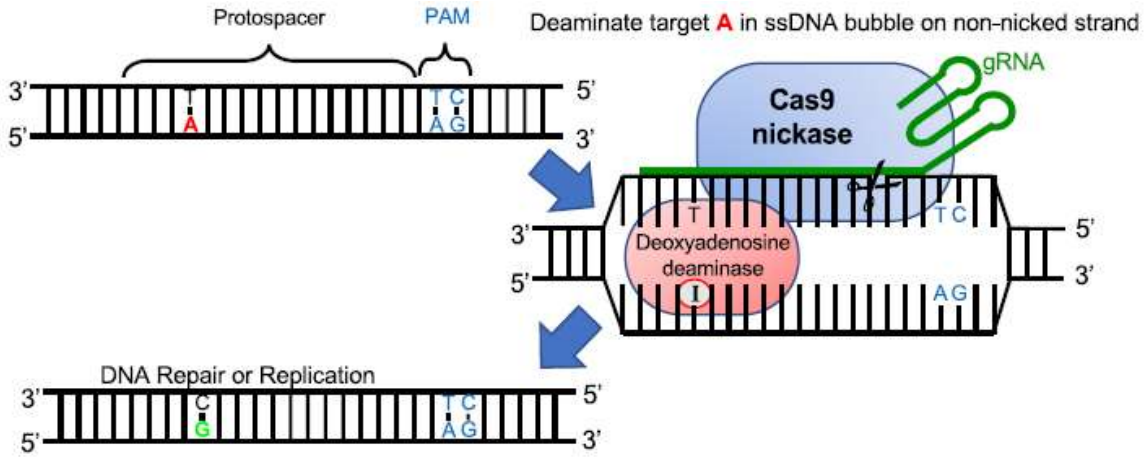

Figure 12. ABE system functioning: *ABEs are composed of a deoxyadenosine deaminase fused to a catalytically impaired SpCas9 with nickase activity. ABE, guided by a gRNA, binds the target DNA, producing a single-stranded DNA, in which deoxyadenosine deaminase converts adenine to inosine, which is recognized as guanine during DNA repair or replication. In this way, the original A•T pair is replaced with a G•C pair at the target site (Krishnamurthy S. et al., 2021).*

2.6.2 mRNA-based therapy

The *in vitro* transcription mRNA (IVT mRNA) represented the first study step in the development of mRNA-based therapy, introducing an external mRNA in the cells to produce any protein or peptide via the same cell's protein synthesis machinery, showing high transfection efficiency with low toxicity, with no opportunistic insertional mutagenesis, although the main issues are related to mRNA instability, immunogenicity and cell membrane passage (Qin S. et al., 2022). This approach, in the last decades, is gaining promising results and some companies have developed

new strategies to treat also rare genetic pathologies; for instance, in CF field, some inhaled mRNA therapy have been patented by Arcturus Therapeutics that have produced ARCT-032 and ACTR-810 (NCT05712538) delivered by LUNAR system, that are under studies by clinical trials with promising results for safety, tolerability, and kinetics (Clarke L.A. and Amaral M.D., 2023; Ricci D. et al., 2025), while, Moderna and Vertex Pharmaceuticals have developed VX-552, which is in Phase I clinical trials for safety evaluation (NCT05668741). In addition, several groups have demonstrated that the use of mRNA therapy based on splice-modulating ASOs, causing the exon 23 skipping, can successfully restore CFTR protein not only in 16-HBE cells engineered with W1282X variant but also in W1282X-homozygous pwCF primary cultures of nasal or bronchial cells (Michaels W.E. et al., 2022; Oren Y.S. et al., 2022; Kim Y.J. et al., 2022). To date, an approach based on mRNA therapy has been developed to correct the mutations that cause methylmalonyl-CoA mutase deficiency, responsible for methylmalonic acidemia, a rare metabolic disease with high morbidity and mortality (Coughlan K.A. et al., 2024). This mRNA-3705 shows a potent rescue and a wide therapeutic window, representing a robust preclinical profile supporting clinical development. In addition, it has already entered an international, multicenter Phase 1/2 clinical trial for patients with MMUT-deficient MMA. Indeed, Mrna-3705 has been selected by the FDA for the START program (Support for Clinical Trials Advancing Rare Disease Therapeutics), which aims to accelerate the clinical development of drugs for rare diseases. Lastly, Moderna is preparing to launch pivotal studies by the end of the current year (2025) (NCT04899310).

2.6.3 Anticodon engineered tRNA (ACE-tRNA): a post-translational gene recovery for nonsense variants

Among the different approaches, the strategy based on anticodon-engineered tRNA (ACE-tRNA), namely suppressor tRNA, can recover protein expression in a genetic context characterized by nonsense variants. Those tRNAs are charged with specific amino acids by the endogenous cell aminoacyl-tRNA synthetase. Still, they also own an altered anti-codon sequence that can recognize a PTC in the mRNA, allowing the correct protein synthesis as shown in **Figure 13** (Lin T.Y. and Glatt S., 2022).

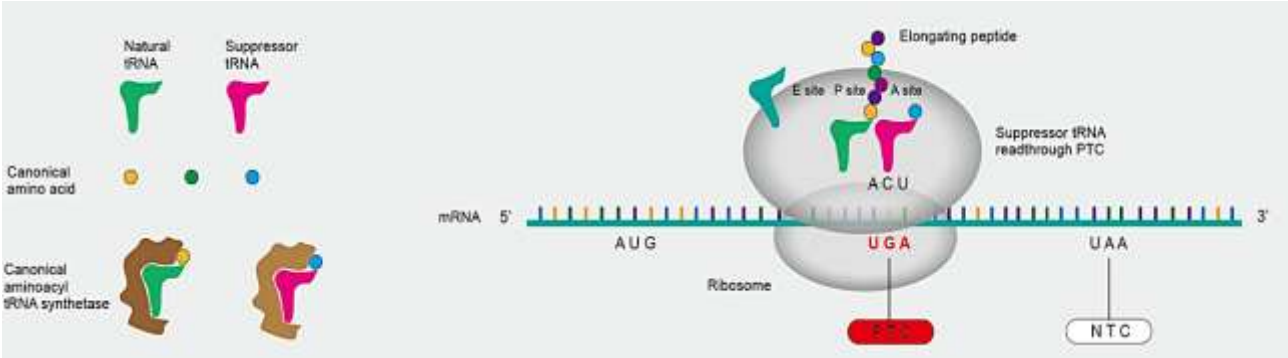

***Figure 13**. **Functional scheme showing the correct mechanism of action of suppressor ACE-tRNA:** these tRNAs are charged with a canonical amino acid and own an engineered anticodon that recognizes PTC, allowing the insertion of the amino acid and the production of a full-length protein (adapted from Ruan J. et al., 2024).*

Several groups are currently investigating ACE-tRNAs and their activity. Recently, this strategy has shown promising results in suppressing nonsense variants in CF. In particular, the Lueck group has demonstrated that these tRNAs can rescue CFTR protein expression *in vitro* in G542X, R1162X, and W1282X nonsense variant models, as well as *in vivo* in a NLuc-UGA PTC mouse model (Lueck J.D. et al., 2019). Notably, in 16HBEge cells, they reported a rescue of nearly 90% of wild-type CFTR channel function at two PTC positions in cells with efficient ACE-tRNA delivery, which was also supported by evidence of CFTR protein restoration (Ko W. et al., 2022). In addition, the Cooperman group has demonstrated that ACE-tRNA^{Arg} can suppress various nonsense variants, as shown in their studies using the PURE-LITE system with mRNA sequences harbouring CFTR patient-specific nonsense variants (Bhat S. et al., 2025). Although the ACE-tRNA strategy is promising, further analyses are needed to assess biosafety, bioavailability, and the development of efficient delivery systems (Lin T.Y. and Glatt S., 2022).

2.6.4 Suppression Therapy: using translational readthrough-inducing drugs (TRIDs) for the recovery of gene function

Among the various therapeutic approaches described so far, suppression therapy has yielded particularly promising results. This strategy is based on the pharmacological induction of readthrough at premature termination codons (Bidou L. et al., 2012; Campofelice A. et al., 2019). During protein synthesis, the ribosome translates information encoded by messenger RNA, producing a polypeptide chain that is released upon encountering a natural termination codon (NTC). However, when a premature termination codon (PTC) arises in the mRNA sequence due to a DNA nonsense variant, protein synthesis is interrupted, leading to the production of a truncated and non-functional protein (Lombardi S. et al., 2020) (**Figure 14**).

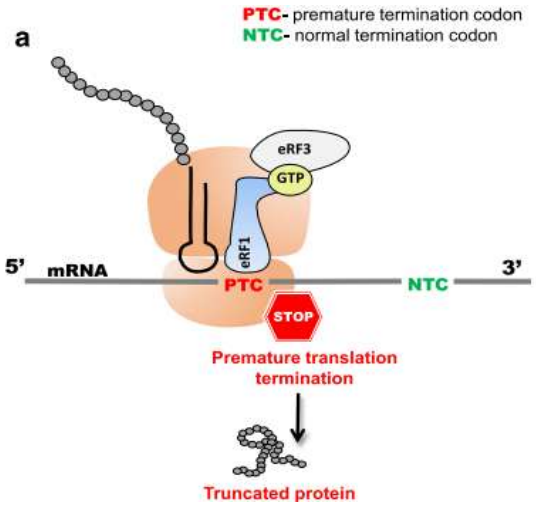

Figure 14. Premature termination translation: *The ribosome encounters a PTC in the mRNA sequence due to a nonsense variant, leading to the interruption of protein translation and the production of a truncated protein (Dabrowski M. et al., 2018).*

It has been demonstrated that cells can attempt to recover protein synthesis through a natural mechanism: the non-programmed translational readthrough. In this process, a near-cognate tRNA (nc-tRNA), that is a transfer RNA whose anticodon sequence partially matches a given mRNA codon, matching base pairs at two out of the three positions within the codon-anticodon interaction, is inserted at the site of the PTC, allowing translation to continue and potentially producing a full-length protein. Despite this mechanism, natural readthrough is rare, occurring in less than 0.1% of cases in over 80% of transcripts (Palma M. and Lejeune F., 2021). Over the last 20 years, various molecules have been identified that induce readthrough during translation. These molecules, known as translational readthrough-inducing drugs (TRIDs), possess the ability to "force" the translation in the presence of a premature stop codon in the mRNA (Palma M. and Lejeune F., 2021) (**Figure 15**).

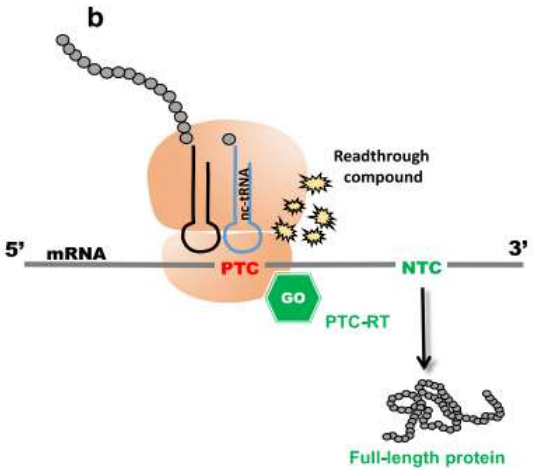

Figure 15. Pharmacologically induced readthrough: *a near-cognate tRNA is inserted at the PTC site during translation, thanks to the activity of a readthrough compound (Dabrowski M. et al., 2018).*

In literature, various classes of compounds with readthrough activity have been identified. Among them, aminoglycosides were the first to be discovered; their mechanism of action (MoA) consists of the binding of the ribosomal A-site, inducing a conformational change, causing the codon misreading at a PTC, and allowing the translation and the production of a full-length protein. Among aminoglycoside antibiotics, gentamicin and geneticin (G418) have played a key role as the first compounds showing readthrough activity, as well as tobramycin and paromycin. However, despite their great translational readthrough activity, chronic treatment with aminoglycosides induces cytotoxic effects, particularly ototoxicity and nephrotoxicity (Martins-Dias P. and Romão L., 2021; Dabrowski M. et al., 2018). In 2007, PTC Therapeutics discovered a new non-aminoglycoside compound with high readthrough activity, showing very low toxicity effects, named PTC124 (commercially known as Ataluren). PTC124 is an achiral compound showing an oxadiazole core characterized by fluorobenzene and benzoic acid rings (**Figure 16**), which does not show structural resemblance to aminoglycosides or any other clinically developed drugs, and whose possible mechanism of action is based on competitive inhibition of release factor-dependent termination binding several ribosome active sites (Welch E. et al., 2007; Huang S. et al., 2022).

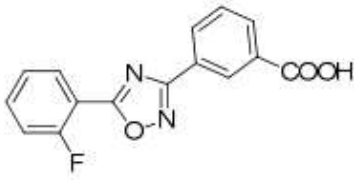

PTC124 - Ataluren

Figure 16. Structure of Ataluren (PTC124) *(Welch E. et al., 2007).*

This molecule showed promising results in both *in vitro* and *in vivo* applications in several diseases such as CF and DMD. However, the endpoints in Phase III clinical trials for CF failed, and although it was initially approved for the treatment of DMD, its use was permitted only until January 2025, when the European Commission (EC) adopted the opinion of the Committee for Medicinal Products for Human Use (CHMP) of the EMA, deciding not to renew the conditional marketing authorization for PTC124. Nevertheless, the EC indicated that individual EU Member States may allow the use of PTC124 if they consider it appropriate for patients with nonsense variants who have no therapeutic alternatives (Kerem E. et al., 2014; Michorowska S. et al., 2021; Aslam A.A. et al., 2023; Ricci D. et al., 2025, PTC therapeutics report, 28 March 2025).

To identify novel molecules as true alternatives to previously used compounds, with effective readthrough activity and potential clinical applicability, research has advanced and led to the development of a new compound, NB124, a synthetic aminoglycoside also known as ELX-02, which

has shown absence of toxic effects under various conditions (Ricci D. et al., 2025). Its MoA is similar to the one of aminoglycosides, mainly binding the decoding site of the ribosome's small subunit, causing the reduction of the ribosome's ability to distinguish between cognate and near-cognate aminoacyl-tRNAs, and thus increasing the production of a full-length protein. In addition, it has been demonstrated that this ability to mediate its function attenuates nonsense-mediated mRNA decay (NMD), leading to a higher steady-state level of transcripts available for protein synthesis (Kerem E., 2020). ELX-02 has overcome, in 2023, the Phase II clinical trial for CF and Alport syndrome, and, most importantly, Eloxx Pharmaceuticals announced essential advancements in patient conditions for both diseases, and NCT04135495 regarding CF patients has shown an improvement of lung function (Eloxx Pharmaceuticals report, 14 September 2022, NCT04135495).

In this scenario, in 2020 the Lentini-Pibiri group, through *in silico* optimization of PTC124 and by using several compound libraries, designed and synthesized three new small molecules containing a 1,2,4-oxadiazole as the heterocyclic core. These compounds have shown promising results not only in terms of high readthrough activity and consequent protein rescue, as demonstrated by the restoration of CFTR protein in Fisher rat thyroid (FRT) cells carrying G542X and W1282X *CFTR* mutations, but also in terms of protein functionality in F-luc assay (Pibiri I. et al., 2020).

In particular, as shown in **Figure 17**, although NV848, NV914, and NV930 share the common oxadiazole core, their structures display notable differences compared to Ataluren: NV848 lacks aryl substituents, both NV848 and NV930 lack fluorine atoms and acidic moieties, whereas NV914 is characterized by a high fluorine content (Pibiri I. et al., 2020).

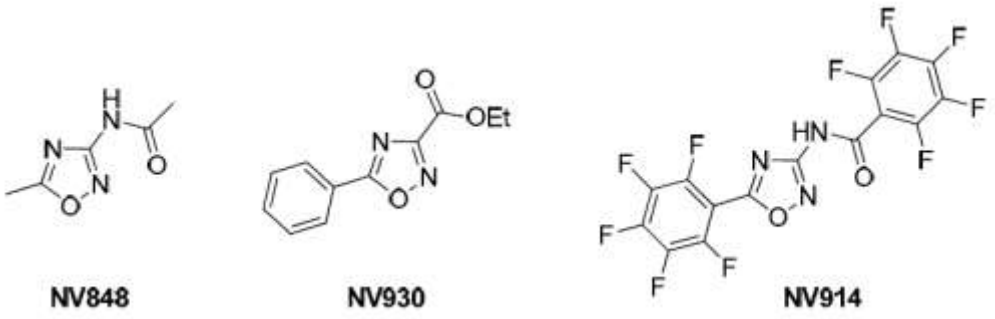

Figure 17. NV molecule structures: *scheme showing the chemical structures of the three oxadiazole molecules NV848, NV914, and NV930 (Pibiri I. et al., 2020; Italian Patent No 102017000134511, European Patent No. 3713934, US Patent No 11,203,578).*

In vitro experiments explored the specificity of these molecules against PTCs and demonstrated no off-target effects on NTCs of TP53 and housekeeping gene expression (Perriera R. et al., 2023). To evaluate the therapeutic potential of these molecules, *in vivo* analyses were performed, confirming their readthrough activity not only in CF nonsense variants but also in Shwachman-Diamond

Syndrome, as well as the absence of toxicity in zebrafish models (Bezzerri V. et al., 2022). Moreover, *in vivo* acute toxicity studies in mice confirmed good tolerability for all compounds, classifying NV848 and NV930 as Category 4 and NV914 as Category 5 under the Globally Harmonized System (GHS), thereby confirming these molecules as low-risk health candidates (Corrao F. et al., 2022). More recently, it has been demonstrated that NV848 reaches the main target organs of CF and, most importantly, acts as a readthrough agent capable of rescuing the CFTR protein in a CF G542X nonsense variant homozygous mouse model (Fiduccia I. et al., 2024). Further studies are needed to evaluate the mechanism of action of these molecules and to clarify the possible biological target.

2.7 The PURE-LITE system: an *in vitro* tool for the evaluation of new compounds with readthrough activity

Recently, personalized medicine has emerged as a strategy to treat patients; indeed, by studying the patient's genomic, biochemical, and behavioral profile, it may be possible to identify drugs tailored to specific conditions (Goetz L.H. et al., 2018). Therefore, it is essential to investigate as many new molecules as possible, including TRIDs, to increase the chances of finding treatments for nonsense variants underlying these diseases. At the same time, identifying the biological targets of existing compounds with readthrough activity can reveal the active sites involved in the process. Such knowledge can then be exploited to design new, more potent compounds capable of interacting with the same sites and inducing readthrough. Several assays and tools are applied to screen new molecules for the evaluation of readthrough activity, such as the reported luciferase assay (Campofelice A. et al., 2019), or the PURE-LITE system (Ng M.Y. et al., 2021). This reconstituted *in vitro* model system not only allows for the screening of different molecules but also other analyses, for instance, the separate determination of TRIDs' effects on both readthrough and termination activities (Huang S. et al., 2022).

This system is composed by different purified components: eukaryotic 80S ribosomes constructed with the cricket paralysis virus (CrPV) internal ribosome entry site (IRES) mRNA, that allows the production of polypeptides without the need of protein initiation factors, different aminoacylated tRNA isoacceptors, the release factors eRF1 and eRF3 and, finally, the elongation factors eEF1A and eEF2 (Ng M.Y. et al., 2021). As shown in **Figure 18,** the IRES mRNA sequence codifies for an octapeptide.

In particular, to study standard peptide elongation, a WT Trp-IRES mRNA sequence is used; instead, to investigate readthrough activity of compounds or translation termination, a Stop-IRES mRNA sequence is used. The use of this *in vitro* model system allowed the Cooperman group to determine

PTC124's mechanism of action, demonstrating that this molecule binds to multiple sites on the ribosome, competitively inhibiting the release factor-dependent termination (Huang S. et al., 2022). The PURE-LITE system is highly versatile and, thanks to its features, allows us to perform different measurements. At each step, a tRNA can be added to monitor, amino acid by amino acid, the growth of the octapeptide. This enables the evaluation of the incorporation of a nc-tRNA and the readthrough activity of specific molecules using a specific mRNA containing a stop codon. All of this is achieved through the use of specific tRNAs that can be charged with tritium-labeled amino acids, or, assays employing specialized instruments capable of detecting fluorescence, with tRNAs conjugated to specific fluorophores (Ng M.Y. et al., 2021).

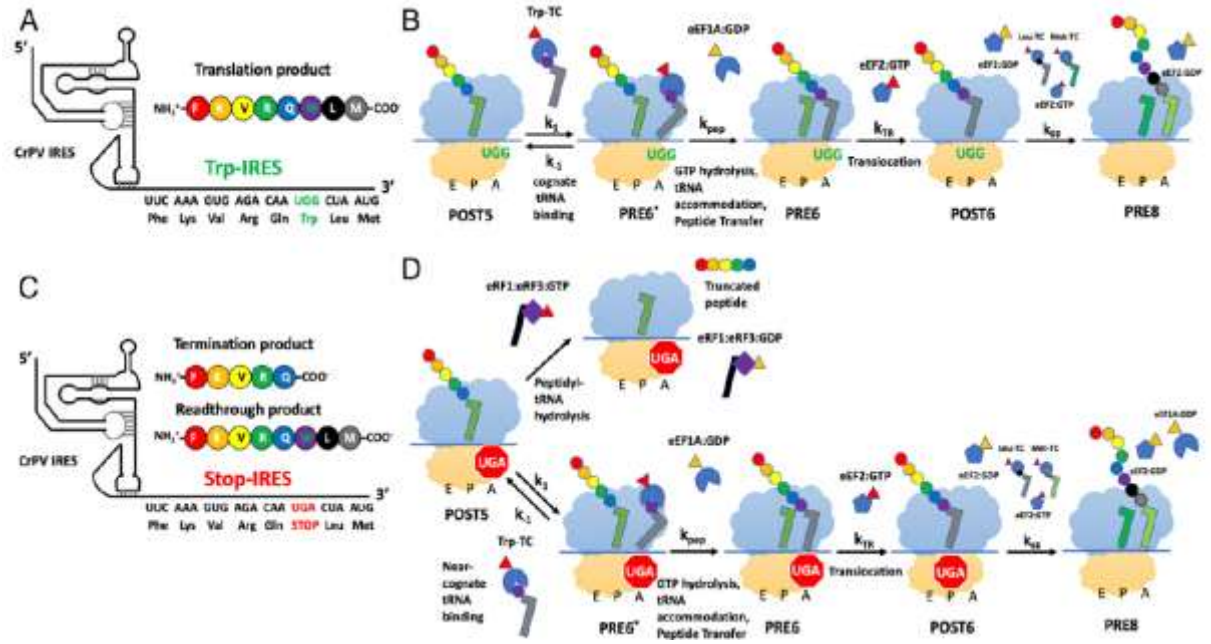

Figure 18. PURE-LITE system structure and functioning: *A) Trp-IRES construct encoding for FKVRQWLM polypeptide;* ***B****) Translation elongation of Trp-POST5 complex;* ***C****) Stop-IRES construct encoding for FKVRQX truncated peptide;* ***D****) Readthrough (down) and Termination (up) reactions of Stop-POST5 complex (Ng MY. et al., 2021).*

2.8 The CFTR G542X mouse as model to study cystic fibrosis and new treatments

Different models have been employed to study drug activity, from 2D and 3D cell systems to non-mammalian organisms, primarily to generate preliminary data (Freires I.A. et al., 2023). Among animal models, the mouse model has been extensively used as a translational tool to investigate human diseases, elucidate molecular mechanisms, and explore potential therapeutic strategies. Its widespread adoption is due to its genetic manipulability, physiological similarities to humans, and the availability of well-characterized disease models. However, to ensure scientific validity and ethical responsibility, it is essential that such studies incorporate appropriate controls, robust

statistical analysis, and adhere strictly to the 3Rs principle (Reduction, Replacement, Refinement) (Justice M.J. et al., 2016; MacArthur C.J. et al., 2018).

Preclinical research in CF caused by nonsense variants has also involved mouse models. For instance, the Hodges group has produced two different mouse models, each reporting a different nonsense variant: G542X and W1282X. For the production of both murine models, CRISPR/Cas9 based gene editing was applied. Based on this technique, different guide RNA (gRNAs) targeting exon 12 or 23 depending of nonsense variant, have been designed and tested *in vitro* for Cas9. The most effective gRNA for each variant, a 120 bp single stranded oligonucleotide containing the G542X or W1282X mutation, and Cas9 protein were injected in the pronucleus of C57BL/6 one-cell embryos, that has been implanted into pseudo-pregnant females (Michicich M. et al., 2025; McHugh D.R. et al., 2018). The G542X CF mouse model generated through gene editing represents a valuable tool to investigate *in vivo* potential therapies for cystic fibrosis, including suppression therapy, ACE-tRNAs, and mRNA-based approaches, as it shows CF manifestations such as impaired growth and low survival due to intestinal obstruction (McHugh D.R. et al., 2018).

Direct observation in our animal facility of the murine model homozygous for the G542X nonsense mutation revealed a distinct and severe phenotype. These mice exhibited delayed growth, significantly reduced weight gain compared to age-matched wild-type controls, and markedly shortened survival, primarily due to fatal intestinal obstructions. Strikingly, nearly 50% of the homozygous animals died before the onset of experimental procedures, limiting their availability for in vivo studies. Furthermore, colony maintenance through successive crossings of heterozygous carriers proved challenging, as these matings consistently produced fewer viable offspring than wild-type pairings, underscoring the reproductive and survival limitations associated with the G542X genotype (Fiduccia I. et al., 2024).Hodges and collaborators produced organoids from these mouse model tissues to investigate not only the effect of the readthrough compound G418 alone, but also its activity in combination with SMG1 inhibitor (a kinase involved in inhibiting the NMD pathway to increase CFTR mRNA levels) as well as with the CFTR correctors VX-445 (Elexacaftor, which promotes proper CFTR protein folding) and VX-661 (Tezacaftor, which stabilizes CFTR). Hodges group demonstrated that G542X mouse-derived organs had greater CFTR restoration than W1282X when treated with G418 alone, G418+SMG1i, and G418+SMG1i+VX-445+VX-661. Interestingly, both the models have demonstrated to be useful tools not only for the evaluation of possible therapies against nonsense variant in CF but also for their *in vivo* efficiency; in addition although the models share different features, both the models responded differently to the same pharmacological treatment, highlighting the need to evaluate a different therapeutic option based on genotype (Michicich M. et al., 2025).

In light of the aforementioned studies and the clinical manifestations observed in mice, this murine model represents a valuable system for the study of cystic fibrosis, and in particular for investigating CFTR protein rescue strategies within a genetic background defined by the G542X nonsense variant.

3. AIM OF THE PROJECT

Choroideremia and cystic fibrosis are two paradigmatic examples of monogenic diseases caused, in a significant fraction of cases, by nonsense mutations. In choroideremia, pathogenic variants in the *CHM* gene prevent the production of Rab Escort Protein-1 (REP1), a key component of the prenylation pathway required for the proper functioning and survival of retinal cells. The loss of REP1 leads to progressive degeneration of the retinal pigment epithelium and photoreceptors, ultimately resulting in blindness. In cystic fibrosis, stop mutations in the *CFTR* gene, such as G542X, result in the production of truncated chloride channel proteins that fail to mediate ion transport across epithelial membranes, leading to the accumulation of thick mucus and chronic inflammation in multiple organs, particularly the lungs.

Given that both conditions stem from a single-gene defect resulting in truncated, non-functional proteins, therapeutic strategies aimed at restoring full-length protein expression have gained significant attention. Among these, translational readthrough has emerged as a particularly promising approach. This method employs small molecules known as translational readthrough-inducing drugs (TRIDs), which facilitate the insertion of near-cognate aminoacyl-tRNAs at premature termination codons (PTCs). By allowing the ribosome to bypass the PTC, TRIDs enable the synthesis of a full-length protein that may retain partial or complete biological activity, offering potential therapeutic benefit in disorders caused by nonsense mutations. Several potential TRIDs have been identified and characterized over the past two decades, including aminoglycosides, such as gentamicin, and non-aminoglycoside compounds, such as PTC124 (Ataluren). However, the clinical translation of these molecules has been limited by their variable efficacy, cytotoxicity, and inconsistent readthrough efficiency. Therefore, the development of new TRIDs with improved pharmacological profiles and broader applicability remains a critical goal in the field of genetic disease therapeutics.

In this context, the present work investigates three novel experimental compounds: NV848, NV914, and NV930, as potential TRIDs. Preliminary studies have shown that these molecules can promote readthrough of premature stop codons and partially restore the expression of full-length proteins *in vitro* and *in vivo (*Pibiri I. et al., 2020; Perriera R. et al., 2023; Bezzerri V. et al., 2022; Corrao F. et al., 2022; Fiduccia I. et al., 2024). NV848, in particular, has demonstrated promising activity in preclinical models of Duchenne muscular dystrophy and cystic fibrosis carrying nonsense mutations (Fiduccia I. et al., 2024).

Building on these findings, this study aims to explore the capacity of NV848, NV914, and NV930 to rescue the expression and function of two disease-relevant proteins: REP1, which is deficient in choroideremia, and CFTR, which is defective in cystic fibrosis. By employing engineered cell lines, patient-derived fibroblasts, and *in vivo* mouse models carrying nonsense mutations, the work seeks

to evaluate the efficacy of TRID-mediated readthrough, define the molecular mechanisms underlying compound activity, and assess their potential as mutation-specific therapeutic agents.

Therefore, the rationale of this work is rooted in the concept that restoring even a modest amount of correctly translated protein can lead to meaningful improvements in disease phenotypes. As a final component of my thesis, I conducted an experimental study at the University of Pennsylvania (UPENN). During this period, the project was focused on the study of the biological target of the three NV compounds, on a new *in vitro* model known as the PURE-LITE system (Ng M.Y. et al., 2021).

Understanding the capacity of NV compounds to promote readthrough and to stabilize mutant mRNAs could therefore provide a proof of concept for their therapeutic potential.

4. MATERIALS AND METHODS

4.1 Cell culture conditions

H1299 cells (human non-small cell lung carcinoma cell line), RPE (retinal pigment epithelium) and HCT116 (human colon rectal tumor 116) were grown in DMEM (Dulbecco's Modified Eagle Medium, GIBCO, Waltham, MA, USA) implemented with 10% FBS (fetal bovine serum, GIBCO) and 1% Penicillin and Streptomycin (Corning, USA), while patient-derived fibroblasts, purchased by Coriell Institute (New Jersey, USA), characterized separately by S190X, R253X and R270X nonsense variants were grown in MEM (Minimum Essential Medium Eagle, Thermo Fisher Scientific, Waltham, MA, USA) implemented with 2% Ultroser G (Thermo Fisher Scientific, Waltham, MA, USA), 1% non-essential amino acids (Thermo Fisher Scientific, Waltham, MA, USA), 1% L-glutamine (Thermo Fisher Scientific, Waltham, MA, USA) and 1% Penicillin and Streptomycin (Corning, USA). Cells were cultured at 5% CO_2 and 37 °C, and media were changed every 48 hours.

4.2 TRIDs preparation

4.2.1 Cell and Animal procedures

Ataluren was synthesized as previously described by Lentini and colleagues (Lentini L. et al., 2014), whereas NV848, NV914, and NV930 were synthesized according to the protocol reported by Pibiri and colleagues (Pibiri I. et al., 2020). For the efficacy studies in mice, a dosage of 60 mg/Kg body weight was selected based on Du M. et al., 2008. Stock solutions of PTC124, NV914, and NV930 in DMSO (Merck, Darmstadt, Germany) were first prepared according to the solubility properties of each compound (i.e. PTC124 at 100 mg/ml, NV914 at 500 mg/ml, and NV930 at 161 mg/ml) and subsequently resuspended in extra-virgin olive oil as delivery vehicle. Mouse daily dosages were calculated individually based on body weight, with a maximum administration volume of 100 µl per animal. For *in vitro* cell studies, compounds were prepared as 100 mM stock solutions in DMSO and diluted in 1X PBS to the 1mM final concentration.

4.2.2 PURE-LITE procedures

Ataluren sodium salt was received from PTC Therapeutics and dissolved in DEPC water. G418 was purchased from Gibco (Thermo Fisher Scientific, Waltham, MA, USA). NV848, NV914, and NV930 were synthesized by the Pibiri-Lentini group at the University of Palermo and dissolved

respectively in DEPC water for NV848 and in DMSO for NV914 and NV930 to the 1mM final concentration.

4.3 Homozygous CFTR$^{G542X/G542X}$ mouse colony production

CFTR$^{WT/G542X}$ mice were gently donated by the Hodges group in Cleveland (McHugh D.R. et al., 2018) and housed in the ATeN Center animal facility of the University of Palermo. Breeding was carried out among 30 pairs of heterozygous G542X mice. Twenty-one days after birth, all pups underwent genotyping. The Genomic DNA was extracted from ear punch biopsies using DNeasy Blood and Tissue Kits for DNA Isolation (Qiagen, USA) according to the manufacturer's instructions, followed by endpoint PCR analysis. Specifically, primers P1 (forward primer recognizing the *CFTR* G542X allele), P2 (reverse primer recognizing the *CFTR* wild type allele), P3 (forward primer recognizing the *CFTR* wild type allele) were used (**Table 1**).

Primer	**Sequence 5'- 3'**
P1	**5'**-ACAAGACAACACAGTTCTCT-**3'**
P2	**5'**-TCCATGCACCATAACAACAAGT -**3'**
P3	**5'**-ACAAGACAACACAGTTCTTG-**3'**

Table 1. Primer sequences for mice genotyping analyses.

All the 159 newborn mice were genotyped by endpoint PCR, using the DreamTAQ DNA Polymerase (Thermo Fisher Scientific, Waltham, MA, USA), according to the manufacturer's instructions. Each DNA sample was separately amplified by using two reaction mixes (**Table 2**) containing the P1/P2 primers pair targeting the *CFTR* G542X allele, or the P3/P2 primers pair targeting the *CFTR* wild type allele. The thermal profile in **Scheme 1** was used.

Reagent	**C_i**	**C_f**	**Volume 20µl**
DreamTaq Buffer	10X	1X	2 µl
dNTPs Mix	2 mM	0,2 mM	2 µl
Primer forward (P1/P3)	10 µM	0,1 µM	0,2 µl
Primer reverse (P2)	10 µM	0,2 µM	0,2 µl
DreamTaq	5U/µl	1U/µl	0,2 µl
DNA sample	/	50-100 ng	X
H_2O DNAse/RNAse free	/	/	to final volume

Table 2. PCR mix for mice genotyping analyses.

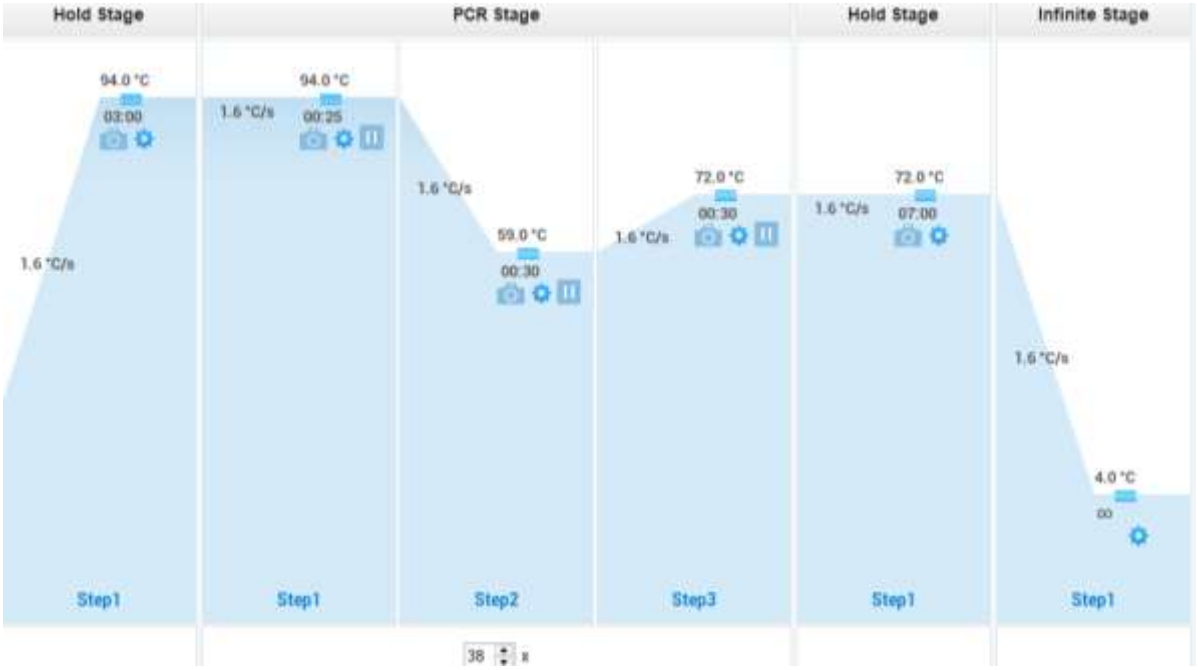

Scheme 1. Thermal profile adopted for genotyping analysis: *the genotyping was performed by endpoint PCR with 2720 Thermal Cycler, in particular 38 cycles of amplification were performed (Applied Biosystems, Waltham, MA, USA).*

PCR products were separated by electrophoresis on a 1% agarose gel in 1X TBE buffer and stained with GelRed Nucleic Acid Gel Stain (Biotium, USA).

4.4 Chronic treatment for a drug efficacy study

All the animals were housed in a temperature-controlled animal facility with 21-23 °C, 50-60% humidity, and a 12 h light/dark cycle. C57BL/6 CFTR$^{WT/WT}$ and C57BL/6 CFTR$^{WT/G542X}$ mice were fed with standard pellet chow and water, *ad libitum*, while C57BL/6 CFTR$^{G542X/G542X}$ mice in order to avoid intestinal obstruction caused by solid food in this mouse model, were fed with a specific liquid diet characterized by fresh milk (Peptamem, Nestlè).

The experimental protocol was conducted in conformity with the Italian D.Lgs 26/2014, and all procedures and care were approved by the authorization of the Italian Ministry of Health (Authorization n.1235/2020; Authorization n° 2/2022-PR) and by the University of Palermo Animal Care and Use Ethics Committee, following the national and EU Directive 2010/63/EU for the handling and use of experimental animals.

A daily administration of PTC124, NV914 and NV930 at 60 mg/kg for 15 days was performed, starting 23 days after birth and genotyping. A total of 13 C57BL/6 CFTR$^{G542X/G542X}$ mice were administered with the molecules. Moreover, five C57BL/6 CFTR^{WT} mice (as positive control) and 5 C57BL/6 CFTR$^{G542X/G542X}$ mice (as negative control), received an oral dose of vehicle (H_2O), only one C57BL/6 CFTR$^{G542X/G542X}$ mice (as negative control), received an oral dose of vehicle (Olive oil

and DMSO). The use of water as a vehicle was motivated by the parallel experimentation performed with a water-soluble molecule, for which the negative controls were carried out using water. Moreover, the limited survival of the mouse model and the low number of animals obtained did not allow for a sufficient number of homozygous G542X mice to be available for the administration of a second vehicle (oil and DMSO), except in the case of a single mouse. At the end of the treatment, mice were euthanized through cervical dislocation, blood and organs were collected, weighed, and stored at -80 °C for Western blot and Real-Time qPCR, and in formaldehyde 4% for IHC analyses.

4.5 H&E and IHC

Formalin-fixed, paraffin-embedded (FFPE) samples of the lung and intestine of mice were collected at the end of the treatments, while has been processed by the Belmonte group at the Tumor Immunology Unit, Department of Health Sciences, University of Palermo. The study involved cases of vehicle-treated $CFTR^{WT/WT}$ mice, vehicle-treated $CFTR^{G542X/G542X}$ mice, NV914-treated $CFTR^{G542X/G542X}$ mice, and PTC124-treated $CFTR^{G542X/G542X}$ mice as positive control.

Lung and intestine samples were fixed in 10% neutral-buffered formalin, processed, and embedded in paraffin. Three-micrometers-thick tissue sections were cut and routinely stained with hematoxylin and eosin (H&E) for histopathological analysis. For the histopathological evaluation of tissue damage, a semiquantitative scoring system was applied. All the variables were morphologically evaluated and scored according to the degree of severity (0, absent; 1, normal; 2, mild; 3, moderate; 4, discrete; 5, severe) and extension (0, absent; 1, focal; 2, multifocal; 3, diffuse).

Three-micrometer-thick sections of lung tissue were deparaffined, rehydrated and subjected to antigen retrieval using Novocastra Epitope Retrieval Solution (pH 6; Leica Biosystems) in a thermostatic bath at 98.5 °C for 30 minutes. Sections were then cooled to room temperature and rinsed in phosphate-buffered saline (PBS). Endogenous peroxidase activity was quenched with 3% H_2O_2, followed by Fc blocking with 0.4% casein in PBS (Leica Biosystems). Tissue sections were incubated with rabbit polyclonal anti-CFTR (1:500 pH 6; ACL-006 Alomone labs). IHC staining was developed using IgG (H&L)-specific secondary antibodies (Life Technologies, 1:500) and DAB (3,3′-Diaminobenzidine, Novocastra) as substrate chromogen. Nuclei were counterstained with Mayer's hematoxylin. Slides were analyzed under a Zeiss Axioscope A1 microscope and microphotographs were collected using a Zeiss Axiocam 503 Color digital camera with the Zen 2.0 Software (Zeiss).

4.6 RNA extraction

RNA extraction from tissues and cells was performed using the RNeasy Mini Kit (Qiagen, Germany) following manufacturer's instructions. The main difference between the two procedures

lies in the first step: up to 24 mg of tissue were disrupted by mechanical homogenization, whereas less than 10^6 cells were lysed by brief vortexing. Instead, for both the procedure an in-column DNase treatment was performed and finally RNA was eluted in 40 µL of DNase- and RNase-free water. This protocol was used to extract RNA from mice lung tissues, and from different cell cultures including H1299, H1299 CHM^{WT}-tGFP, H1299 CHM^{R253X}-tGFP and H1299 CHM^{R293X}-tGFP, Fibro CHM^{S190X} and Fibro CHM^{R253X}. After the extraction for each sample, RNA was quantified using a NanoDrop 2000 (Thermo Fisher Scientific, Waltham, MA, USA), and its integrity was checked by electrophoresis on a 1% agarose gel with SYBR™-SAFE DNA Gel Stain (10,000X, Thermo Fisher Scientific, Waltham, MA, USA) staining and UV exposition.

4.7 Reverse transcription and Real Time PCR

RNAs extracted from mouse lungs, from H1299 cells (untransfected or transfected with pRG213610 CHM^{WT}-tGFP, $pCHM^{R253X}$-tGFP, or $pCHM^{R293X}$-tGFP), and from $CHM^{S190X/y}$ fibroblasts and $CHM^{R253X/y}$ fibroblasts were reverse-transcribed into cDNA using the High-Capacity cDNA Reverse Transcription Kit (Thermo Fisher Scientific, Waltham, MA, USA), according to the manufacturer's instructions and following the thermal profile presented in **Scheme 2.**

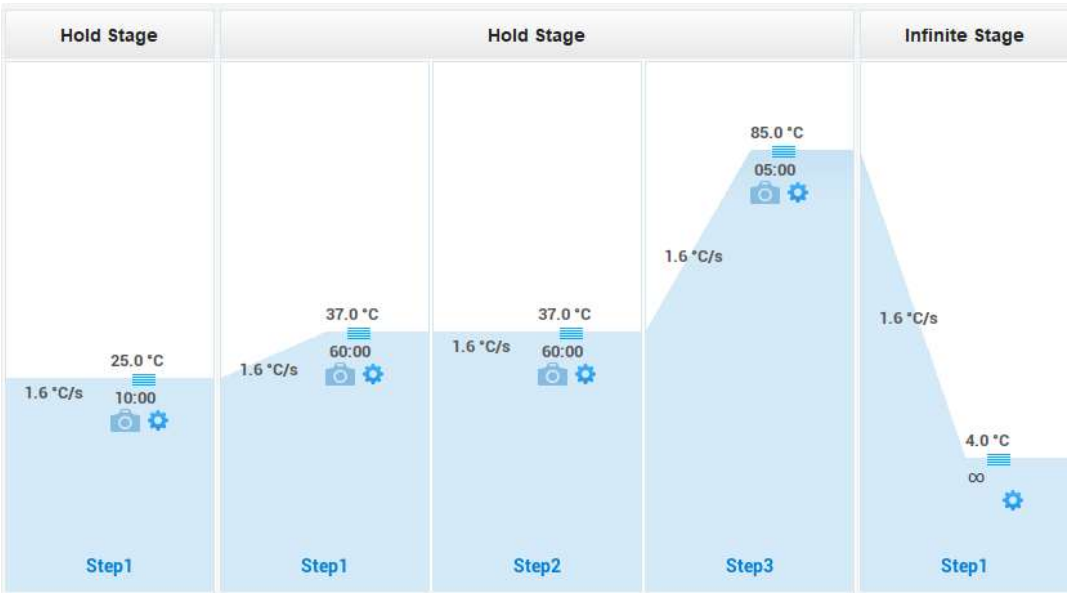

Scheme 2. Thermal profile used for retro-transcription process.

Real-time PCR was then performed using the synthesized cDNA. To assess *CFTR* expression, the primers pair CFTR For. and CFTR Rev. was used, with ACTIN For. and ACTIN Rev., recognizing ACTIN as housekeeping control. To evaluate TurboGFP expression, GFPturbo For. and GFPturbo Rev. primers pair were employed, with GAPDH For. and GAPDH Rev., recognizing GAPDH as

housekeeping control. Lastly, to evaluate *CHM* expression in the primary cell cultures the primers pair CHM For. and CHM Rev. was used, GAPDH as housekeeping control, as detailed in **Table 3.**

Primer	Sequence 5' - 3'
CHM For.	**5'**-GATCCAGAGAATGCGCTAG-**3'**
CHM Rev.	**5'**-AATGACCCGAACAGCAAAAGTTC-**3'**
GAPDH For.	**5'**-CTCATGACCACAGTCCATGCC-**3'**
GAPDH Rev.	**5'**-GCCATCCACAGTCTTCTGGGT-**3'**
GFPturbo For.	**5'**-AGGACAGCGTGATCTTCACC-**3'**
GFPturbo Rev.	**5'**-CTTGAAGTGCATGTGGCTGT-**3'**
CFTR For.	**5'-**CTACATGGAACACATACCTTCG-**3'**
CFTR Rev.	**5'-**GGTGATAATCACTGCATAGC-**3'**
ACTIN For.	**5'-**ACCGTCAAAAGATGACCCAGA-**3'**
ACTIN Rev.	**5'-**GAGGCATACAGGGACAGCACA-**3'**

Table 3. Primer sequences involved in Real-time qPCR.

For each couple of primers, the reaction mix was assembled as follows:

- PowerUp™ SYBR™ Green Master Mix (Thermo Fisher Scientific, Waltham, USA): 5 µl;
- Primers (Forward 1 µM + Reverse 1 µM): 2 µl;
- H_2O DNase/RNase-free: 1 µl;
- cDNA: 2 µl.

The samples were loaded in triplicate with a final volume of 10 µl each. Lastly, the 96-plate was centrifuged at 2500 rpm for 5 minutes. The amplification was performed using the QuantStudio 3 machine, and the results were analyzed with QuantStudio Design & Analysis Software.

4.8 Protein extraction and western blot analyses

Protein extraction from tissues and cells was performed using RIPA lysis solution (Thermo Fisher Scientific, Waltham, MA, USA) and 1% protease inhibitors (Thermo Fisher Scientific, Waltham, MA, USA). The main difference between the two procedures concerns the first step: up to 50 mg of tissue were disrupted by mechanical homogenization with a homogenizer, whereas cells were lysed by brief up and down with a pipette. Thus, the mixtures were incubated for 1.5 h on ice at 4 °C. Then, the samples were centrifuged at 12,000 rpm for 20 min at 4 °C, and the supernatants were collected and stored at -80 °C. For each sample, a quantification was performed using the Bradford colorimetric assay.

For the protein analysis, 50 µg of proteins from each sample were loaded onto a 3%-8% SDS-PAGE gel and electrophoresed at 150 V and 100 mA for 45 minutes. After that, proteins were transferred to a PVDF membrane (Thermo Fisher Scientific, Waltham, MA, USA) overnight at 4 °C, 12 V, and 50 mA. A 5% non-fat milk in TBS-TWEEN 1X solution (Thermo Fisher Scientific, Waltham, MA, USA) was used to block for 1 h at room temperature to prevent non-specific binding. The primary antibodies used were anti-CFTR (ACL-006, 1:10,000, Alomone lab), anti-β-actin antibody (A5441, 1:10,000, Sigma-Aldrich), anti-TurboGFP (TA150041, 1:1,000, Thermo Fisher Scientific), and anti-REP1 (sc-23905, 1:1,000, Santa Cruz Biotechnology), incubating overnight at 4 °C. After three 15-minute washing with 1X PBS-Tween, the membranes were then incubated with horseradish peroxidase (HRP)-conjugated secondary antibodies: anti-rabbit (W4011, 1:3,000, Promega) or anti-mouse (1:5,000, Thermo Fisher Scientific). Lastly, after three 15-minute washes with 1X PBS-Tween. Protein detection was conducted by SuperSignal West Femto Maximum Sensitivity Substrate (Thermo Fisher Scientific, Waltham, MA, USA). To analyze membranes Chemidoc XRS (BioRad) and Quantity One software (BioRad) were used. Protein bands were quantified using ImageJ software (NIH).

4.9 Plasmid pRG213610 preparation

The pRG213610 CHM^{WT}-tGFP (**Figure 19**) plasmid was bought from Origene Technologies, Inc. (Rockville, US). It was dissolved in 100 µL of D-R-free water, briefly vortexed, and incubated for 10 minutes at room temperature. The solution was stored at -20 °C.

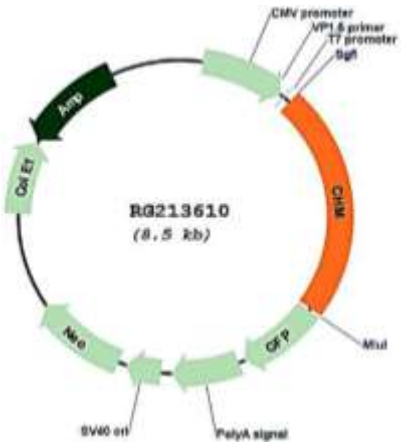

Figure 19. pRG213610 plasmid map: *The vector contains the CHM sequence with an in-frame sequence for turbo GFP, an Amp cassette for the selection in bacterial cells, and a Neo cassette for selection in eukaryotic cells.*

4.10 Site-directed mutagenesis and Colony PCR

The site-directed mutagenesis of the pRG213610 CHM^{WT}-tGFP vector consists of introducing nonsense mutation c.757C>T (R253X) or c.877C>T (R293X) in the *CHM* coding sequence with the QuickChange II kit (Statagene, CA, USA). The assay required the Pfu-Turbo DNA polymerase, plasmid template, and the following specifically designed couples of oligonucleotides, CHM-R253X For and CHM-R253X Rev, or the introduction on R253X nonsense mutation, and CHM-R293X For and CHM-R293X Rev, for the introduction on R293X nonsense mutation, (**Table 4)**.

Primer	Sequence 5' - 3'
CHM-R253X For.	**5'**-ATTGATCTTCTAATCAAATCTAATGTTAGT**T**GATATGCAGAG TTTAAAAATATTACCA-**3'**
CHM-R253X Rev.	**5'**-TGGTAATATTTTTAAACTCTGCATATC**A**ACTAACATTAGATT TGATTAGAAGATCAAT-**3'**
CHM-R293X For.	**5'**-GCAAACAACTTACTATGGTAGAAAAG**T**GAATGCTAATGAAA TTTCTTACATTT-**3'**
CHM-R293X Rev.	**5'**-AAATGTAAGAAATTTCATTAGCATTC**A**CTTTTCTACCATAGT AAGTTGTTTGC-**3′**

Table 4. Primer sequences for site-directed mutagenesis: *primer sequences used for the introduction of the nonsense variants in the pRG213610 CHM^{WT}-tGFP.*

Reactions were performed as follows: 25 ng of template were incubated with 62.5 ng of each primer and with 1X reaction buffer, 0.5 µl dNTP mix, and 0.5 µl of Pfu Ultra from the kit, following the thermal cycles shown in **Scheme 3.**

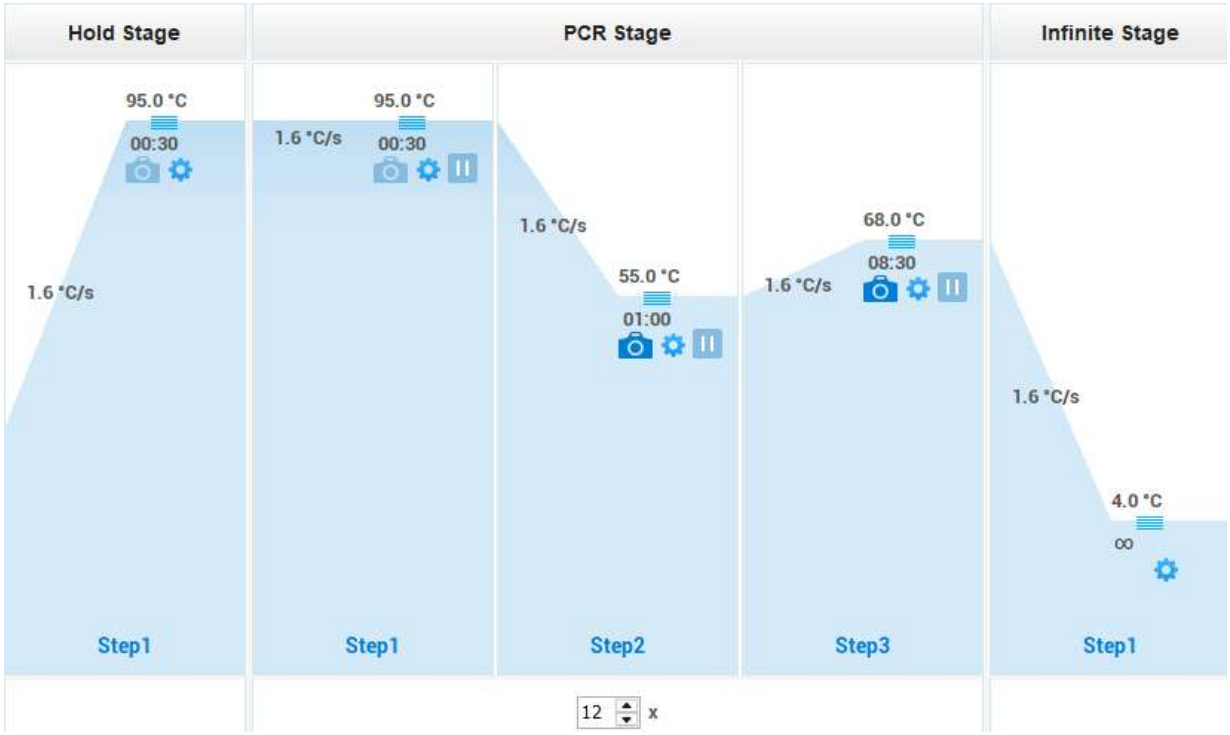

Scheme 3. Thermal profile: *this profile was applied to introduce nonsense variants into the pRG213610 CHM^{WT}-tGFP.*

At the end of the PCR, 0.5 µl of DpnI enzyme was added, and the reactions were incubated at 37 °C for 1 h. The plasmids obtained after the mutagenesis reaction were transformed into Top10 *E. coli* competent cells, which were plated on LB agar containing ampicillin.

To select plasmid-positive colonies, colony PCR was performed with two pairs of primers, reported in Tables **3** and **4**, CHM For. and CHM Rev. for the R253X variant, and CHM For. and CHM-R293X Rev. for the R293X variant. The expected ~400 bp (for R293X mutation) and 1 kb (for R253X mutation) amplicons were visualized on 1% agarose gel, with SYBR Green I staining and UV exposition, and then sequenced by BMR genomics. Only one clone per mutation was used to purify mutagenized plasmid DNA by Hi-Pure Plasmid Midi-prep Kit (Thermo Fisher Scientific, Waltham, MA, USA), according to manufacturer instructions. After extraction and purification, 1 µg of each DNA preparation, pCHM^{R293X}-tGFP and pCHM^{R293X}-tGFP, was sent to BMR genomics for sequencing.

4.11 Cell Transfections

3×10^5 H1299 cells were seeded into each well of a 6-well plate (Corning, ME, USA). After 24 h, a transfection was performed. Specifically, 1 µg of pRG213610 CHM^{WT}-tGFP, 1 µg of pCHM^{R253X}-tGFP, or 1 µg of pCHM^{R293X}-tGFP was diluted separately in 200 µl of DMEM (without

supplements). The transfection reagent Turbofectamine (Thermo Fisher Scientific, Waltham, MA, USA) was vortexed, and 3 µl was added to each tube containing the different plasmids. The mixtures were incubated at room temperature for 20 minutes and then dispensed into wells containing H1299 cells. After 5 h, the medium was replaced. Seventy-two hours later, selection with G418 (Geneticin) at 600 µg/mL was carried out each 72 hours for 15 days.

4.12 Cell DNA extraction

2 x 10^5 H1299, H1299 CHM^{WT}-tGFP, H1299 CHM^{R253X}-tGFP, and H1299 CHM^{R293X}-tGFP cells were seeded and, after 48 h, were detached with trypsin 0.05% (Thermo Fisher Scientific, Waltham, MA, USA), collected, and pelleted. Lastly, extraction was performed using PureLink™ Genomic DNA Mini Kit (Thermo Fisher Scientific, Waltham, MA, USA), following the kit instructions. For each sample, DNA was quantified using a NanoDrop 2000 (Thermo Fisher Scientific, Waltham, MA, USA), and its integrity was checked by electrophoresis in a 1% agarose gel.

4.13 PCR analysis

Genomic DNA extracted from each cell line was amplified using a DreamTaq DNA Polymerase, 5 U/µL (Thermo Fisher Scientific, Waltham, MA, USA), according to the manufacturer's instructions and following the thermal profile in **Scheme 1**. The primers CHM For. and GFPturbo Rev., which target the plasmid region of interest, were used for the amplification (see **Table 3**) of an expected amplicon of 2049 base pairs. The PCR amplicons were visualized in a 1% agarose TAE 1X gel.

4.14 PURE-LITE system procedures

4.14.1 tRNAs

The single tRNA isoacceptors were isolated from bulk tRNA from cake yeast via hybridization to complementary oligoDNAs immobilized in beads (as described in Ng MY. et al., 2018 and in Zhang H. et al., 2016). This last complex is prepared by overnight incubation of DNA oligo's with beads. Initially, the bulk tRNAs were quantified by spectrometry. Contemporary, 250 mL of 10 mM Tris-HCl (pH 7.6) and a 2X TMA buffer (20 mM Tris pH 7.6, 1.8 M Tetramethylammonium chloride, 0.2 mM EDTA) solutions were prepared. Thus, the beads were washed twice with 10 mL 10 mM Tris pH 7.6 through vacuum suction. The tRNA bulk solution was then incubated at 80 °C for 10 min, after that, the 2X TMA was added and incubated at 65 °C for 10

min. Thus, the mixture was added to beads and incubated at 65 °C for 10 min. Subsequently, the temperature was decreased to 37 °C, mixing the beads every 15 minutes. Different washes with 10 mL of 10 mM Tris-HCl (pH 7.6) were performed, continuing until the absorbance at 260 nm was minimal to remove all the unbound tRNA in the mixture and get pure desired tRNA which is bound to beads. The optical density (OD) absorbance at 260 nm was measured to evaluate the nmol of tRNA on the beads. Lastly, 5-9 mL 10 mM Tris-HCl (pH 7.6) was added and incubated at the target temperature, then the supernatant, which contains eluted tRNA, was decanted and saved. Next, the same yeast tRNAs isoacceptor was deaminoacylated and charged with the desired cognate radioactive amino acids (as described in Pan D. et al., 2006 and in Pan D. et al., 2009). Yeast tRNATrp and tRNALeu were charged with [3H]-Trp or [3H]-Leu for the hexa/heptapeptide assay.

4.14.2 POST5 complexes preparation

The preparation of POST5 complexes was adapted from Ng M.Y. et al., 2018. The protocol was conducted in Buffer 4 (40 mM Tris HCl, pH 7.5, 80 mM NH_4Cl, 5 mM $Mg(Ac)_2$,100 mM KOAc, and 3 mM β-mercaptoethanol). The first step requires an 80S-IRES complex, which was produced by incubating 2 μM of 80S ribosome and 4 μM IRES mRNA at 37 °C for 30 min. POST5 complex was formed by incubating 1 μM 80S-IRES with 1 μM each of Phe-tRNAPhe, Lys-tRNALys, Val-tRNAVal, Arg-tRNAArg, and Gln-tRNAGln, 2 μM eEF1A, 2 μM eEF2, and 2 mM GTP at 37 °C for 45 min. POST5 was then purified by layering into a 1.1-M sucrose solution in Buffer 4 (250 μL) and performing ultracentrifugation at 110,000 × rpm for 90 min at 4 °C. The POST5 pellet was resuspended in Buffer 4. POST5 complexes used in peptide formation assays were prepared using [3H]-Trp-tRNATrp for radioactive count studies, while for fluorescence studies, [ATTO647]-Trp-tRNATrp was used. S-POST5 production follows the same protocol using an 80S-Stop-IRES.

4.14.3 $Trp^{[3H]}$-PRE6 and $Trp^{[3H]}$-POST6 complexes preparation

The procedure was adapted from Zhang H. et al., 2016. Trp-PRE6 was formed by incubating 100 μL of 0.05 μM Trp-POST5, 0.5 μM [3H]Trp-tRNATrp, 1 μM eEF1A, and 1 mM GTP for 30 s at 37 °C. Trp-POST6 was formed similarly but with 1 μM eEF2 added. Trp-PRE6 and Trp-POST6 were purified by ultracentrifugation as described for POST5 complexes.

4.14.4 $Leu^{[3H]}$-POST7 complexes preparation

Leu-POST7 was formed by incubating Stop-POST5 (0.05 μM), 0.5 μM [3H]Trp-tRNATrp, 0.5 μM [3H]Leu-tRNALeu, 1 μM eEF1A, 1 μM eEF2, 0.1 μM eRF1, 0.2 μM eRF3 and 1 mM GTP

for 5 minutes at 37 °C. Leu-POST7 was purified by ultracentrifugation as described for POST5 complexes.

4.14.5 Assays

All assays were performed in Buffer 4 at 37 °C. In assays involving ribosome pelleting, *E. coli* 70S carrier ribosome (100 pmol 70S) was added. Pellets were layered by a 1.1-M sucrose solution in Buffer 4 (350 µL), and the mixture was subject to ultracentrifugation at 110,000 rpm for 90 min at 4 °C.

4.14.6 Elongation assay

The assay was performed by mixing POST5 mix (POST5 0.05 µM, GTP 1 mM, Buffer 4 10X, MQ water) and TC mix (Trp-tRNA$^{[3H]}$, eEF1A, eEF2, GTP Buffer 4 10X, MQ water) and incubating at 37 °C for 5 minutes. Subsequently, the reaction was quenched with 100 µL MES buffer and placed on ice, 70S carrier was added for ribosome pelleting. POST6 was then purified by layering into a 1.1-M sucrose solution in Buffer 4 (250 µL) and performing ultracentrifugation at 110,000 × rpm for 90 min at 4 °C. The POST6 pellet was resuspended in Buffer 4 and quantified by radioactive count and spectrometer.

4.14.7 Readthrough assay

The assay was performed by mixing Stop-POST5 mix (Stop-POST5 0.05 µM, GTP 1 mM, Buffer 4 10X, test molecule, MQ water) and TC mix (Leu-tRNA$^{[3H]}$, eEF1A, eEF2, eRF1, eRF3, GTP, Buffer 4 10X, MQ water) and incubating at 37 °C for 5 minutes. Subsequently, the reaction was quenched with MES buffer 100 µL and placed on ice, and 70S carrier was added for ribosome pelleting. POST7 was then purified by layering into a 1.1-M sucrose solution in Buffer 4 (250 µL) and performing ultracentrifugation at 110000 × rpm for 90 min at 4 °C. The POST7 pellet was resuspended in Buffer 4 and quantified by radioactive count and spectrometer.

4.14.8 Termination assay

The assay was performed by mixing Stop-POST5 mix (Stop-POST5 0.05 µM, GTP 1 mM, Buffer 4 10X, test molecule, MQ water) and RFC mix (eRF1, eRF3, GTP, Buffer 4 10X, MQ water) and incubating at 25 °C for 10 minutes. Subsequently, the reaction was quenched with MES buffer 100 µL and placed on ice, and 70S carrier was added for ribosome pelleting. Stop-POST5 was then purified by layering into a 1.1-M sucrose solution in Buffer 4 (250 µL) and performing

ultracentrifugation at 110,000 × rpm for 90 min at 4 °C. The supernatant was analyzed, in particular, the released peptide was quantified by radioactive count and a spectrometer.

4.14.9 Peptide release assay

The assay was performed by preparing separately Stop-POST5 mix (Stop-POST5 0.05 µM labelled with ATTO647, GTP 1 mM, Buffer 4 10X, MQ water) and RFC mix (eRF1 0.12 µM, eRF3 1.6 µM, GTP 1 mM, Buffer 4 10X, test molecule, MQ water). Stop-POST5 mix was splatted in a 96-well plate and the reaction began only after the addition of RFC mix. Immediately, the plate was placed inside the Tecan Spark plate reader at 25 °C and data were acquired. The fluorescence emitted by the fluorophore was analyzed.

4.14.10 PRE6 formation assay

The assay was performed by preparing separately Stop-POST5 mix (Stop-POST5 0.05 µM labelled with ATTO647, GTP 1 mM, Buffer 4 1X, MQ water) and TC mix (eEF1A 100 µM, eRF1 2 µM, eRF3 10 µM, GTP 1 mM, Buffer 4 1X, Ataluren 1 mM, NV848 12µM, MQ water). Stop-POST5 mix was splatted in a 96-well and the reaction began only after the addition of TC mix. Immediately, the plate was inserted in the Tecan Spark plate reader at 25 °C and data were acquired. The fluorescence emitted by the fluorophore was analyzed.

5. RESULTS

Objective 1

5.1 Rescue of the CFTR protein expression by readthrough experimental molecules in a Cystic Fibrosis mouse model characterized by the CFTR^{G542X} nonsense variant

The first objective of this work was to study the recovery of CFTR protein expression in a murine model of cystic fibrosis carrying the G542X nonsense mutation. This mutation, located in exon 12 of the CFTR gene, introduces a premature stop codon that prevents the synthesis of the full-length chloride channel, leading to a complete loss of function. To address this defect, the study aimed to evaluate the ability of experimental readthrough-inducing compounds to restore CFTR expression *in vivo*. Using the C57BL/6 CFTR$^{G542X/G542X}$mouse model, the effects of selected compounds were analyzed at both molecular and protein levels.

5.1.1 Production of a Cystic Fibrosis mouse model characterized by the CFTR G542X nonsense mutation

To obtain a consistent number of mice (N=5 per condition) for the experimental treatment with the NV914 and NV930 compounds, heterozygous mice carrying the G542X mutation were used for breeding. According to Mendelian inheritance, the mating of heterozygous animals yields approximately 25% homozygous offspring carrying the G542X mutation, as illustrated in **Figure 20**.

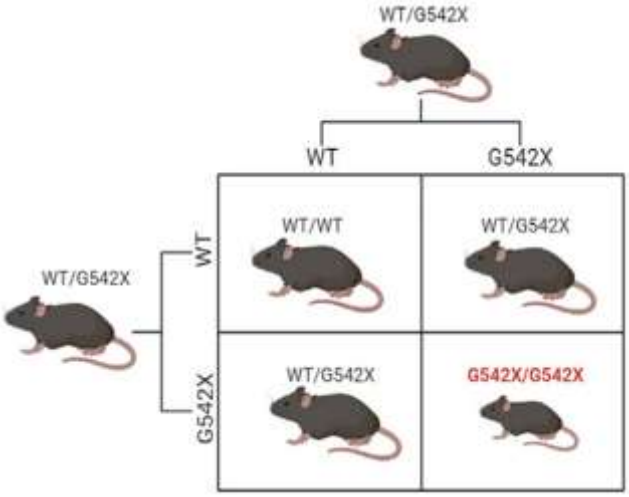

***Figure 20**. **Punnett's scheme:** the scheme illustrates the breeding strategy employed to generate G542X mutant CFTR mice (Fiduccia I. et al, 2024).*

During this project, a total of 30 couples between heterozygous C57BL/6 CFTR$^{WT/G542X}$ mice have been made, and a total of 159 mice have been produced.

As shown in the timeline in **Figure 21,** after the birth of the mice, which usually occurs between the eighteenth and twenty-first day after setting up the mating pairs, the newborns remain with the mother

for the following 20 days. At the end of this period, an ear biopsy is performed, and the mice are separated into groups of three, divided by sex, and fed for the following days with a specially formulated milk designed for children with cystic fibrosis to avoid intestinal obstructions. The biopsy samples are used to genotype mice to identify homozygous mice for the CFTR G542X mutation, which are then included in the experimental study.

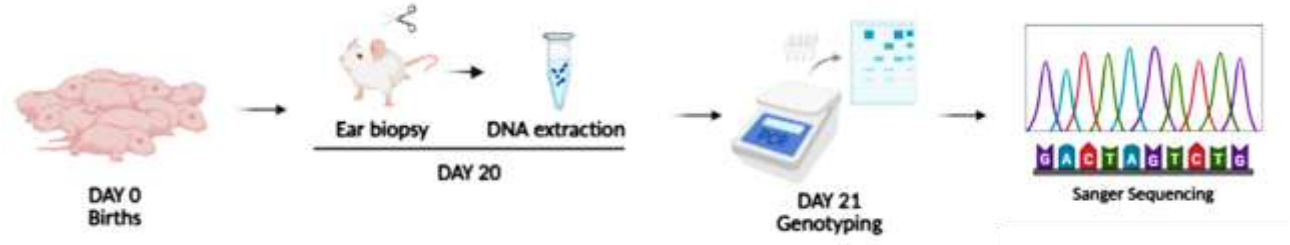

Figure 21. Experimental timeline: *the figure illustrates the workflow for genotyping newborn mice.*

Genomic was DNA extracted from ear biopsies, and all the experimental protocols involving the mice were performed in accordance with the Italian D.Lgs 26/2014. In addition, all the procedures were approved by the University of Palermo Animal Care and Use Ethics Committee and by the authorization of the Italian Ministry of Health (Authorization n.1235/2020; Authorization n° 2/2022-PR) and following the national and EU Directive 2010/63/EU for the handling and use of experimental animals. A PCR analysis using appropriate kits and specific primers designed to identify both the WT and G542X alleles (as detailed in Materials and Methods, **Table 1**) was performed. Specifically, primers P1 (primer forward recognizing $CFTR^{G542X}$ allele), P2 (primer reverse recognizing $CFTR^{WT}$ allele), and P3 (primer forward recognizing $CFTR^{WT}$ allele) map on a defined CFTR gene region comprising nucleotides c.84714 _85032, generating an amplicon of 319 bp. All 159 mice were genotyped.

In detail, for each sample shown in **Figure 22**, the presence of a single band in the lane corresponding to the mix containing the WT-specific primers indicated a wild-type genotype. Conversely, a single band in the lane with the G542X-specific reaction identified homozygous G542X mice. The simultaneous presence of both amplification products revealed heterozygous animals carry the G542X nonsense variant.

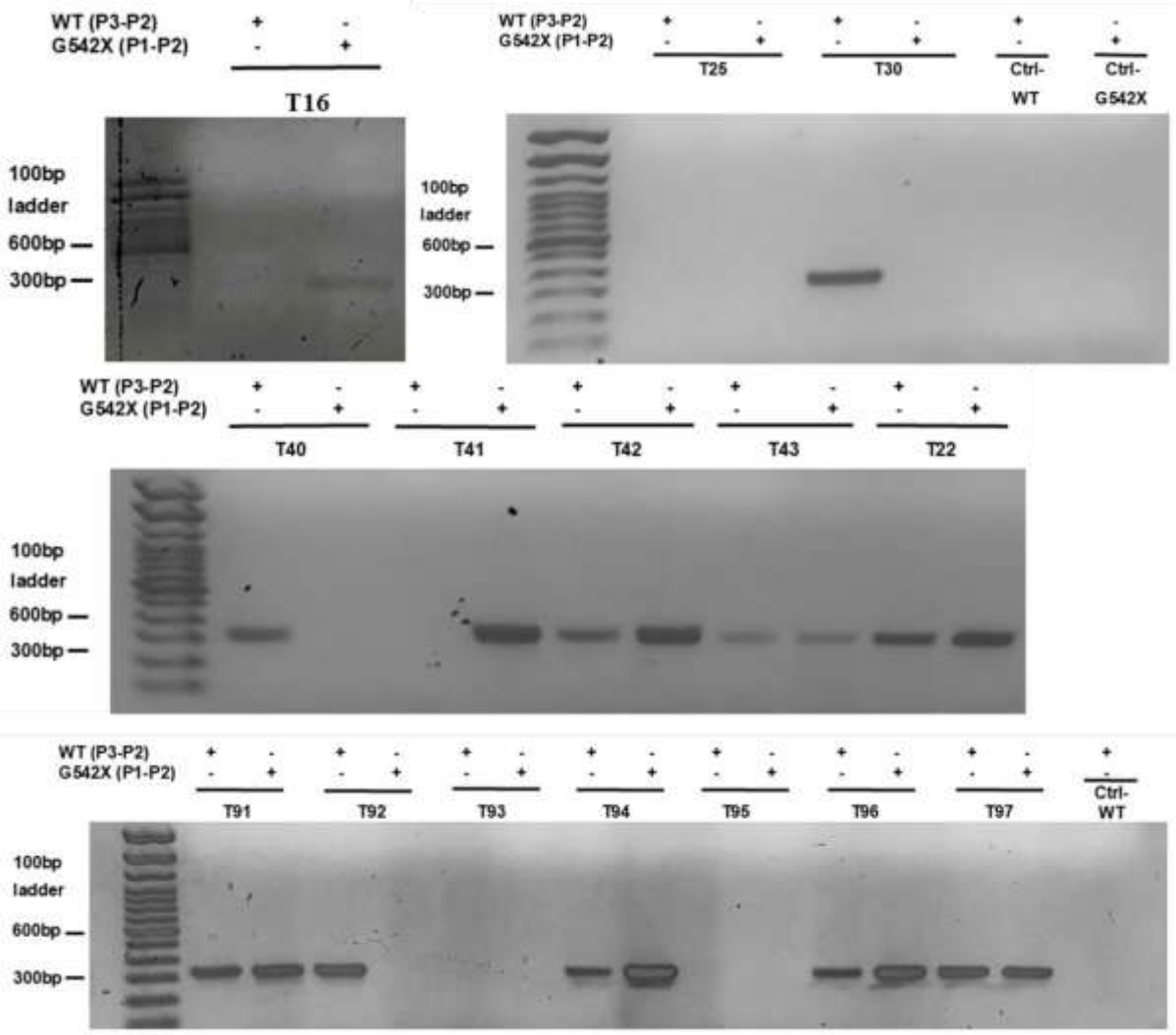
WT (P3-P2)
G542X (P1-P2)
T16
100bp
ladder
600bp
300bp
T25
T30
Ctrl-
WT
Ctrl-
G542X
T40
T41
T42
T43
T22
T91
T92
T93
T94
T95
T96
T97

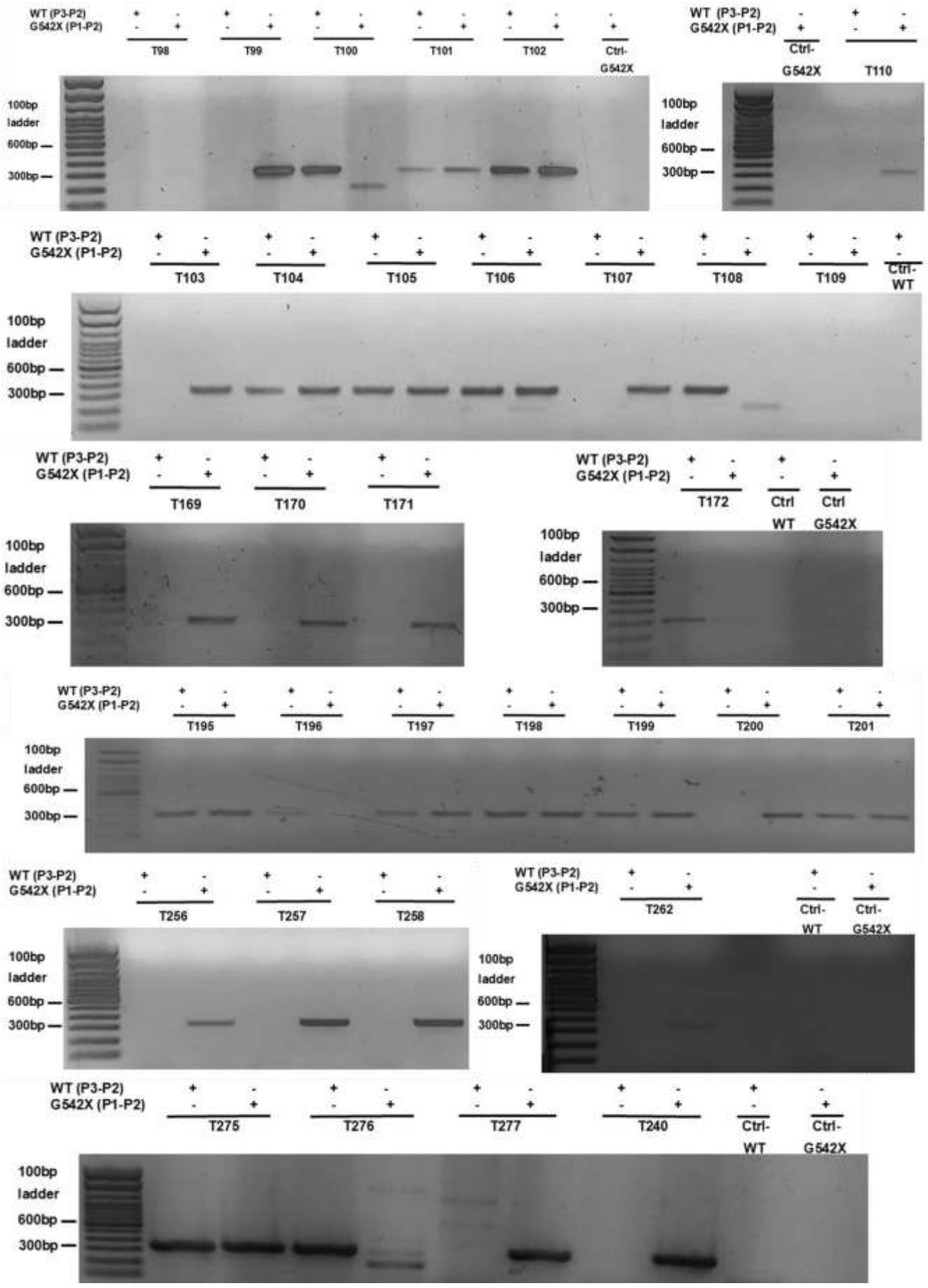
WT (P3-P2)
G542X (P1-P2)
T98
T99
T100
T101
T102
Ctrl-G542X
100bp ladder
600bp
300bp
WT (P3-P2)
G542X (P1-P2)
Ctrl-G542X
T110
100bp ladder
600bp
300bp
WT (P3-P2)
G542X (P1-P2)
T103
T104
T105
T106
T107
T108
T109
Ctrl-WT
100bp ladder
600bp
300bp
WT (P3-P2)
G542X (P1-P2)
T169
T170
T171
100bp ladder
600bp
300bp
WT (P3-P2)
G542X (P1-P2)
T172
Ctrl WT
Ctrl G542X
100bp ladder
600bp
300bp
WT (P3-P2)
G542X (P1-P2)
T195
T196
T197
T198
T199
T200
T201
100bp ladder
600bp
300bp
WT (P3-P2)
G542X (P1-P2)
T256
T257
T258
100bp ladder
600bp
300bp
WT (P3-P2)
G542X (P1-P2)
T262
Ctrl-WT
Ctrl-G542X
100bp ladder
600bp
300bp
WT (P3-P2)
G542X (P1-P2)
T275
T276
T277
T240
Ctrl-WT
Ctrl-G542X
100bp ladder
600bp
300bp

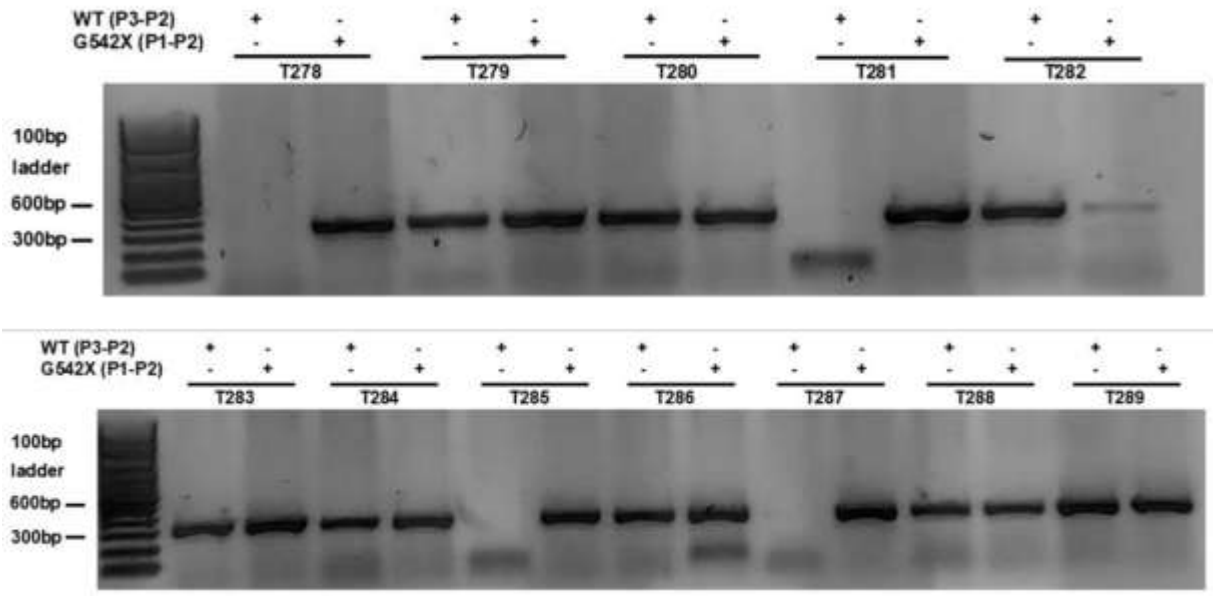

Figure 22. PCR-based genotyping: *the CFTR WT or CFTR G542X genotype is indicated by the single band in the respective line, while the presence of two bands indicates the heterozygous ones.*

The complete results of this analysis are reported in **Table 4,** and the sequencing analyses that confirmed this result are reported in supplementary **Figure S1-2**.

GENOTYPE	**N. MICE**
$CFTR^{WT/WT}$	39
$CFTR^{WT/G542X}$	92
$CFTR^{G542X/G542X}$	28

Table 4. Identified genotypes.

The **Figure 23** shows a homozygous mutant mouse carrying the G542X mutation (left), compared with a wild-type mouse (right); both are male and of the same age. In particular, the homozygous mouse carrying the mutation appears smaller, which is also reflected in the typically lower body weight observed in these animals.

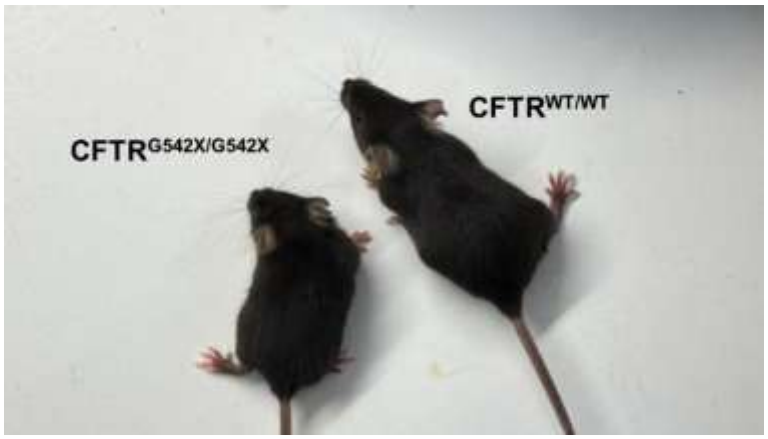

Figure 23. Homozygous CFTR$^{G542X/G542X}$ and CFTR$^{WT/WT}$ mice phenotype.

5.1.2 CFTR protein rescue after 15 days of NV914 and NV930 chronic administration in G542X nonsense mouse model

To evaluate whether chronic daily administration could promote *in vivo* the rescue of CFTR protein expression, CFTR$^{G542X/G542X}$ mice, received a daily dose of 60 mg/kg of NV914 or NV930 for 15 consecutive days as shown in the experimental timeline in **Figure 24**.

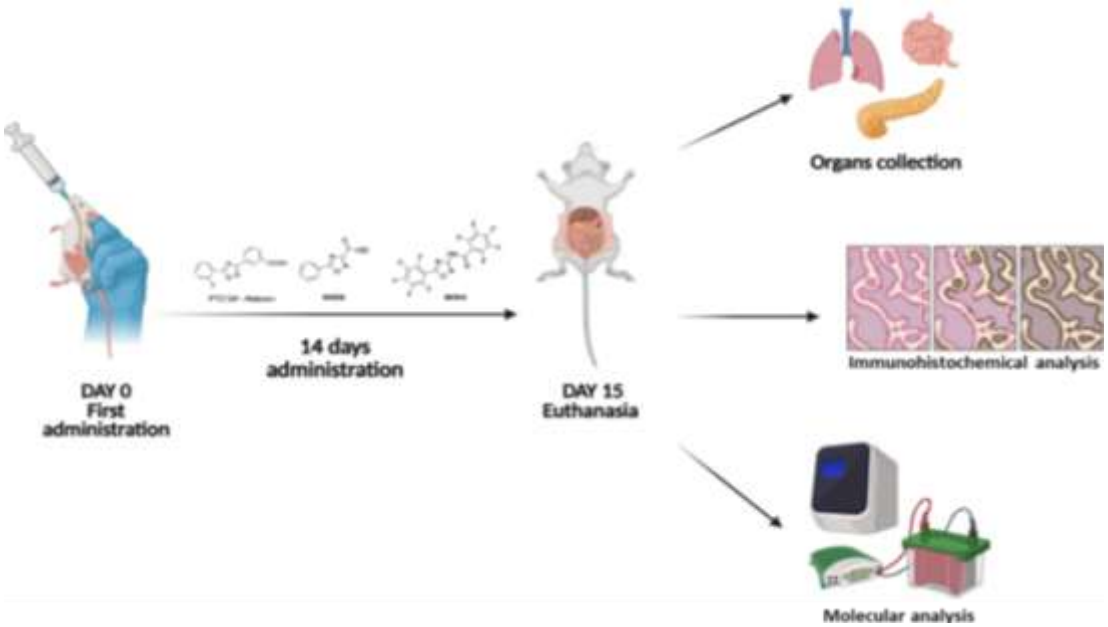

Figure 24. Study design for CFTR rescue in homozygous CFTR$^{G542X/G542X}$ mice.

Each compound (NV914, NV930) was administered once per day to assess its long-term efficacy and tolerability in 4 mice per condition. While 3 mice were treated with PTC124 as positive control, and olive oil with DMSO or water were used as negative control (**Table 5**).

ID number	*Genotype*	*Administration*
T40	$CFTR^{WT/WT}$	*Vehicle*
T246	$CFTR^{WT/WT}$	*Vehicle*
T247	$CFTR^{WT/WT}$	*Vehicle*
T248	$CFTR^{WT/WT}$	*Vehicle*
T250	$CFTR^{WT/WT}$	*Vehicle*
T254	$CFTR^{WT/WT}$	*Vehicle*
T16	$CFTR^{G542X/G542X}$	*Vehicle*
T287	$CFTR^{G542X/G542X}$	*Vehicle*
T41	$CFTR^{G542X/G542X}$	*Vehicle*
T58	$CFTR^{G542X/G542X}$	*Vehicle*
T194	$CFTR^{G542X/G542X}$	*Vehicle*
T238	$CFTR^{G542X/G542X}$	*Vehicle*
T169	$CFTR^{G542X/G542X}$	*PTC124 60 mg/Kg*
T171	$CFTR^{G542X/G542X}$	*PTC124 60 mg/Kg*
T200	$CFTR^{G542X/G542X}$	*PTC124 60 mg/Kg*
T99	$CFTR^{G542X/G542X}$	*NV914 60 mg/Kg*
T103	$CFTR^{G542X/G542X}$	*NV914 60 mg/Kg*
T107	$CFTR^{G542X/G542X}$	*NV914 60 mg/Kg*
T219	$CFTR^{G542X/G542X}$	*NV914 60 mg/Kg*
T256	$CFTR^{G542X/G542X}$	*NV930 60 mg/Kg*
T257	$CFTR^{G542X/G542X}$	*NV930 60 mg/Kg*
T258	$CFTR^{G542X/G542X}$	*NV930 60 mg/Kg*
T262	$CFTR^{G542X/G542X}$	*NV930 60 mg/Kg*

Table 5. Experimental mice included in molecular studies: *the table shows all the mice involved in experimental procedures that were used for the molecular analyses.*

During the period of treatment, the body weight was measured daily. The body weight variation is reported in **Figure 25,** presented as the mean of absolute values (grams). The graph shows that, across all 21 mice treated with different molecules and vehicle, there is no toxicity or statistically significant change in body weight.

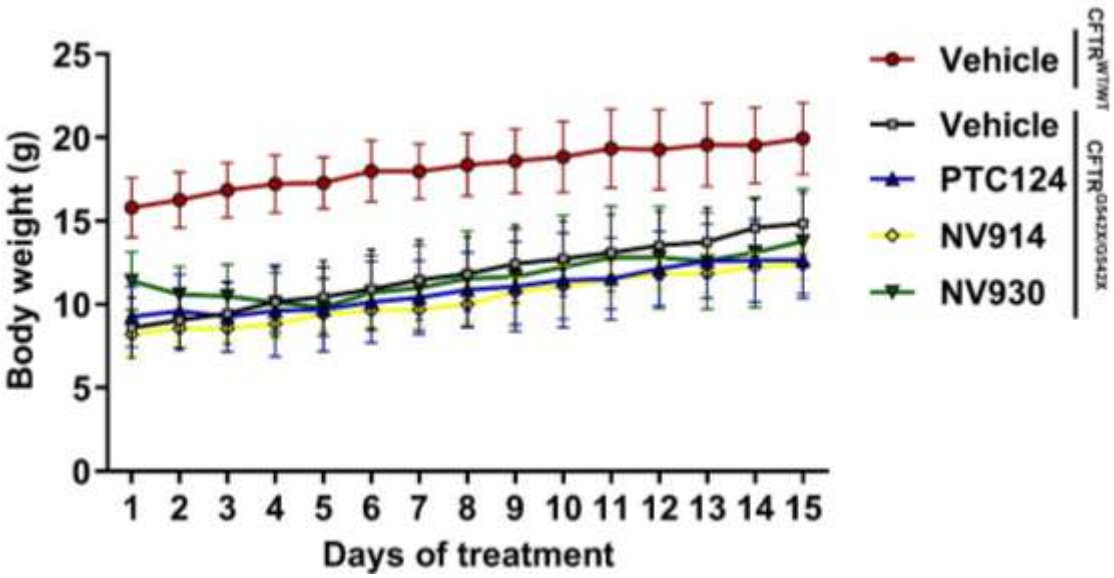

Figure 25. Body weight graph: *each line represents the mean value for each day of treatment of the 5 WT and G542X mice, 4 mice for NV914 and NV930 treated-mice, and 3 mice for PTC124 treated mice; the positive control is represented by the group of WT mice treated with the vehicle (H_2O), while the negative control is represented by the group of homozygous G542X nonsense mutation treated with the vehicle (H_2O).*

To evaluate CFTR mRNA and protein expression in the lung tissue after NV914 and NV930 molecule administration, four $CFTR^{G542X/G542X}$ mice treated with each molecule were analysed. Two homozygous mice for the G542X nonsense variant have been used as negative controls, and one WT mouse as positive control. Lastly, 3 homozygous $CFTR^{G542X/G542X}$ mice treated with PTC124 (Ataluren) were used as a positive control for the treatment. Real-time RT-PCR and Western-blots were performed to assess mRNA and protein expression. As shown in **Figure 26**, Real-time RT-PCR analysis highlighted a low quantity of CFTR mRNA in G542X homozygous mice and about two and threefold increase of the CFTR mRNA when mice were treated with PTC124 and NV914 respectively. While in the presence of the treatment with NV930, there was no significant increase of transcript.

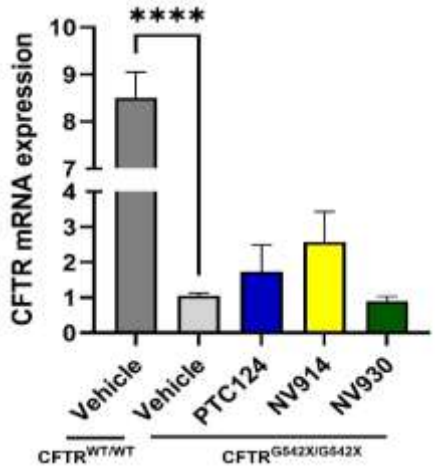

Figure 26. Gene expression analyses resulting from NVs treatment: *Real-Time RT PCR on RNAs extracted from mice lungs, mean values for each category are shown, homozygous G542X mice untreated and treated with PTC124, NV914, and NV930; mice were treated for 15 days with 60 mg/Kg of each compound. All the data were analyzed with GraphPad Prism 6, and a probability value (p) was calculated using a one-way ANOVA test; four symbols (****) indicate p < 0.0001.*

Western blot analysis was performed on lung protein extracts from G542X homozygous mice. The study showed a rescue of the CFTR protein in PTC124, NV914 and NV930 treated mice (**Figure 27 A-B-C**). **Figure 27** shows a mature band of CFTR in all G542X homozygous treated mice. This increase is particularly significant for the NV914 treatment (**Figure 27-D**).

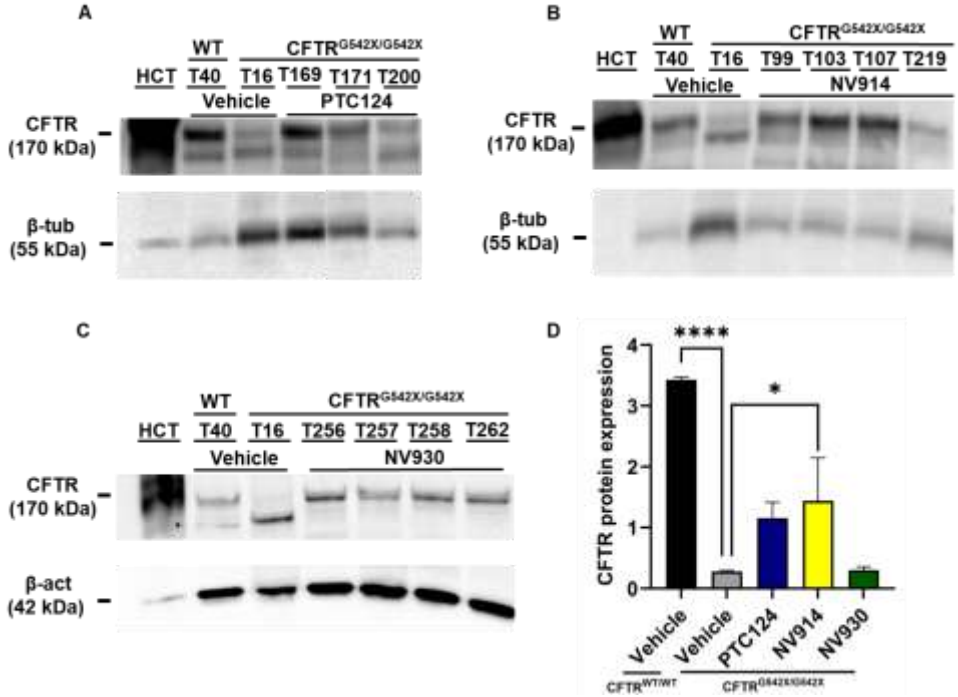

Figure 27. CFTR protein rescue results following NVs treatment: *(**A-B-C**) Western blot analyses were presented as gels for each treatment: PTC124 (**A**), NV914(**B**), and NV930 (**C**. T40 is a positive control represented by a WT mouse, while T16 is represented by an untreated homozygous G542X mouse; **D**) Quantification of band mean value, using ImageJ.*

For the NV914-treated mice, immunohistochemical analyses were also performed. Specifically, all lung samples were collected in 4% formaldehyde and subsequently processed in collaboration with the Belmonte group at the Tumor Immunology Unit, Department of Health Sciences, University of Palermo. The analyses suggested a recovery of CFTR protein expression in lung tissue, as indicated by the positive CFTR staining observed in the NV914 treated $CFTR^{G542X/G542X}$ (T107) mouse, shown in **Figure 28** (representative example). Moreover, it was observed that the epithelium in the pulmonary ducts of the NV914 treated $CFTR^{G542X/G542X}$ mice appears compact and uniform similarly to the positive control samples $CFTR^{WT/WT}$ and $CFTR^{WT/G542X}$ and respect to the $CFTR^{G542X/G542X}$ negative control.

This finding provides further confirmation of the functional restoration of CFTR *in vivo* following NV914 treatment, supporting the molecular data.

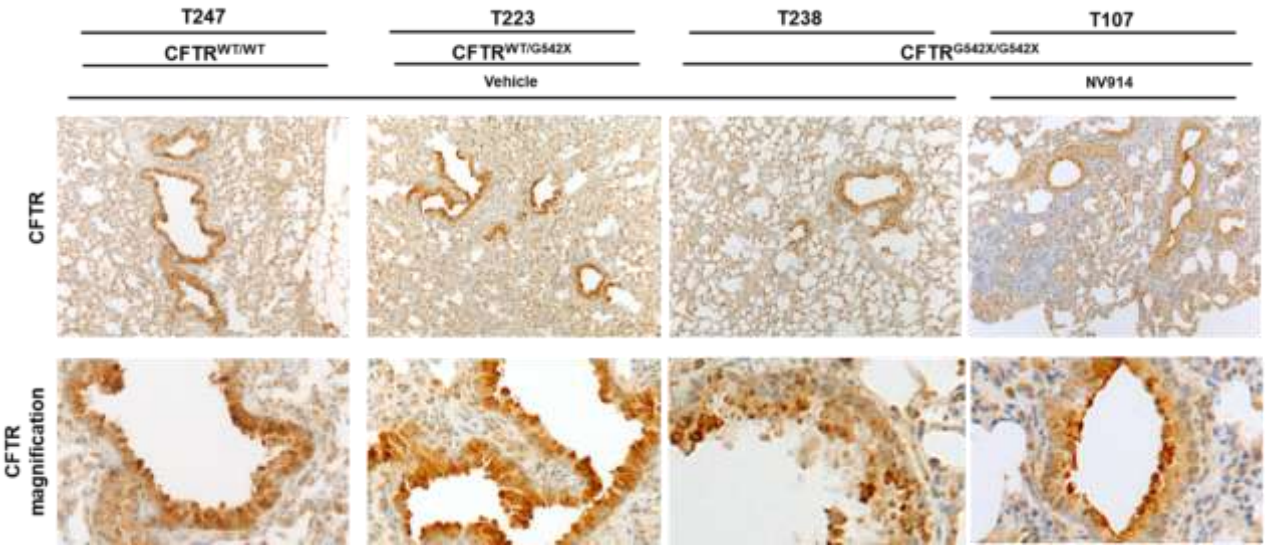

Figure 28. Immunohistochemical analysis on NV914-treated mice: *The rabbit polyclonal anti-CFTR antibody (ACL-006, Alomone Labs) was used for CFTR IHC staining. IgG (H&L)-specific secondary antibodies and DAB (3,3'-diaminobenzidine) as the substrate chromogen were used. Nuclei were counterstained with Mayer's hematoxylin. Slides were analyzed under a Zeiss Axioscope.*

Objective 2

5.2 Assessment of REP1 protein rescue following NV848, NV914 and NV930 treatment on different *in vitro* nonsense Choroideremia cell model systems

5.2.1 Generation of a stable Choroideremia cell model system to evaluate the rescue of the expression of the REP1-tGFP protein following NVs molecule treatment.

The first goal of this second objective was to evaluate the rescue of the REP1-tGFP protein in an engineered Choroideremia nonsense model following treatment with NV compounds promoting translational readthrough. To this end, the initial step was the development of an in vitro model system carrying, separately, two of the most common nonsense variants in the CHM gene (cDNA), R253X and R293X. To generate these variants, the pRG213610 CHM^{WT}-tGFP vector was used as a template for site-directed mutagenesis. In the pRG213610 CHM^{WT}-tGFP plasmid, the CHM cDNA, under the CMV promoter control, is fused in-frame with the coding sequence of turbo Green Fluorescent Protein (tGFP), enabling visualization of the CHM-tGFP fusion protein through fluorescence microscopy. Specifically, the c.757C>T (R253X) and c.877C>T (R293X) nonsense mutations were inserted into the CHM coding region via site-directed mutagenesis (**Figure 29**), as detailed in the Materials and Methods section. In both instances, the wild-type CGA codon for arginine (R253 or R293) was converted into a premature termination codon, specifically the TGA (*opal*) codon.

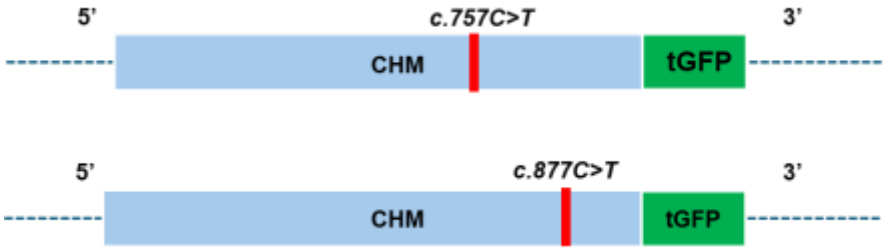

Figure 29. R253X and R293 nonsense variants insertion: *schematic representation of the nonsense mutations introduced into the CHM cDNA sequence in the pRG213610 CHM^{WT}-tGFP plasmid.*

After mutagenesis, the newly mutagenized plasmids were transformed into two separate batches of E. coli competent cells, which were then seeded onto agar petri dishes and selected with ampicillin. The presence of the mutagenized plasmids was assessed by colony PCR, performed on bacterial clones selected from the plates, and the expected 400 bp or 1,000 bp bands confirmed the presence of the CHM-tGFP vector in almost all clones from both batches (**Figure 30-A and 30-B**). Furthermore, to evaluate the correct introduction of the nonsense mutations in the plasmid CHM sequence, the amplicons, derived by colony PCR, were purified and sequenced (Sanger) by BMR Genomics. In all the evaluated amplicons, the nonsense mutations R293X or R253X were confirmed.

Finally, a single clone for each introduced mutation was selected, and the plasmid DNA was purified. The identity was confirmed by Sanger sequencing by BMR Genomics (**Figure 30-C** and **30-D**).

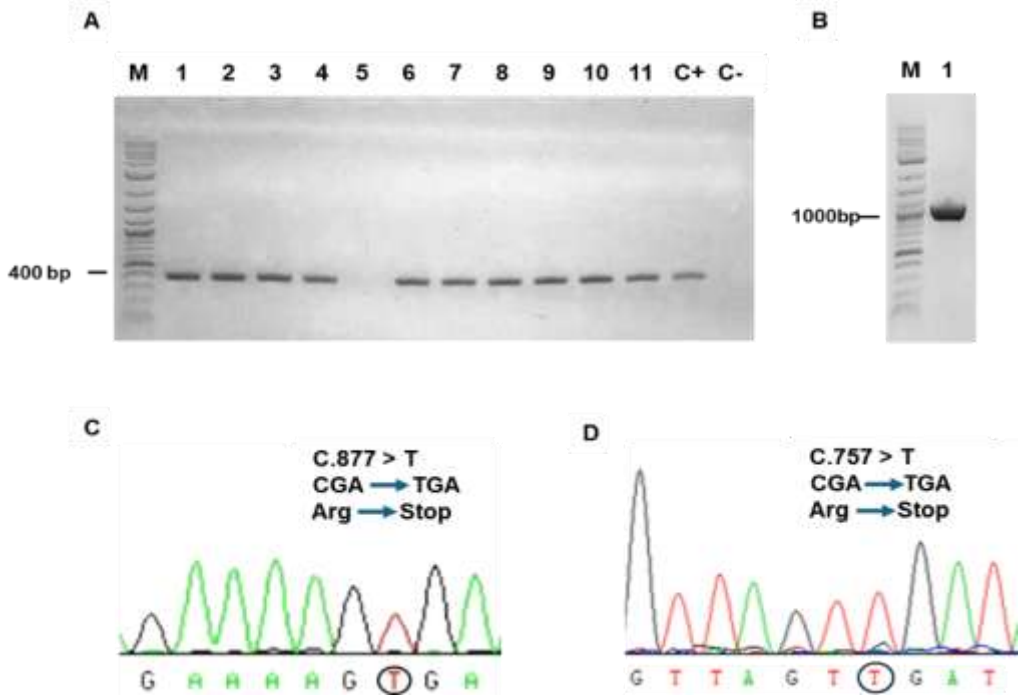

Figure 30. Validation of CHM Nonsense Mutations (R293X and R253X) by Colony PCR and Sanger Sequencing: *(**A-B**) Colony PCR assay to evaluate the presence of the pRG213610 CHM^{R293X}-tGFP (**A**) or pRG213610 CHM^{R253X}-tGFP (**B**) in bacterial cells. Each lane represents a clone; M: 2-log ladder; C+: positive control (pRG213610 CHM^{WT}-tGFP); C-: No Template control. (**C-D**) The substitutions c.877C>T (R293X) (**C**) or c.757C>T (R253X) (**D**) in CHM cDNA were evaluated by Sanger sequencing and are presented as chromatograms.*

5.2.2 Engineering stable cell populations harboring the R253X (c.757C>T) and R293X (c.877C>T) nonsense variants within the pRG213610 CHM^{WT}-tGFP.

The H1299 pCHM^{R253X}-tGFP or pCHM^{R293X}-tGFP were generated by the transfection of the mutagenized vectors to produce two stable cell lines (as described in Materials and Methods). To evaluate the expression of REP1-tGFP protein in the cells, 24 hours post-transfection, tGFP fluorescence was assessed by the Zeiss Axios fluorescence microscope (**Figure 31**). As expected, a bright fluorescence was observed in CHM^{WT}-tGFP transfected cells, while CHM^{R253X}-tGFP or CHM^{R293X}-tGFP did not show any fluorescence.

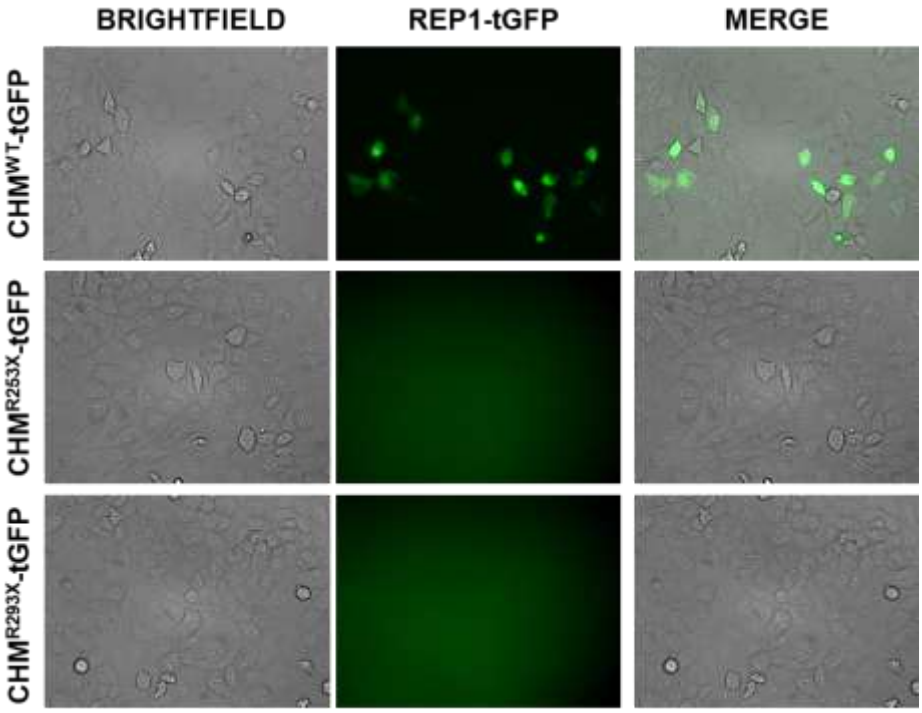

Figure 31. tGFP fluorescence emission after 24 hours post-transfection: *the panel shows tGFP fluorescence 24 hours post-transfection in H1299 cells transfected with pCHM^{WT}-tGFP, while the H1299 cells transfected with mutagenized plasmids do not show tGFP expression.*

Cells were selected with G418 (600 µg/mL) for 15 days, and genomic DNA and total mRNA were subsequently extracted to evaluate integration and expression of the constructs, respectively.

In detail, a PCR analysis on genomic DNA was performed by specific primers (detailed in material and methods, **table 2**) these primers recognize two specific plasmid region, the forward one anneals on CHM sequence, while the reverse one on the tGFP region, both amplifying a region of 2049 bp. As expected, the results confirmed the integration of the three vectors into the genomic DNA of H1299 transfected cells, as indicated by the presence of a 2049 bp band (**Figure 32-A**). To further evaluate the expression of the specific cDNAs the CHM-tGFP mRNA expression was evaluated by Real-time qPCR. As shown in **Figure 32-B** all the three cell lines express at almost the same level the CHM-tGFP mRNA.

Subsequently, the evaluation of REP1-tGFP protein expression was performed by a western blot analysis. As expected, H1299 CHM^{WT}-tGFP expressed REP1-tGFP protein in addition to the endogenous REP1, in contrast H1299 CHM^{R253X}-tGFP and CHM^{R293X}-tGFP cells revealed only the endogenous REP1 form (**Figure 32-C**). The result was confirmed by the tGFP fluorescence emission revealed in H1299 CHM^{WT}-tGFP cells, that is not present in cells transfected with mutagenized vectors (**Figure 32-D**). Taken together, these results demonstrated that these cells can be used as a stable cell model system of CHM R253X or R293X nonsense variants.

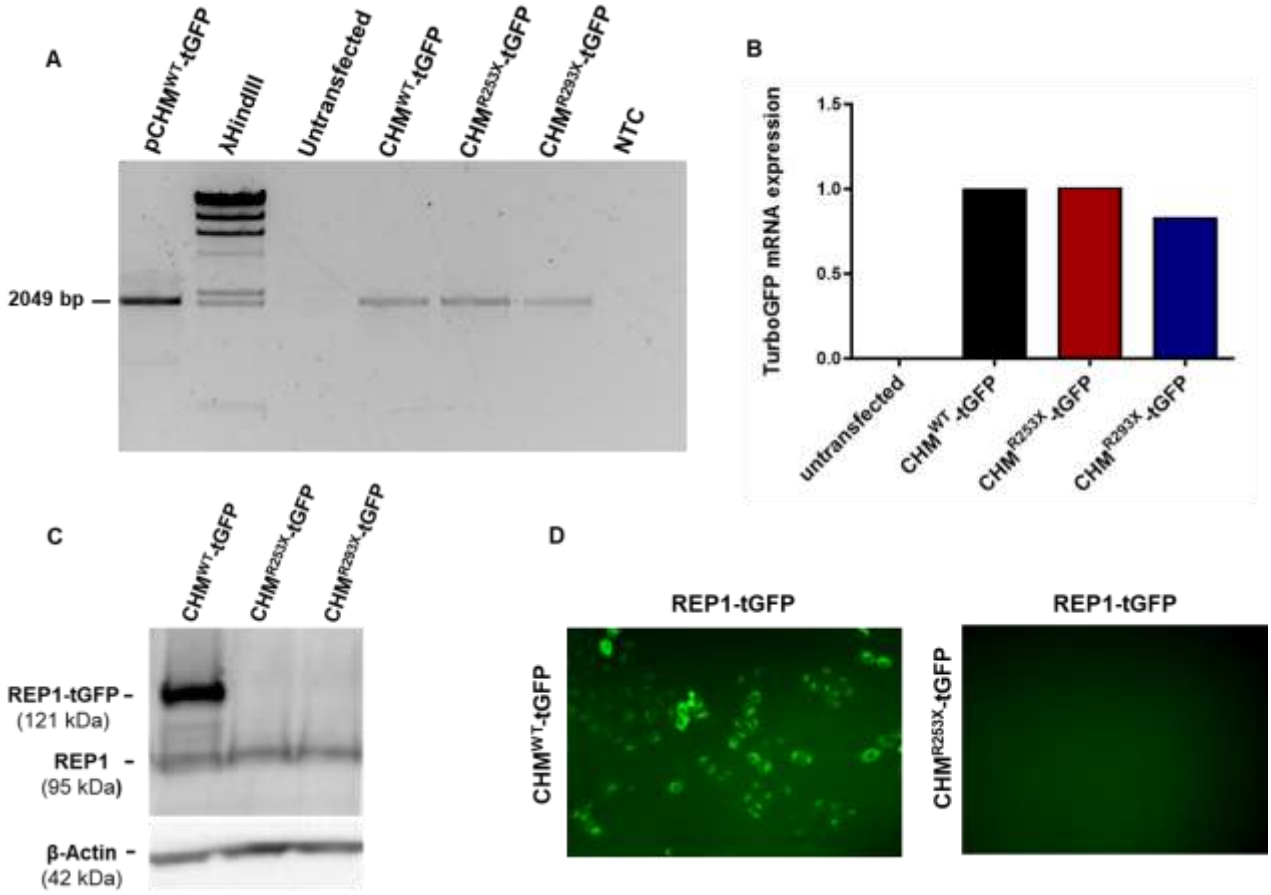

Figure 32. Production of stable H1299 CHM^{R253X}-tGFP and CHM^{R293X}-tGFP cell lines: *A) PCR analysis showing the integration of the mutagenized vector in the genomic DNA of H1299 cells. The pCHMWT-tGFP vector was used as a positive control; DNA from untransfected cells and a no-template control (NTC) were used as negative controls.* ***B****) tGFP mRNA expression assessed by Real Time RT-PCR;* ***C****) Western blot analysis on H1299 cells transfected with pCHMWT-tGFP, pCHMR253X-tGFP, or pCHMR293X-tGFP. The REP1 antibody (Santa Cruz) has been used to detect the REP1-tGFP protein (121 kDa) and the endogenous REP1 (95 kDa).* ***D****) Stable H1299 CHMWT-tGFP cells showing tGFP fluorescence.*

5.2.3 Immunofluorescence analyses reveal REP1-tGFP protein rescue in H1299 pCHM^{R253X}-tGFP and pCHM^{R293X}-tGFPcells after treatment with NV compounds.

The production of those cell model systems hosting, separately, those two nonsense variants, represent a useful tool to evaluate the rescue of REP1-tGFP protein expression and its proper subcellular localization. In particular, the H1299 CHM^{R253X}-tGFP and H1299 CHM^{R293X}-tGFP cells were used to evaluate the ability of rescue of REP1-tGFP protein by NV compounds. To investigate a potential dose-dependent readthrough activity of NV compounds and PTC124, immunofluorescence analyses were performed at concentrations of 12μM, 24 μM and 48 μM, while G418 was included as a positive control at 430 μM. As shown in **Figure 33-A** a dose-dependent increase in PTC124 concentration was associated with enhanced readthrough activity in H1299

CHM^{R253X} cell line, as well as NV914 used at 48µM (**Figure 33-C**). While a dose-dependent increase in readthrough activity was observed with increasing concentrations of NV930 in the H1299 CHM^{R293X} cell line (**Figure 34-D**), no comparable dose-dependent effect was detected for the NV compounds or for PTC124 in the other experimental conditions.

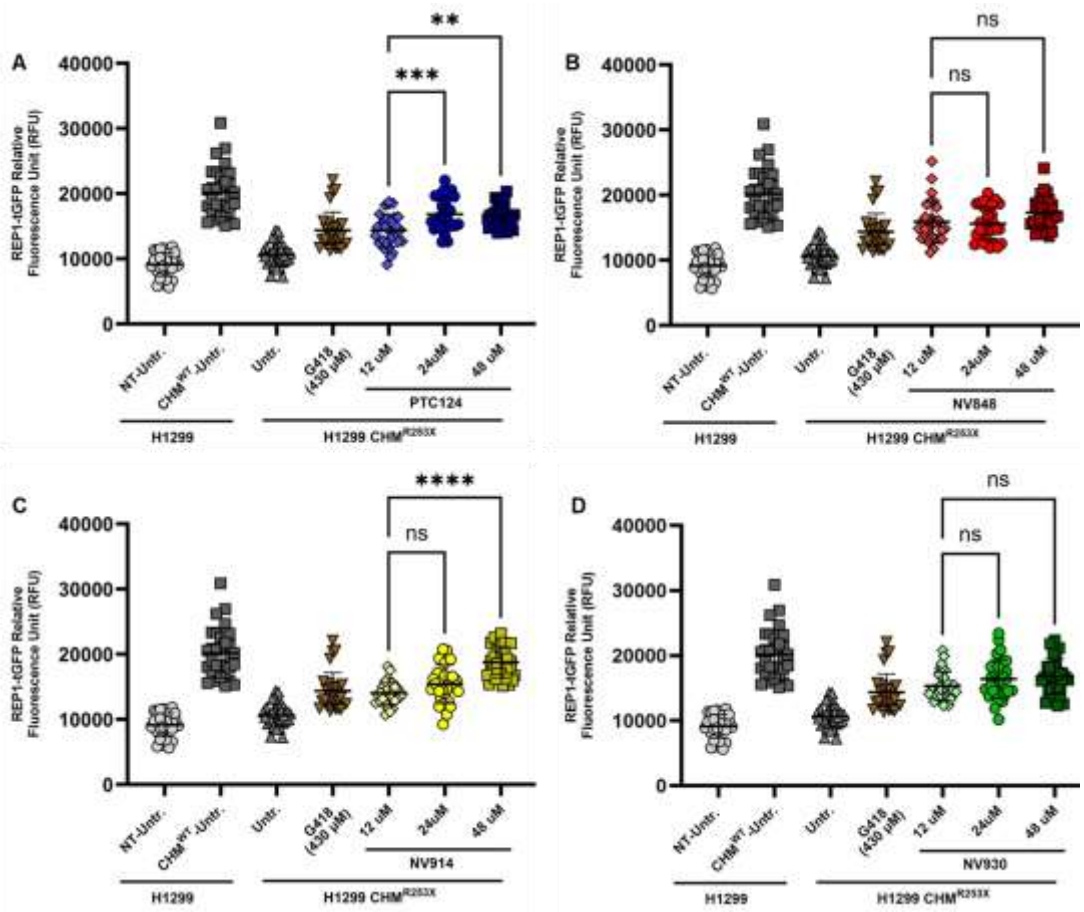

Figure 33. Immunofluorescence analysis: *Treatment were performed with PTC124 (**A**), NV848 (**B**), NV914 (**C**), and NV930 (**D**) at concentrations of 12, 24, and 48 µM in stable H1299 CHM^{R253X}-tGFP cell line. Not-transfected H1299 cells and untreated stable cell lines were used as negative controls, while G418 at 430 µM served as the positive control.*

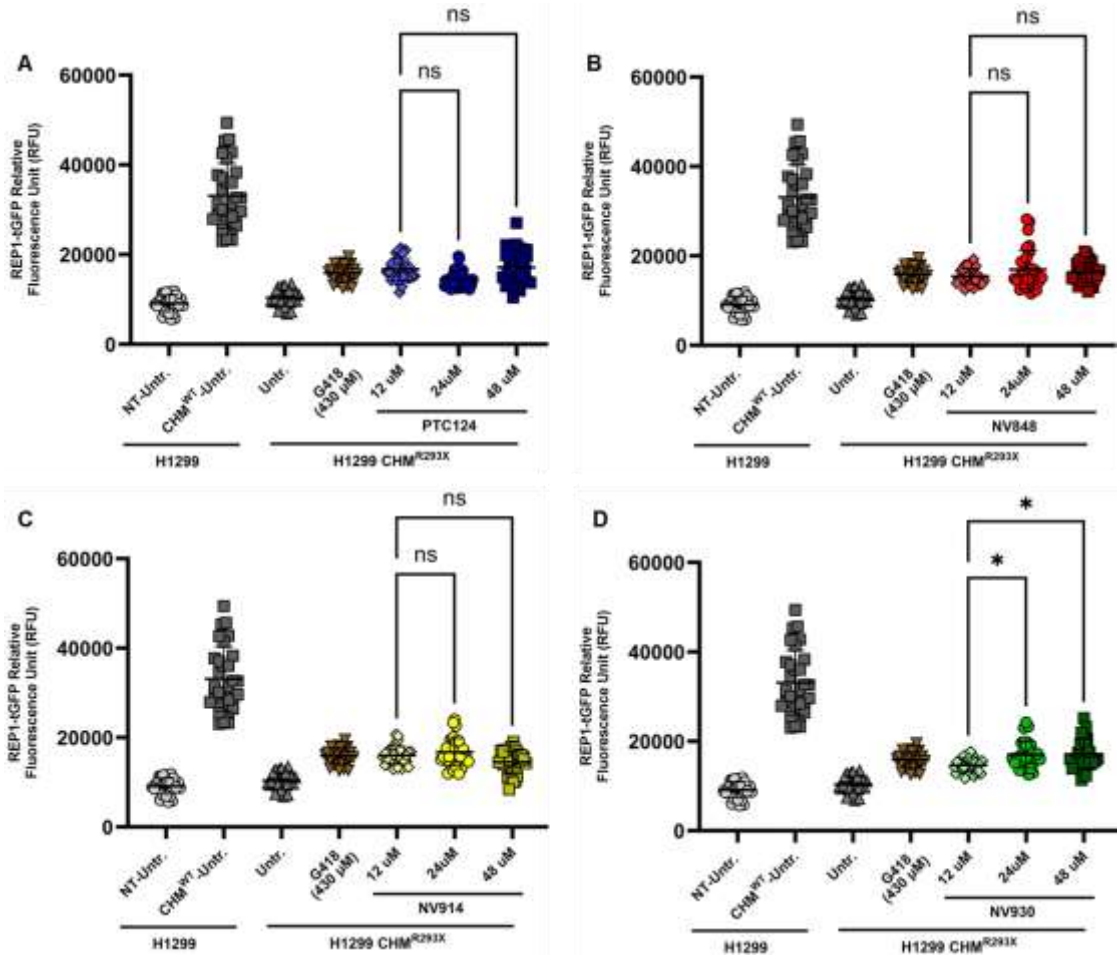

Figure 34. Immunofluorescence analysis: *Treatments were performed with PTC124 (**A**), NV848 (**B**), NV914 (**C**), and NV930 (**D**) at concentrations of 12, 24, and 48 µM in stable H1299 CHM^{R293X}-tGFP cell line. Not-transfected H1299 cells and untreated stable cell lines were used as negative controls, while G418 at 430 µM served as the positive control.*

Taken together, these results allow us to continue the experimental procedures using for all the molecules at the same concentration of 12 *µM,* as also conducted in previous studies. Thus, the same selected cell populations, designated H1299 CHM^{R253X}-tGFP and H1299 CHM^{R293X}-tGFP, were chronically treated for 72 hours with G418 (430 µM, concentration required for the readthrough) and PTC124 (12 µM), contemporary NV compounds were tested at 12 µM to evaluate REP1-tGFP protein rescue. Cells were fixed and incubated with a primary antibody against the tGFP protein. As shown in the panel NV848, NV914, and NV930 molecules can induce the readthrough of the two PTCs in the R253X (**Figure 35**) and R293X (**Figure 36**) stable cell lines, allowing the rescue of REP1-tGFP protein and its presence inside the cells (**Figure 35 A-B and 36 A-B**). Conversely, western blot analyses did not detect any detectable REP1-tGFP rescue signal (**Figure S3**).

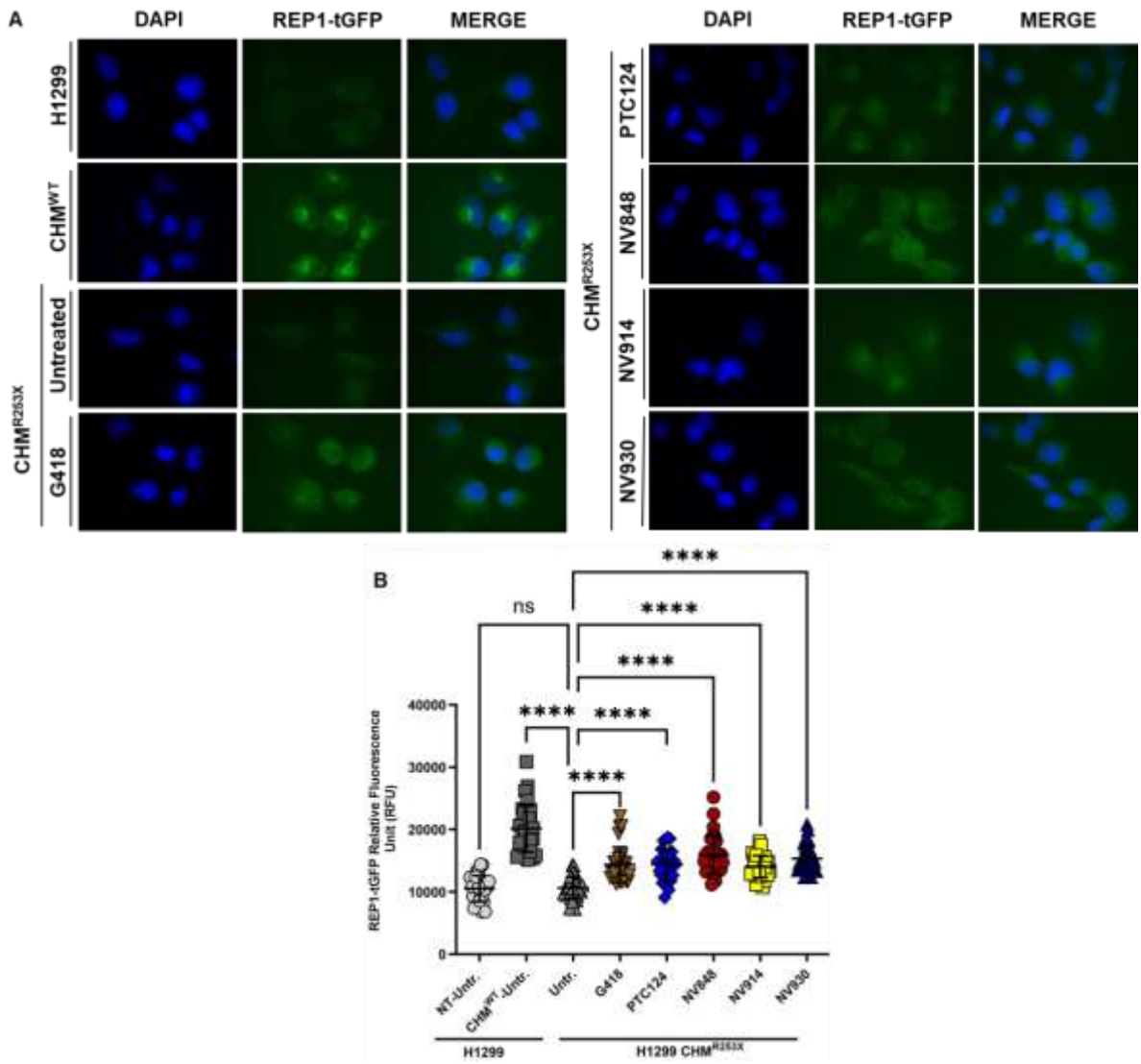

Figure 35. Panel showing immunofluorescence and quantification analyses: ***A)*** *Panels representative of immunofluorescence analyses performed on H1299 CHM^{R253X}-tGFP. H1299 not transfected untreated (NT-Untr.) and H1299 CHM^{R253X}-tGFP untreated represent the negative control, while H1299 CHM^{WT}-tGFP represents the positive control;* ***B)*** *Quantification of immunofluorescent analyses performed on H1299 CHM^{R253X}-tGFP. All the images were collected by Zeiss AxioSkope microscope at 63X. All the data were analyzed using GraphPrism6, and a probability value (p) was calculated by one-way ANOVA test statistical analysis; four asterisks (****) were used to denote $p < 0.0001$.*

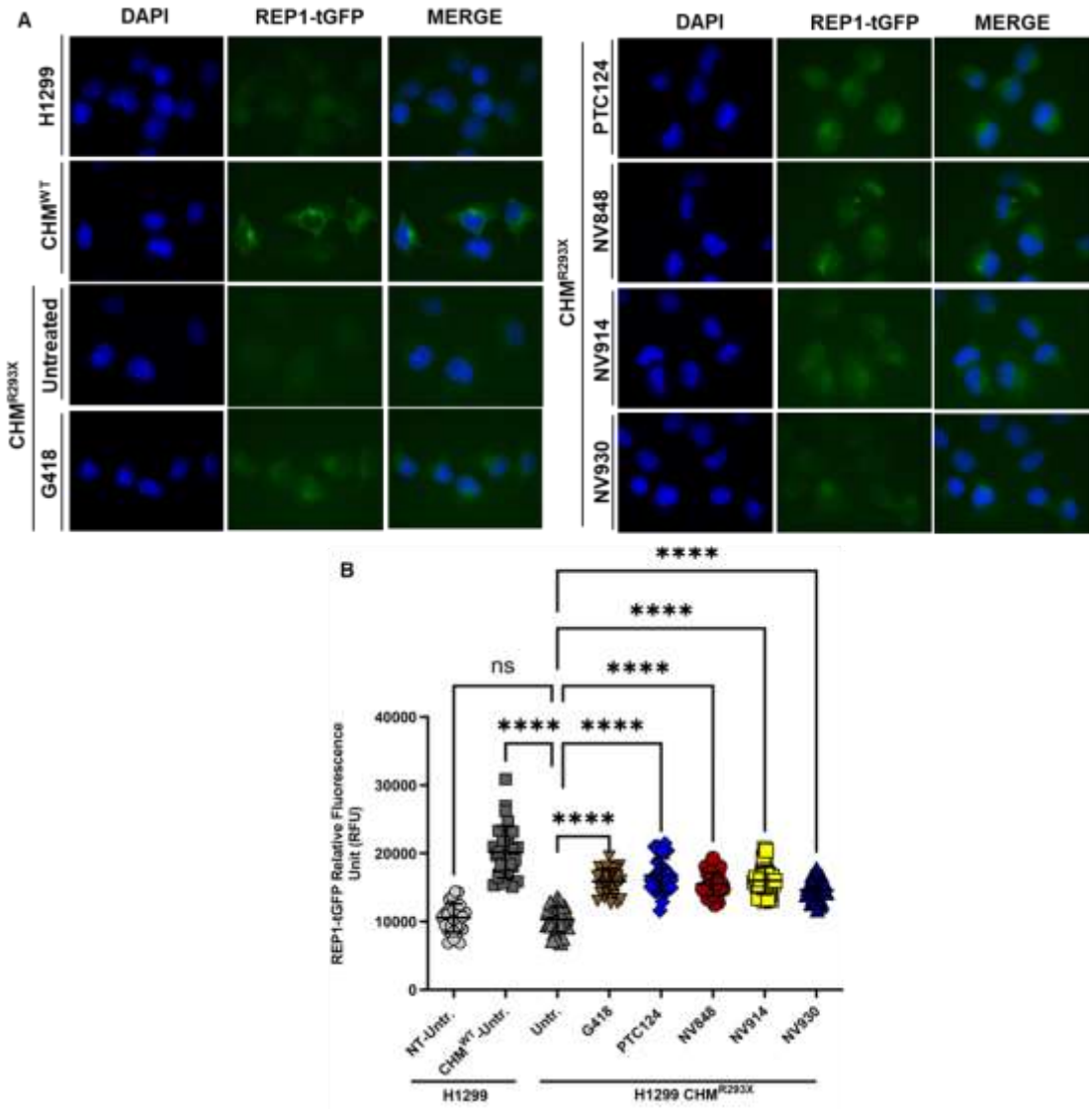

Figure 36. Panel showing immunofluorescence and quantification analyses: A) *Panels representative of immunofluorescence analyses performed on H1299 CHM^{R293X}-GFP. H1299 (NT-Untr.) and H1299 CHM^{R293X}-tGFP untreated represent the negative control, while H1299 CHM^{WT}-tGFP represents the positive control;* ***B)*** *Quantification of immunofluorescent analyses performed on H1299 CHM^{R293X}-tGFP. All the images were collected by Zeiss AxioSkope microscope at 63X. All the data were analyzed using GraphPad Prism 6, and a probability value (p) was calculated using a one-way ANOVA; four asterisks (****) were used to denote $p < 0.0001$.*

Subsequently, in order to detect the REP1-tGFP protein by Western blot analysis after the previous treatment, total proteins were extracted and analyzed. However, despite several attempts, the protein could not be detected. Nevertheless, the same experiments were then carried out using a cell line derived from choroideremia patients. I proceeded to evaluate the activity of the three compounds directly on cells derived from patients affected by Choroideremia caused by nonsense mutations. This is to obtain a preclinical model closely resembling the patient's condition.

5.2.4 Evaluation of the readthrough activity of NV molecules in vitro after 72 hours of chronic treatment in primary male patient-derived fibroblast cultures carrying the R253X, S190X and R270X nonsense variants.

Patient-derived fibroblasts harbouring R253X, S190X and R270X nonsense variants on the CHM gene were used to investigate the rescue of REP1 protein expression after treatment with NV molecules. To evaluate the *CHM* gene expression 300,000 $CHM^{R253X/y}$ or $CHM^{S190X/y}$ fibroblasts for each condition were seeded in t25 flasks and chronically treated for 72 hours with the NV compounds at 12 µM (NV848, NV914, and NV930) and PTC124 treatment at 12 µM was used as positive control. A Real-Time qPCR was performed following the treatment to evaluate the amount of the CHM mRNA in treated and untreated cells. As shown in **Figure 37-A,** all samples showed comparable levels of CHM mRNA, with a slight increase observed upon treatment with NV914 in $CHM^{R253X/y}$ fibroblasts (**Figure 37-B**).

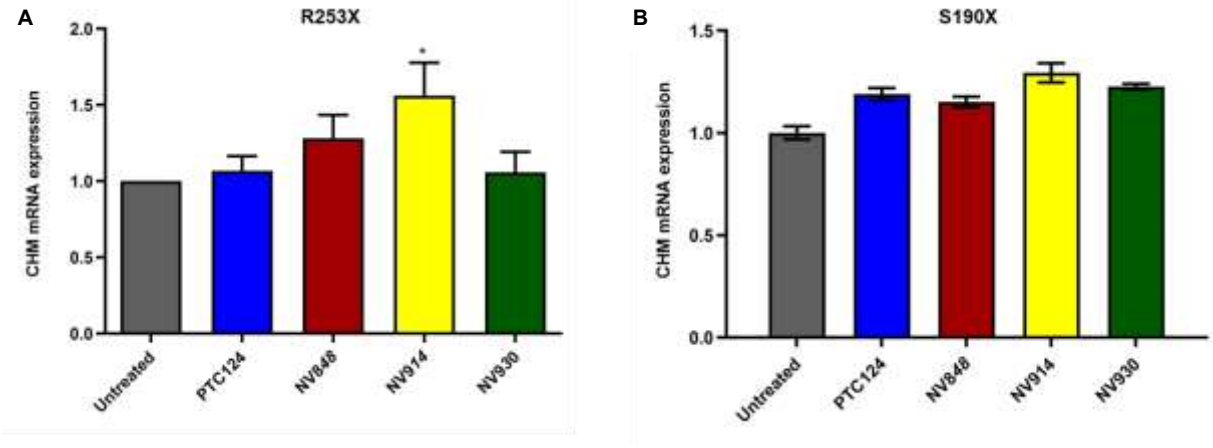

Figure 37. CHM mRNA expression in* $CHM^{R253X/y}$ *and* $CHM^{S190X/y}$ *fibroblasts following 72 hours of chronic treatment: A) *an increase in* $CHM^{R253X/y}$ *transcripts patient patient-derived fibroblast is revealed after NV914 treatment;* ***B)*** *no increase in* $CHM^{S190X/y}$ *transcripts patient patient-derived fibroblast is shown. (*) A p value <0.05 was calculated by one-way ANOVA test statistical analysis.*

5.2.5 REP1 rescue in $CHM^{R253X/y}$*,* $CHM^{S190X/y}$ *and* $CHM^{R270X/y}$ *patient-derived fibroblasts after NV molecule treatment.*

To evaluate the rescue of the REP1 protein, an immunofluorescence analysis was performed. Thus, 50,000 $CHM^{R253X/y}$, $CHM^{R270X/y}$ or $CHM^{S190X/y}$ fibroblasts for each condition were seeded and treated for 72 hours of chronic treatment with NV molecules and PTC124 at 12 µM. Cells were fixed on coverslips and incubated with a specific primary antibody for REP1 and revealed by 488-Alexa-fluor conjugated secondary antibody. The RPE cells and HCT116 were used as positive control of the REP1 expression. As shown, the NV848, NV914, and NV930 molecules induced the readthrough of the $CHM^{R253X/y}$ (**Figure 38-A**), $CHM^{S190X/y}$ (**Figure 39-A**) and $CHM^{R270X/y}$ (**Figure 40-A**)

nonsense codons in patient-derived fibroblasts similarly to the positive control PTC124 (**Figure 38-B, 39-B, 40-B**), as also highlighted by the REP1 image magnification (**Figure 38-C, 39-C, 40-C**).

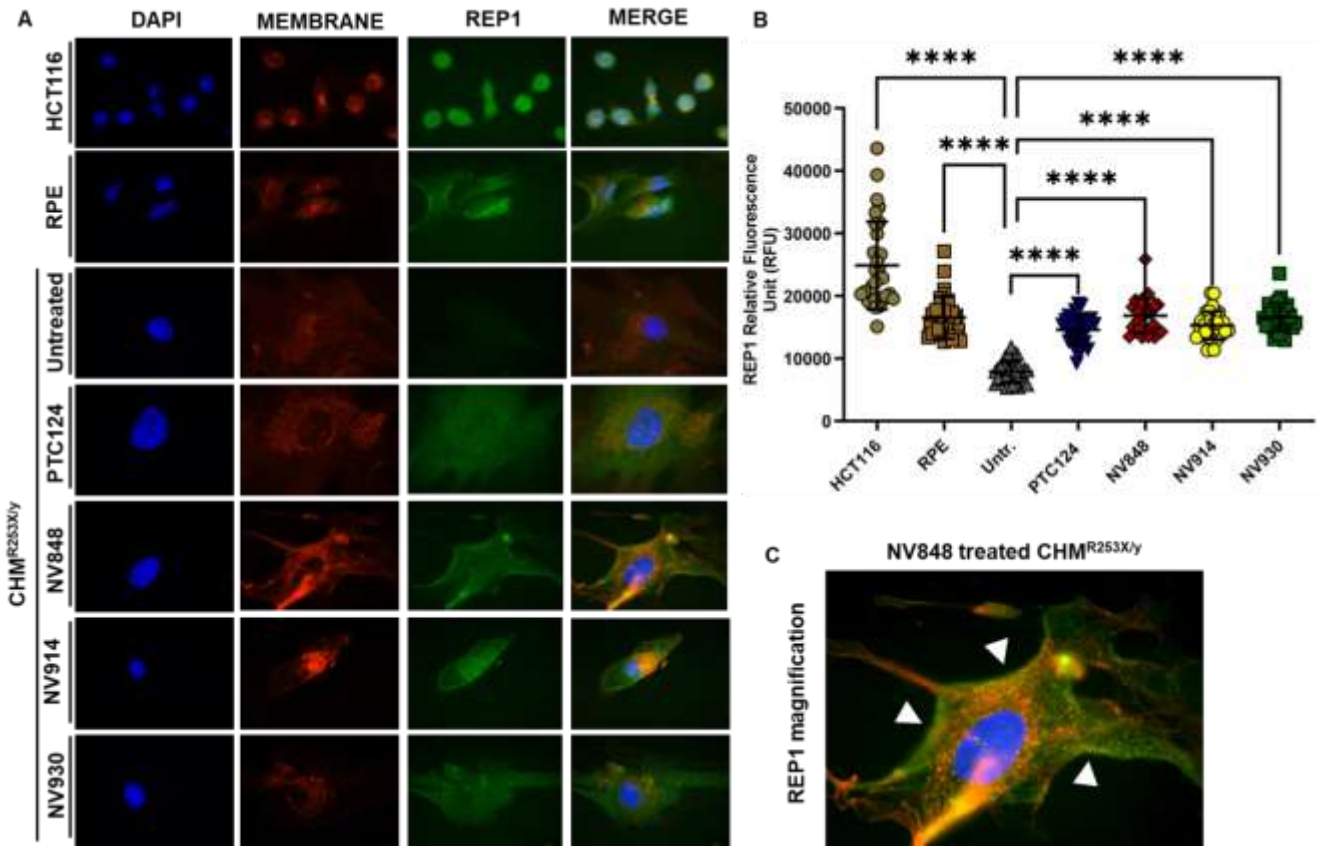

Figure 38. Immunofluorescence analyses on R253X patient-derived fibroblasts, showing the rescue of REP1 protein after 72hours at 12 µM NV molecules treatment: ***A****) REP1 protein (green) was revealed by a specific primary antibody and a fluorochrome-conjugated secondary antibody (AlexaFluor-488). Nuclei (blue) were stained with DAPI (40,6-diamidino-2-phenylindole). PTC124 was used as a positive control for PTCs readthrough.* ***B****) Images were quantified using ImageJ, and the quantifications were analyzed using GraphPad Prism 6 software. A probability value (p), four symbols (****) for p < 0.0001;* ***C****) REP1 magnification image of NV848 treated CHM$^{R253X/y}$, the experiment was performed in duplicate.*

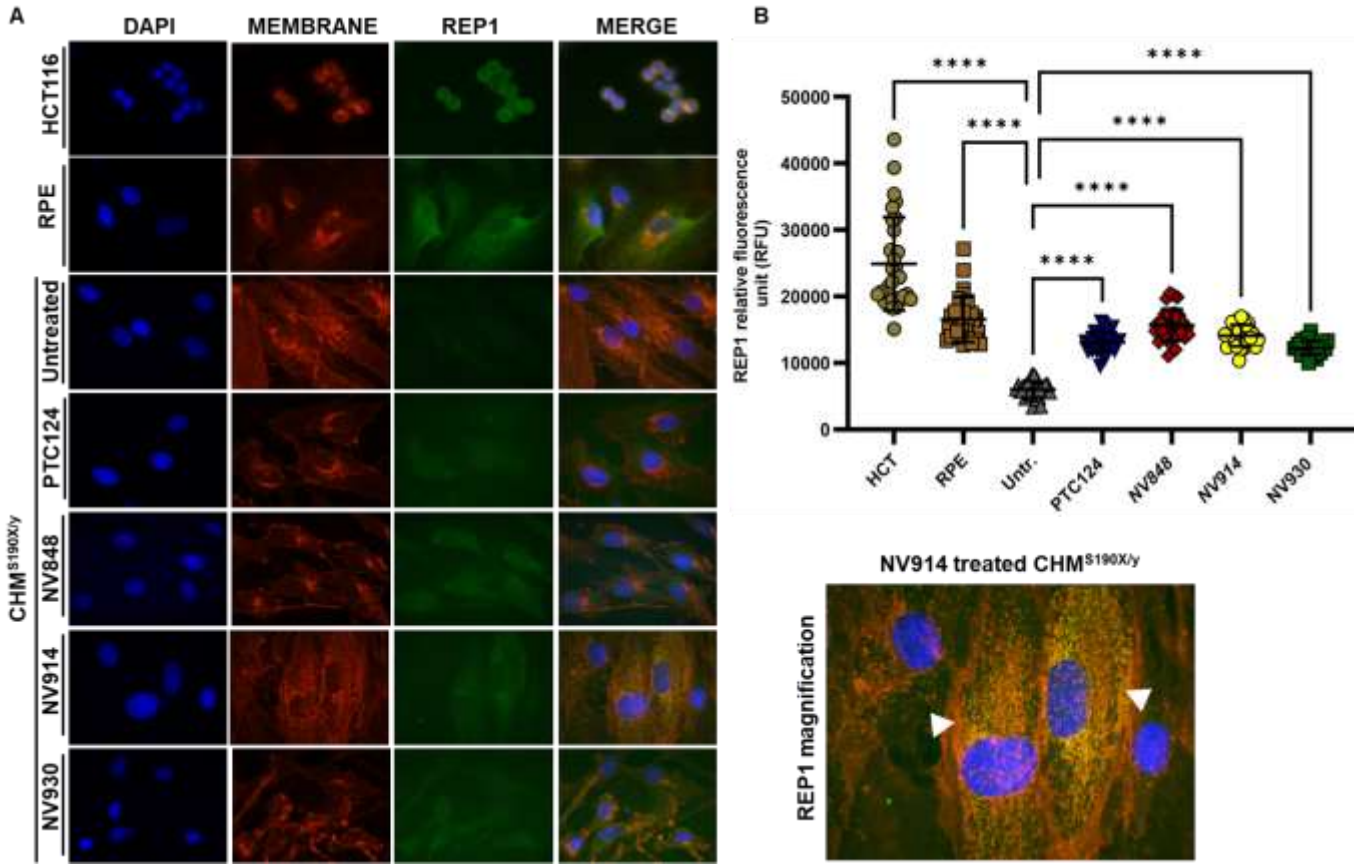

Figure 39. Immunofluorescence analyses on S190X patient-derived fibroblasts, showing the rescue of REP1 protein after 72hours of 12 µM NV molecules treatment: A) *REP1 protein (green) was revealed by a specific primary antibody and a fluorochrome-conjugated secondary antibody (AlexaFluor-488). Nuclei (blue) were stained with DAPI (40,6-diamidino-2-phenylindole). PTC124 was used as a positive control for PTCs readthrough.* ***B****) Images were quantified using ImageJ, and the quantifications were analyzed using GraphPad Prism 6 software. A probability value (p), four symbols (****) for p < 0.0001;* ***C****) REP1 magnification image of NV914 treated CHM$^{S190X/y}$, the experiment was performed in duplicate.*

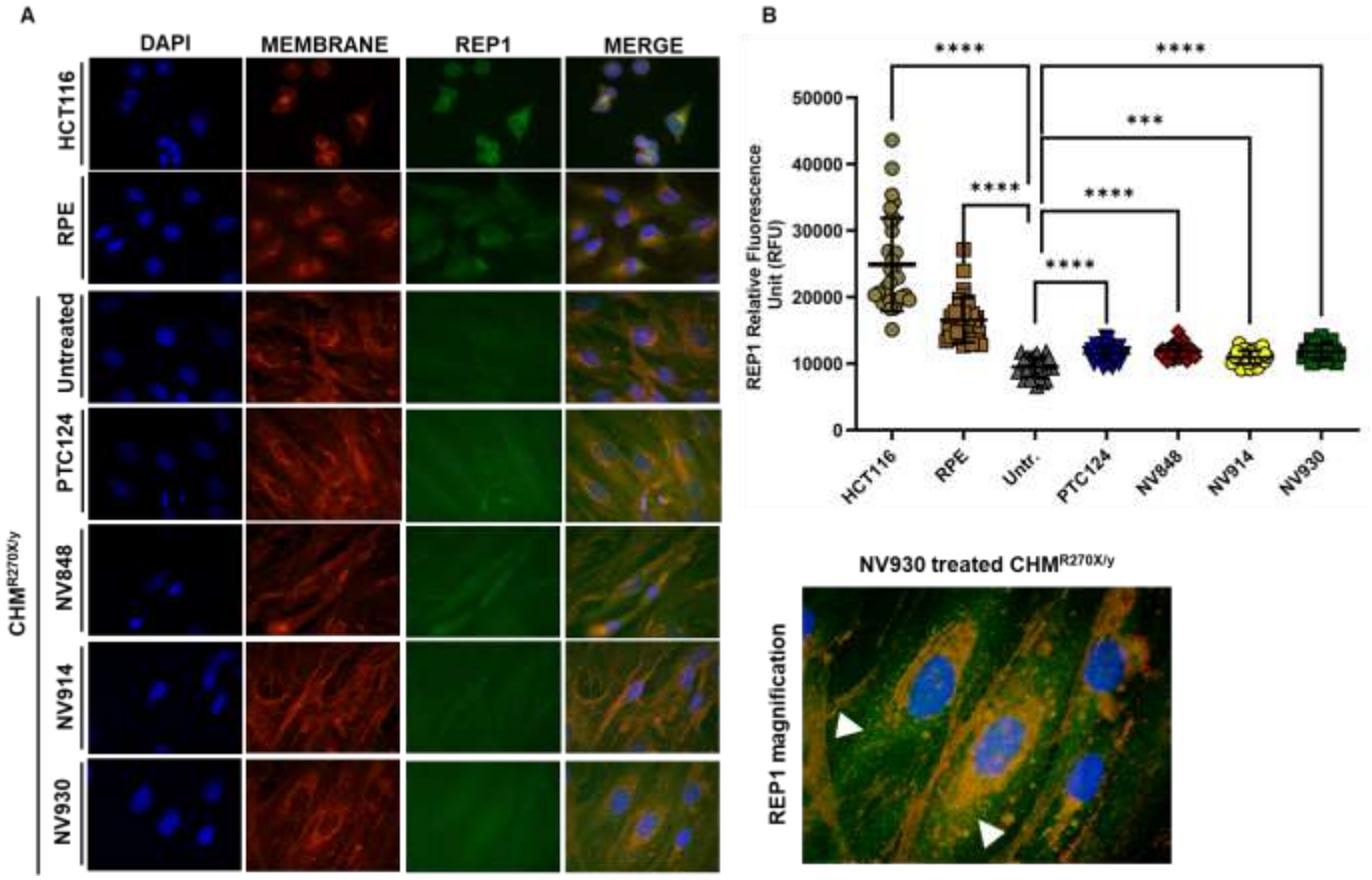

Figure 40. Immunofluorescence analyses on R270X patient-derived fibroblasts, showing the rescue of REP1 protein after 72 hours of 12 µMNV molecules treatment: *A) REP1 protein (green) was revealed by a specific primary antibody and a fluorochrome-conjugated secondary antibody (AlexaFluor-488). Nuclei (blue) were stained with DAPI (40,6-diamidino-2-phenylindole). PTC124 was used as a positive control for PTCs readthrough.* ***B)*** *Images were quantified using ImageJ, and the quantifications were analyzed using GraphPad Prism 6 software. A probability value (p), four symbols (****) for p < 0.0001;* ***C)*** *REP1 magnification image of NV930 treated CHM$^{R270X/y}$, the experiment was performed in duplicate.*

Moreover, immunofluorescence revealed a high percentage of micronucleated cells, reaching 23% in untreated CHM$^{R253X/y}$ cells (**Figure 41-A**). Interestingly, treatment of the same cell line with PTC124, NV848, NV914, and NV930 at 12 µM reduced the frequency of micronucleated cells to 12%, 10%, 15%, and 13.5%, respectively, indicating a marked decrease in micronucleation (**Figure 41-C**), as also highlighted by the picture in **Figure 41-B**.

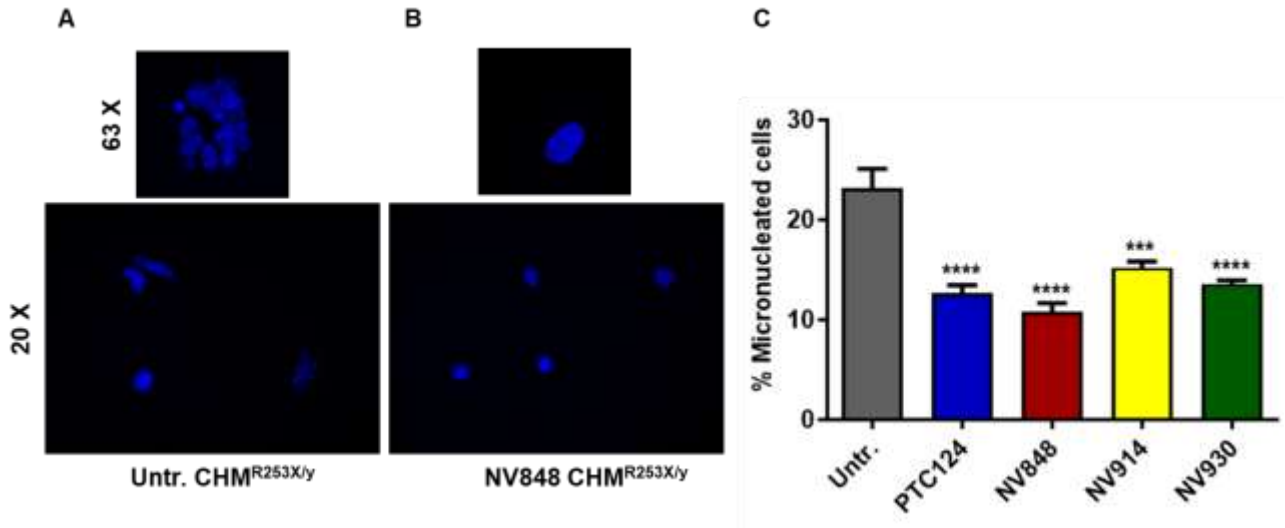

Figure 41. Micronucleated cells and their percentage in the cells: *examples of micronucleated cells present in high percentage in untreated CHM$^{R253X/y}$ (**A**) and NV848-treated CHM$^{R253X/y}$ (**B**) patient-derived fibroblasts; **C**) percentage of micronucleated cells for each condition. Data were collected using ImageJ and analyzed with GraphPad Prism 6 software, which provided a probability value (p) and four symbols (****) for p < 0.0001.*

Western blot analysis on CHM$^{R253X/y}$ and CHM$^{S190X/y}$ patient-derived fibroblasts revealed faint bands, suggesting a partial restoration of REP1 protein (**Figure 42**).

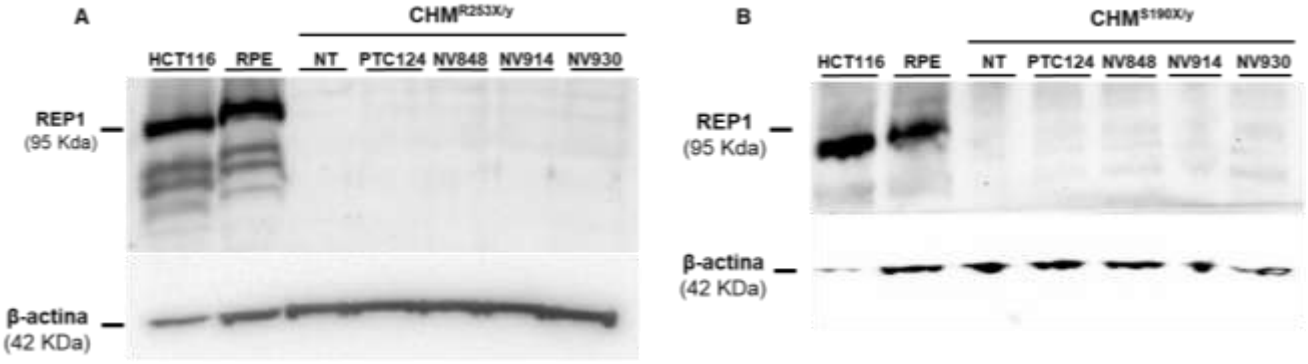

Figure 42. Protein expression analysis on R253X and S190X patient-derived fibroblasts: *western blot analyses show REP1 rescue after TRIDs treatment in CHM$^{R253X/y}$ **(A)** and CHM$^{S190X/y}$ **(B)** patient-derived fibroblasts.*

Objective 3

5.3 Investigation of the biological target of NV compounds using the PURE-LITE *in vitro* translation system

The final objective was to evaluate the biological targets of the NV848, NV914, and NV930 molecules by exploring their potential interactors. This aim was pursued using the PURE-LITE system in collaboration with the Cooperman lab. The PURE-LITE system is a reconstituted *in vitro* assay, performed outside of cells, that serves as a valuable tool to assess possible inhibitory effects of molecules on the ribosome. More importantly, it enables the investigation of their biological targets, shedding light on potential mechanisms of action involving either the release factor termination process or tRNA ribosome mispairing.

5.3.1 Ribosomal peptide elongation in the Trp-IRES PURE-LITE system is not affected by NV compounds

To study the possible biological target of the NV molecules, the PURE-LITE system has been used (Huang S. et al., 2022). In particular, the NV compounds are derivatives of PTC124, sharing its oxadiazole core. Recently, the Cooperman group demonstrated a potential mechanism of action for PTC124, whereby the compound acts by competitively inhibiting translation termination mediated by release factors. Given the structural origin of these compounds, it was therefore investigated whether they might act in a similar manner. Therefore, the three NV compounds were used to perform the same study performed by Cooperman on PTC124. This *in vitro* model system, enabling the assessment of peptide translation outside the cell, eliminating the need for initiation factors as illustrated in the Introduction section (page 20, **figure 18**).

The main components of the PURE-LITE system, and its functioning showed in **Figure 43,** are:

1. Eukaryotic 80S ribosomes constructed with variants of the cricket paralysis virus (CrPV) internal ribosome entry site (IRES) mRNA;
2. aminoacylated tRNA iso-acceptors;
3. elongation factors eEF1A and eEF2;
4. release factors eRF1 and eRF3

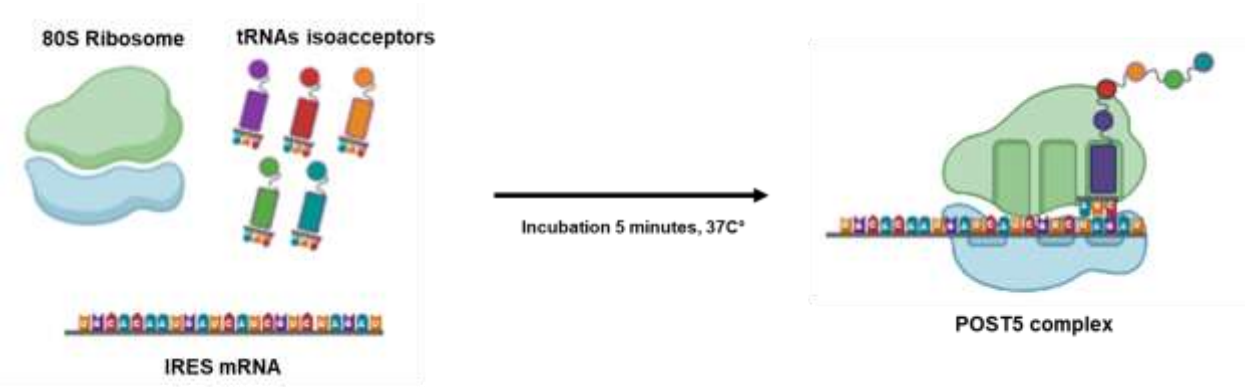

Figure 43. Pure-LITE system: the figure shows the formation process of POST5 complex.

One of the limitations of this system is related to the possible inhibitory effect on peptide elongation that some molecules may exert on it. Therefore, one of the first steps was to evaluate the potential inhibitory effect of NVs molecule on the system. Briefly, the PURE-LITE system allows the study of the translational process underlying protein synthesis. In order to perform the different analyses with the PURE-LITE system, it is always necessary to produce either POST5 or Stop-POST5 complexes, depending on the assay to be performed.

The main difference between the two lies in the use of either a wild-type Trp-IRES mRNA or a Stop-IRES mRNA, the latter containing a UGA stop codon instead of the sixth natural codon encoding tryptophan. One of these mRNAs is inserted into the eukaryotic 80S ribosome by incubation, and step by step, the first five aminoacids are incorporated by the aminoacylate tRNA isoacceptors, to produce either the POST5 or the Stop-POST5 complex. A molecule exerting an inhibitory effect on this system leads to the inhibition of the regular peptide elongation, so for this purpose, a POST5 complex, characterized by a wild-type reference sequence Trp-IRES, was chosen and used as a basis to perform a co-sedimentation assay to study normal elongation peptide. A $Trp^{[3H]}$-tRNATrp was used to check the insertion of the tRNA inside the ribosome, and so the effective and correct progression of peptide translation.

To assess the NV molecules possible inhibitory effect on peptide elongation on PURE-LITE system two different concentration points (100 and 500 μM) were used in a co-sedimentation assay. To induce the formation of the POST6 hexapeptide from the Trp-POST5 pentapeptide, eukaryotic Elongation Factor 1 alpha (eEF1α), eukaryotic Elongation Factor 2 (eEF2), and $Trp^{[3H]}$-tRNAtrp were added to the initial mixture. After incubation at 37 °C for five minutes, the samples under different conditions were centrifuged through a sucrose solution. The supernatants were discarded, and the pellets were resuspended. Radioactivity was then measured for each condition as radioactive count. A statistically lower radioactive count in the test pellet compared to the negative control (mixture without the test molecules) indicates a possible inhibitory effect on peptide elongation induced by the

molecule. As shown in **Figure 44,** no statistically significant difference in the radioactive counts, and consequently in the ratio of Hexapeptide/POST5 formation, after treatment with the three molecules can be seen in comparison with the negative control, represented by only POST5 and the elongation factors. These results indicate that NV848, NV914, and NV930 did not inhibit regular protein elongation in the sample and so did not show an inhibitory effect on peptide elongation on this *in vitro* ribosome model system.

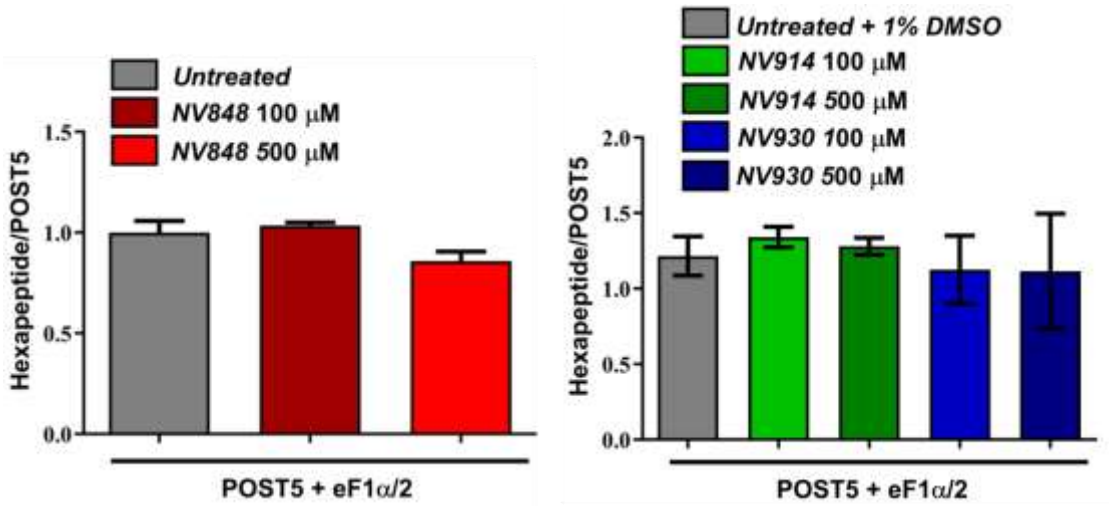

Figure 44. In the PURE-LITE system, ribosomal activity is not affected by the NV compounds: *the figure shows the evaluation of the activity of NV molecules on normal elongation peptide. Trp-POST5 mix was mixed with TC-mix containing Trp$^{[3H]}$-tRNATrp and elongation factors in the presence of NV848, NV914, and NV930 to study their activity in two different concentrations, 500 and 100 μM. A co-sedimentation assay was performed, and no* inhibitory effect on peptide elongation *was shown after the treatment on normal elongation.*

5.3.2 Readthrough is induced in the Stop-IRES PURE-LITE system by NV848, NV914, and NV930.

After the elongation assay, the following step was necessary to study the effective readthrough activity of the three compounds in this system. Specifically, the same experimental model has been used but constructed with a Stop-IRES mRNA characterized by a UGA stop codon. Therefore, a Stop-POST5 complex was produced and a Leu$^{[3H]}$-tRNA Leu was used to check if peptide translation can proceed correctly with the insertion of Leu-tRNA in the growing peptide, only if the molecules induce the readthrough of the stop codon with the occurrence of near-cognate Trp-tRNA previously. To evaluate this possibility, a co-sedimentation assay was performed in which it is possible to directly monitor the formation of a POST7 from a Stop-POST5 complex after treatments with different molecules, thanks to the evaluation of the radioactive count. A positive control with PTC124 was used. In **Figure 45,** NV848, NV914, and NV930 exhibit a three-fold change in readthrough activity at low concentrations compared to the negative control, and this is also observed with PTC124, which

confirms its readthrough activity. These results suggest that NV molecules are able not only to induce readthrough but especially to do that at low concentrations.

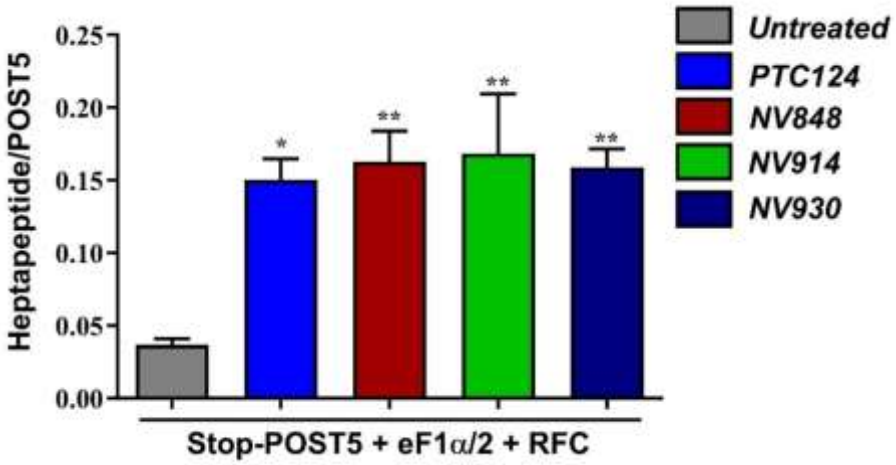

Figure 45. Evaluation of NV molecules readthrough activity on Stop-POST5: *Stop-POST5 mix was mixed with TC-mix containing* $Trp^{[3H]}$*-tRNATrp,* $Leu^{[3H]}$*-tRNALeu, elongation factors, and release factors in the presence of NV848 (12 µM), NV914 (100 µM), and NV930 (100 µM) to study their activity. A co-sedimentation assay was performed, and readthrough activity was tested in comparison with PTC124 1 mM as a positive control.* E*ach experiment* was *analyzed by GraphPad Prism 6 software. A probability value (p), two symbols (**) for* $p < 0.0084$.

5.3.3 The release factor dependent termination is not affected by NV molecules, unlike PTC124

Recently, the Cooperman group has demonstrated the mechanism of action of PTC124 to induce readthrough, showing that this drug competitively inhibits release factor-dependent termination, allowing the insertion of a near-cognate tRNA in the correspondence of the A site inside the ribosome when a PTC occurs (Huang S., et al 2022). Otherwise, the NVs molecule's biological target is still unknown. The hypothesis was that derivatives of PTC124 may show the same mechanism of action or acting on release factors. Thus, to understand in which way these molecules can act, the NV molecules activity on release factors was assessed. In particular, we investigated whether NV molecules could inhibit or influence the components of the release factor complex (RFC), as well as the release factors eRF1 and eRF3. To test this hypothesis, a co-sedimentation assay was performed, assessing not as in previous experiments the radioactive count in the previously resuspended pellets, but directly in the supernatant after centrifugation in sucrose solution. This approach allowed us to determine whether peptide release mediated by the RFC was affected following treatment with the NV molecules. A decrease in the radioactive count in the supernatant would indicate a reduced rate of peptide release, thus suggesting that the molecules might exert an inhibitory or modulatory effect on RFC activity.

The first step was to evaluate the activity of these molecules on the Release Factors Complex (RFC) in the Stop-POST5 PURE-LITE system. In particular, the standard radioactive count of the peptide was used to check the normal termination activity after a co-sedimentation assay in standard conditions and in the presence of NV molecules. As shown in **Figure 46** no statistically significant difference change in peptide radioactive count is appreciable, suggesting that peptide release and so release factors are not affected by NV compounds.

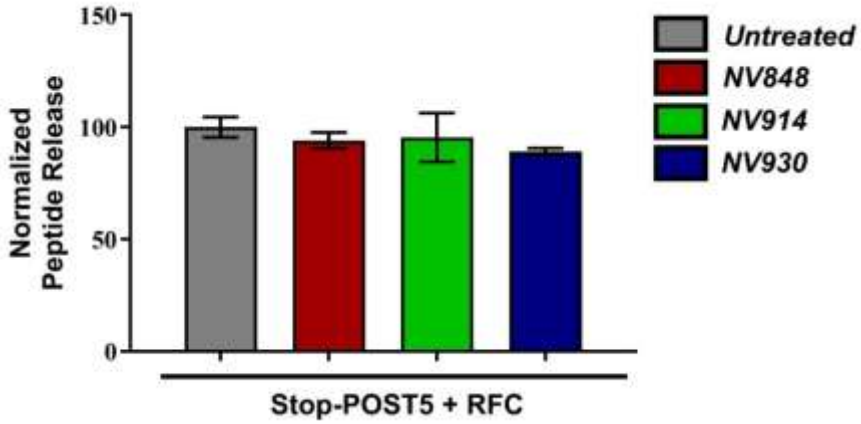

Figure 46. Evaluation of NV molecules on the Release Factor Complex: *Stop-POST5 mix was mixed with RFC-mix containing $Trp^{[3H]}$-tRNATrp, and release factors in the presence of NV848, NV914, and NV930 at 250 μM to study their activity on termination. A co-sedimentation assay was performed, and no change in peptide release was shown.*

To validate this data, the rate of peptide release over time was studied. If NV molecules act similarly to PTC124, the inhibition of release factor-dependent termination will occur. The use of the Stop-POST5 PURE-LITE system allows the evaluation of this parameter, in particular, PTC124 which binds multiple binding sites on the ribosome competitively inhibiting RFC catalysis of termination, in this way the machinery can stay more time on the ribosome and especially on PTC when it occurs, allowing the insertion of a near-cognate tRNA, and so a complete peptide translation.

To study the peptide release rate during termination a fluorescence assay based on ATTO647 was performed, this last one is a red fluorescent dye with high photostability, commonly used to label specific molecules, for instance the Trp-tRNATrp, which shows excitation and emission spectra around 646 nm and 664 nm, respectively. For this purpose, a plate reader assay was performed, using a STOP-POST5 and a $Trp^{[ATTO647]}$-tRNATrp, which is useful and essential for the evaluation of fluorescence emission. With this approach, peptide release can be measured, in particular as already shown in Cooperman's paper when PTC124 is used on this system a statistically significant decrease in the rate of peptide release occurs (Huang S., et al 2022), instead as shown in these new results

(**Figure 47**) no statistically significant difference is detectable when on the same system are used NV848, NV914, and NV930.

This suggests that NV molecules work differently from their precursor PTC124, not by inhibiting release factor-dependent termination, but similarly to aminoglycosides, affecting directly the tRNA mispairing, having no effect on termination activity, and stimulating readthrough in both the absence and presence of RFC, with the effect being greater in the absence of RFC.

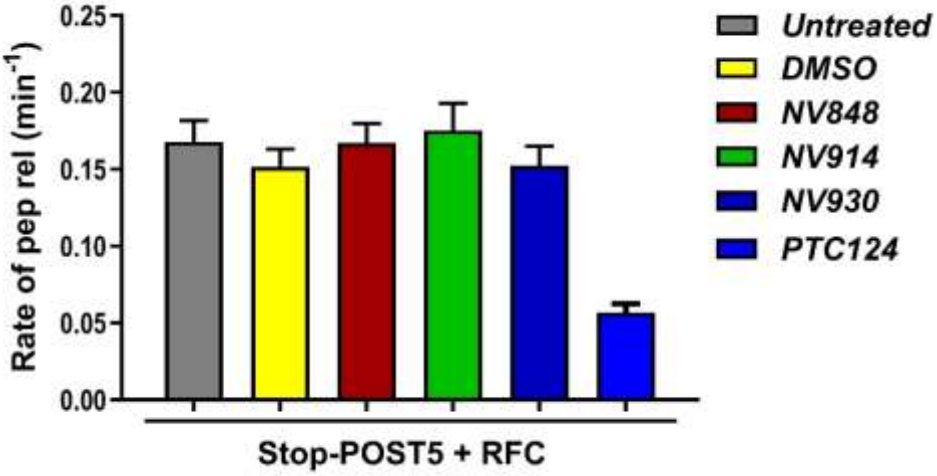

Figure 47. Release Assay: *The graph showing the rate of peptide release after the addition of NV molecules using a Stop-POST5 ATTO647 labelled. NV molecules were tested at 500 μM with a constant concentration of RFC at 0.06μM. PTC124 at 500μM was used as positive control. No statistically significant difference in the rate of peptide release is shown after treatment with NVs molecules.*

5.3.4 The UGA codon readthrough in the PURE-LITE system is induced synergistically by the combination of NV848 and PTC124

Given the distinct mechanisms of action by which PTC124 and NV compounds exert their effects, a potential cooperative activity in promoting PTCs readthrough was evaluated in the PURE-LITE system through the combined treatment with PTC124 and NV848. By employing this *in vitro* reconstituted system, characterized by the Stop-POST5 complex and a proflavine-labeled nc-tRNA, it was possible to evaluate PRE6 complex (as shown in **Figure 18** page 20, a complex in which the near-cognate tRNA is inserted at the ribosomal A site corresponding to stop codons, but does not form a peptide bond with the previous aminoacyl yet) formation and the correct accommodation of the nc-tRNA at the PTC, as assessed by fluorescence emission measured with a plate reader. Consistent with the results obtained from the radioactive readthrough assay, this fluorescence one further confirmed the readthrough activity of PTC124 and NV848. Interestingly, as illustrated in

Figure 48, the combined treatment with both compounds caused an additive effect, markedly enhancing PTC readthrough relative to the effects observed with each compound alone.

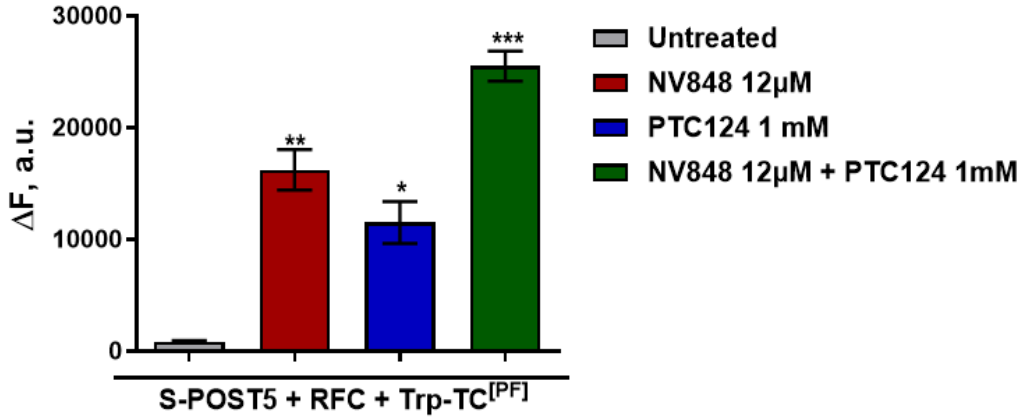

Figure 48. ***Plate reader assay evaluating PRE6 formation:*** *The graph shows the formation of the PRE6 complex from POST5. NV84 was used at 12 μM, while PTC124 1 mM. The figure illustrates the changes in fluorescence emission, indicative of PRE6 complex formation. The stop-POST5 complex was used as a negative control, while treatment with PTC124 served as a positive control. Each experiment was analyzed by GraphPad Prism 6 software. A probability value (p), three symbols (****) for $p < 0.0003$.*

To further investigate the NV848 activity in this proflavine-labelled system, an NV848 titration assay was performed at different concentrations, as shown in **Figure 49**. This analysis confirmed an increase in readthrough activity as the tested concentrations increased, and also the activity of NV848 directly on mispairing of the tRNA as a possible biological target.

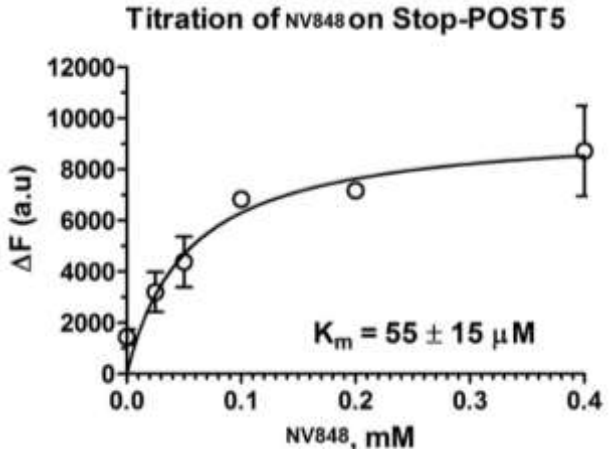

Figure 49. NV848 titration assay: *figure presents the NV848 titration assay with 0.025 μM Stop-POST5 and 0.05μM proflavin-labeled Trp-TC^{W} in absence of RFC, demonstrating a clear dose-dependent relationship between the concentration of NV848 and the observed fluorescence intensity.*

As the amount of NV848 increases, a proportional enhancement in fluorescence signal is detected, confirming the concentration-dependent behaviour of the compound. Thus, NV848 was also tested at 100 µM on the Stop-POST5 complex containing the proflavine-labelled Trp-tRNA, in the presence of the release factor complex, both alone and in combination with PTC124. This experiment aimed to evaluate the formation of the PRE6 complex at higher compound concentrations, as shown in **Figure 50**, confirming the potential readthrough activity of each molecule individually and their synergistic effect when used together.

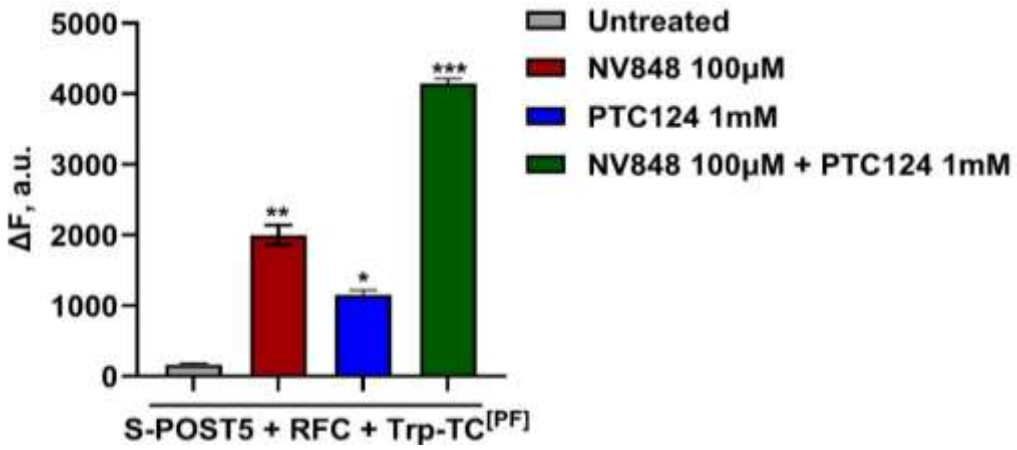

Figure 50. ***Plate reader assay evaluating PRE6 formation:*** *the graph shows the formation of the PRE6 complex from POST5. The figure illustrates the changes in fluorescence emission, indicative of PRE6 complex formation. The stop-POST5 complex was used as a negative control, while treatment with PTC124 served as a positive control. Each experiment was analyzed by GraphPad Prism 6 software. One-way ANOVA followed by Tukey's Multiple comparison test was performed (p value < 0.05).*

Together, these results indicate that NV compounds promote UGA readthrough independently of release factor inhibition.

6. DISCUSSION

Nonsense-related diseases (NRDs) arise from nonsense variants, which account for approximately 11% of rare inherited disorders. These last ones cause premature termination codons in gene sequences, leading to the production of truncated, non-functional proteins. To date, no treatments are available for these diseases, such as Cystic Fibrosis (CF), Choroideremia (CHM), and Duchenne Muscular Dystrophy (DMD). Although different approaches are now under investigation, among these, the suppression therapy approach, based on translational readthrough-inducing drugs (TRIDs), is gaining promising results.

Those compounds permit the insertion of a near-cognate tRNA at the PTCs, allowing the translation of a full-length protein. Our research group has developed three compounds with readthrough activity, NV848, NV914, and NV930, that show very promising results *in vitro* and *in vivo (*Pibiri I. et al., 2020; Perriera R. et al., 2023; Corrao F. et al., 2022; Fiduccia I. et al., 2024).

In particular, all three compounds have shown good readthrough activity across different cell lines carrying distinct nonsense variants *(*Pibiri I. et al., 2020; Bezzerri V. et al., 2022).

Previous studies in our laboratory using CFTR G542X mice provided compelling evidence for the potential rescue of CFTR protein function. Specifically, daily treatment for 14 days with NV848 (60 mg/kg body weight), another readthrough compound synthesized by our group, restored CFTR protein expression and correct localization in these mouse models. Moreover, biodistribution studies confirmed that the molecule successfully reached the primary organ targets typically affected by CF in humans (Fiduccia I. et al., 2024).

Building on these findings, the study carried out during my Ph.D. project focused on evaluating additional potential readthrough compounds, namely NV914 and NV930. This study was conducted both on the aforementioned mouse model and on models of another genetic disease caused by nonsense mutations, namely Choroideremia. This choice is justified by the fact that, in the first case, the Cystic Fibrosis model, it is essential to have compounds that can act on multiple cellular targets. Our previous studies have shown that, although the precise molecular targets of the three NV compounds are not yet fully understood, they may act on distinct targets (Carollo P.S. et al., 2023). Therefore, their combined use, if all three prove effective, could represent a strategy to achieve a synergistic effect. Moreover, at present, there is no specific therapy for cystic fibrosis caused by stop variants, unlike for patients carrying other mutations, most notably F508del. Therefore, identifying a compound capable of restoring CFTR function in this genetic context is of considerable importance.

The choice of the other model, on the other hand, is justified by the fact that more than 30% of patients with Choroideremia carry nonsense variants in the CHM gene.

The study conducted in C57BL/6 CFTR G542X mice over a two-week period, during which the animals were administered a dose of 60mg/Kg, showed a positive trend in CFTR protein expression. This result is particularly significant for the NV914 compound.

However, this study proved to be particularly challenging due to the fragility of mice homozygous for the G542X CFTR mutation.

For this reason, during this period, the mice were fed a special liquid diet. Throughout the two-week treatment period, the body weight of mice treated with the two compounds was also monitored, showing a steady increase similar to that of the negative controls. This indicates that the compounds did not induce adverse or toxic effects and were generally well tolerated.

The most important aspect of the study regarding CFTR protein rescue is the analysis of its expression. Through molecular analyses, including assessments of gene transcript and protein expression, it was observed that treatment with NV914 and NV930 induces CFTR protein expression. Moreover, NV914 appears to affect the potential stabilization of the mRNA. These findings are supported by histological analyses, which revealed the protein in the pulmonary epithelium and a potential effect on overall tissue structure.

Lastly, the restoration of CFTR protein expression after NV914 and NV930 treatments showed by molecular analyses, have demonstrated the potential *in vivo* activity of those compounds not showing toxicity during the administration period but also promoting the correct apical localization of CFTR within the epithelial cells of the pulmonary ducts, thereby reinforcing their relevance as promising therapeutic candidates.

Regarding the second objective of my work, it focused on investigating whether readthrough compounds could also be applied to another disease caused by stop mutations: choroideremia. In addition to the two previously mentioned compounds (NV914 and NV930), NV848 was included for this objective because it had not been tested in this genetic background.

For this purpose, a specific plasmid, pRG213610, produced by Origene, has been purchased, containing the CHM gene sequence cloned in frame with a tGFP sequence, which is fundamental for the next readthrough experiment to evaluate directly the readthrough activity of TRIDs molecules, thanks to the production of the REP1-tGFP chimeric protein. Site-directed mutagenesis was performed on this plasmid to introduce two of the most common nonsense variants, R253X and

R293X, separately, while colony PCR following a midi-prep was performed to obtain the mutagenized DNA.

These vectors were therefore used to engineer H1299 cells, creating a versatile stable model for the preliminary evaluation of the compound concentrations required to induce readthrough. Treatments were thus carried out at different concentrations (12, 24, and 48 μM), and it was ultimately decided to start with 12 μM, a concentration that has previously yielded significant results in our laboratory. Immunofluorescence analyses of the generated models revealed an increase in REP1 protein expression after 72 hours of chronic treatment with NV848, NV914, and NV930, although this was not detected by Western blot analysis.

It was therefore decided to assess the treatment's efficacy in primary human fibroblast lines derived from patients with Choroideremia carrying nonsense variants in the CHM gene.

Three types of primary CHM-mutated fibroblast cell lines, each characterized by a different nonsense variant (R253X, R270X, or S190X), were employed. Similarly to the previous experiments, a chronic treatment every 24 hours was performed using the three NV compounds. The results of these new experiments indicated that the NV treatments do not appear to affect mRNA stabilization, except for a slight effect observed in cells carrying the R253X mutation treated with NV914.

Regarding CHM expression, it was observed across all three fibroblast types, showing a very similar response to all three compounds relative to the mutation considered, with potentially greater responsiveness in cells carrying the R253X mutation, as evidenced by immunofluorescence analysis.

Furthermore, in these cells, fragmented nuclei and micronuclei were clearly observed, and their frequency (23%) decreased significantly following the treatments.

Despite the encouraging data, Western blot analysis did not reveal a substantial recovery of the protein after treatment with the three compounds. It is possible that the protein restored by readthrough is not readily detectable by this technique, and further experimental validation will be required.

Taken together these data suggest that NV molecules can restore REP1 protein expression in the two different model through compounds induced translational readthrough of PTCs. In addition the reduced micronucleated phenotype observed in the patient-derived fibroblasts treated with NVs molecule may suggest a possible functional rescue of REP1 and not only the restoration of protein expression. However, further analyses are required to assess a possible functional recovery.

The final part of my work, on the other hand, focused on investigating the potential biological targets of the three NV compounds and, in addition, on possible interactions with components of the translation machinery, using a system developed at the University of Pennsylvania (UPENN).

For this purpose, an *in vitro* reconstituted model system, the PURE-LITE system, was employed.

This system enables both readthrough and termination assays to determine how the molecules act.

As a starting point, the potential inhibitory effect of the molecules on normal peptide elongation was assessed. For this purpose, a reference POST5 Trp-IRES sequence was used, and the normal translation elongation peptide was evaluated. As observed, none of the three molecules showed an inhibitory effect on the ribosome, thus allowing correct peptide elongation.

The next step was to evaluate the readthrough activity of the NV compounds directly in the PURE-LITE system, using a reference sequence different from the Trp-IRES one but containing a nonsense codon in the sixth position instead of the tryptophan one. In this case as well, NV848, NV914, and NV930 exhibited strong readthrough activity at very low concentrations when compared with the positive control PTC124.

Taken together, these results confirm not only the safety but also the potential readthrough activity of these compounds for NRDs.

Given the chemical structure of these molecules and their ancestor, PTC124, from which they are derived, it was hypothesized that they might share the same biological target. For PTC124, this has recently been demonstrated by the Cooperman group (Huang S. *et al.*, 2022), who showed that PTC124 binds to several ribosomal sites and competitively inhibits release factor-dependent termination. Specifically, PTC124 can bind to the ribosome's active site, where the release factor usually associates, thereby slowing the binding of the release factor complex (RFC). This allows the ribosome to remain longer at the PTC, favoring the incorporation of an nc-tRNA and thus enabling protein translation.

So to assess this possibility, as the first thing, we evaluated the activity of NVs molecules on release factors eRF1 and eRF3, and in particular, all three TRIDs molecules did not affect those factors, showing in the co-sedimentation assay no variation in the peptide release when the molecules were used in the Stop-POST5 complex.

Lastly, the rate of peptide release was evaluated. As already demonstrated by Cooperman and collaborators, treatment with PTC124 in the PURE-LITE system using a plate reader assay causes a marked decrease in the rate of peptide release, due to the mechanism described above. Conversely,

treatment with the NV molecules did not result in the same reduction in peptide release rate, indicating that our compounds do not act like PTC124 by competitively inhibiting release factor-dependent termination, but rather are more likely to act through tRNA mispairing.

7. CONCLUSIONS

In conclusion, the results of this work support the potential of NV compounds as effective agents for promoting readthrough of nonsense mutations across different genetic contexts. Although further validation is required, the observed re-expression of CFTR and CHM proteins, together with the absence of toxic effects, highlights the therapeutic relevance of these molecules. Future studies aimed at elucidating their precise molecular targets will be essential to fully understand their mechanism of action and the specific biological target, to optimize their potential application in personalized treatments for genetic diseases caused by premature stop codons.

8. SUPPLEMENTARY MATERIAL

8.1 Genotyping of all the mice produced during experimental project and Sanger sequences of mice involved in experimental procedures

All the mice that were genotyped are showed in **Figure S1**, while the genotype of mice involved in experimental procedures were confirmed by sanger sequencing by BMR Genomics and showed in **Figure S2.**

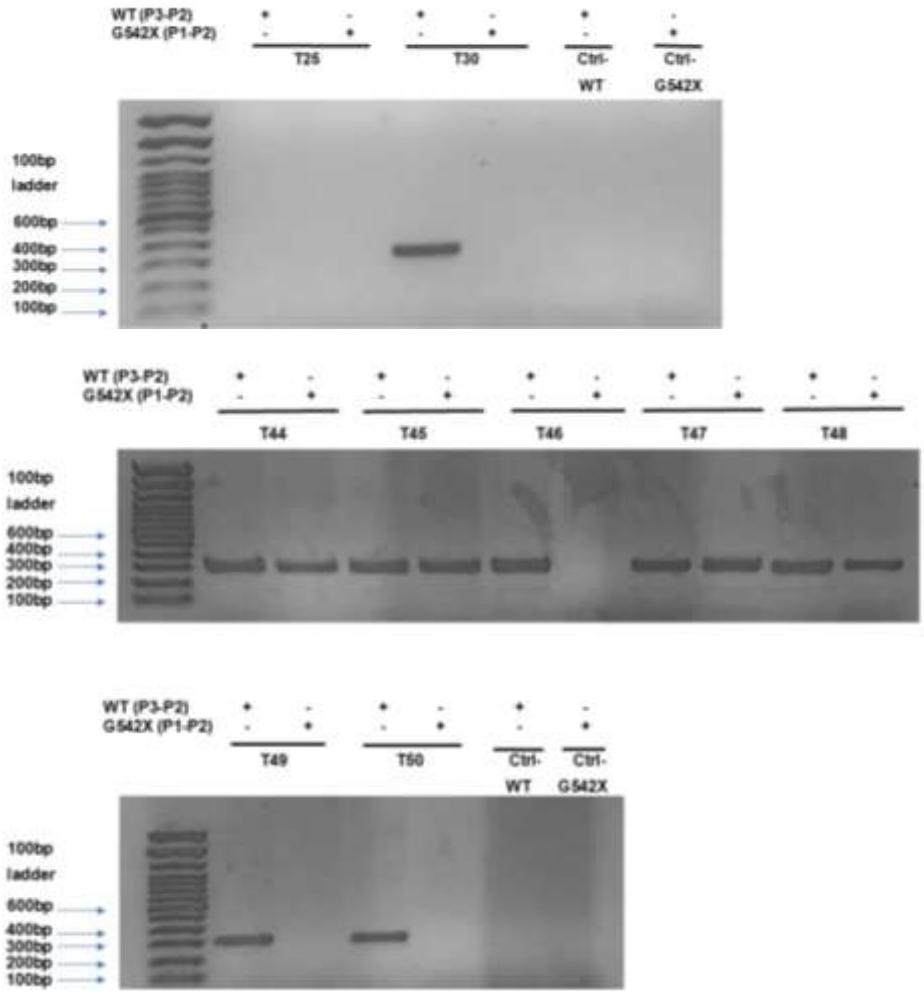

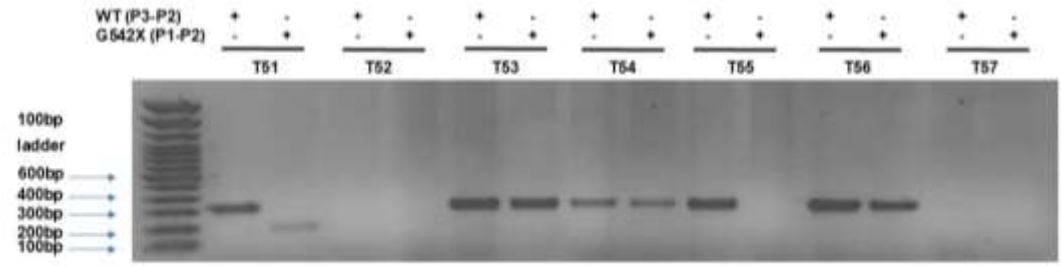
WT (P3-P2)
G542X (P1-P2)
T51
T52
T53
T54
T55
T56
T57
100bp
ladder
600bp
400bp
300bp
200bp
100bp

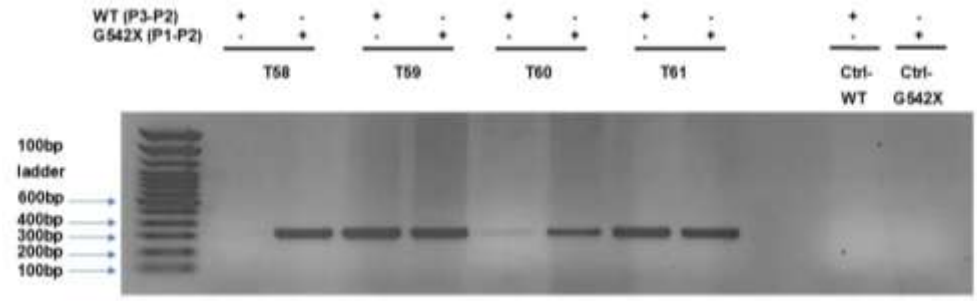
WT (P3-P2)
G542X (P1-P2)
T58
T59
T60
T61
Ctrl-
WT
Ctrl-
G542X
100bp
ladder
600bp
400bp
300bp
200bp
100bp

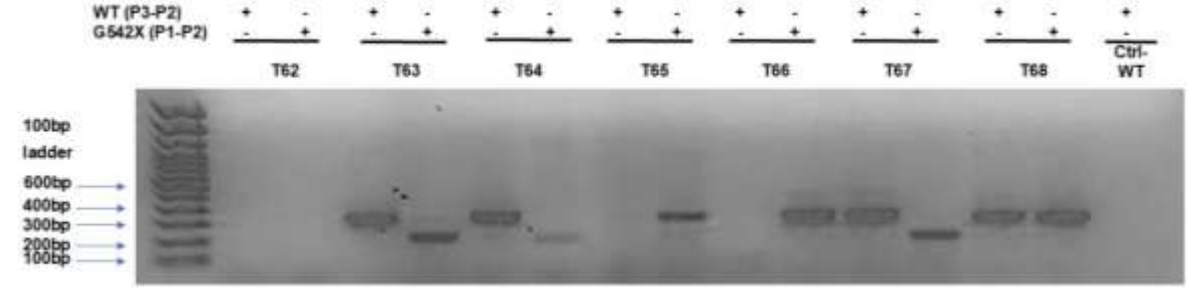
WT (P3-P2)
G542X (P1-P2)
T62
T63
T64
T65
T66
T67
T68
Ctrl-
WT
100bp
ladder
600bp
400bp
300bp
200bp
100bp

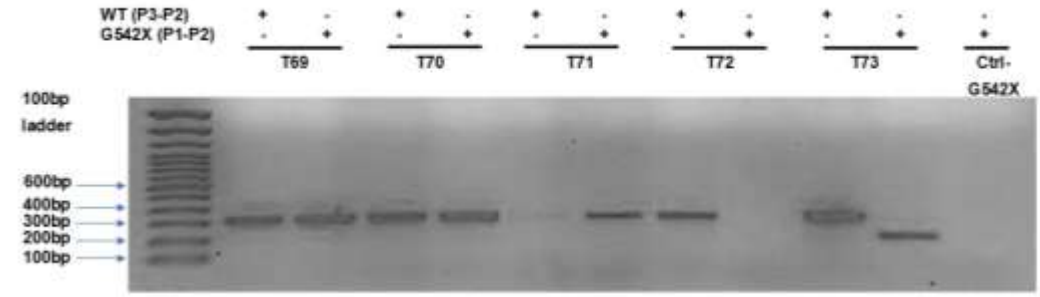
WT (P3-P2)
G542X (P1-P2)
T69
T70
T71
T72
T73
Ctrl-
G542X
100bp
ladder
600bp
400bp
300bp
200bp
100bp

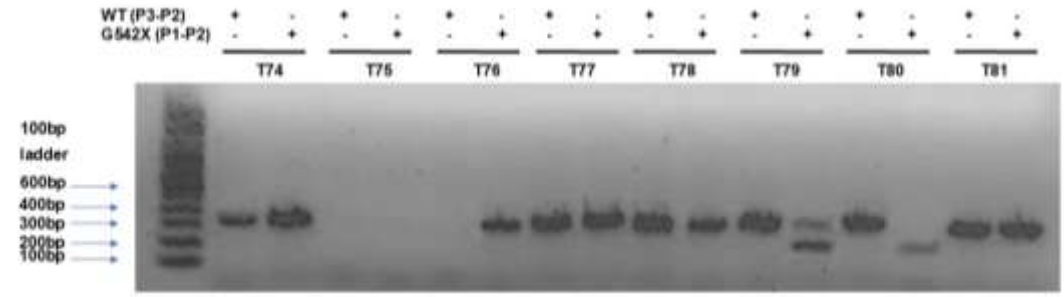
WT (P3-P2)
G542X (P1-P2)
T74
T75
T76
T77
T78
T79
T80
T81
100bp
ladder
600bp
400bp
300bp
200bp
100bp

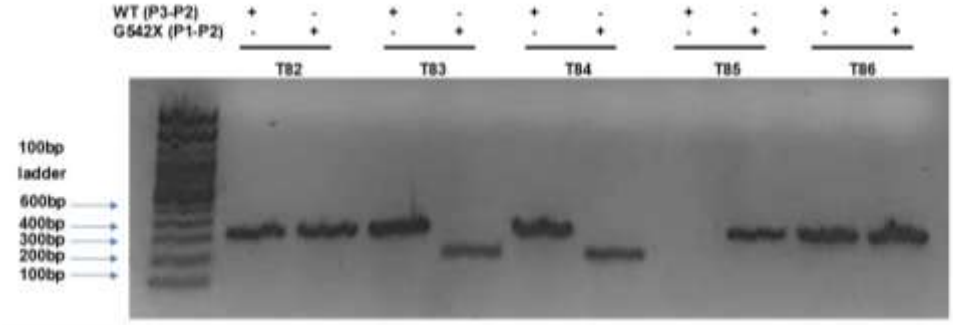
WT (P3-P2)
G542X (P1-P2)
T82
T83
T84
T85
T86
100bp
ladder
600bp
400bp
300bp
200bp
100bp

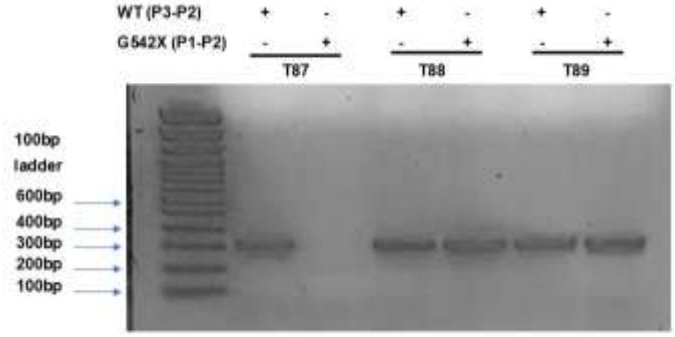
WT (P3-P2)
G542X (P1-P2)
T87
T88
T89
100bp
ladder
600bp
400bp
300bp
200bp
100bp

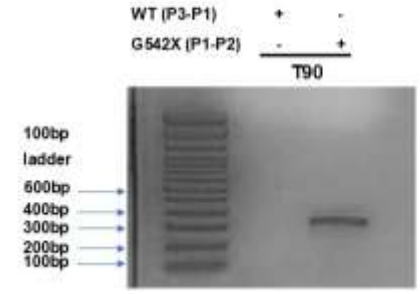
WT (P3-P1)
G542X (P1-P2)
T90
100bp
ladder
600bp
400bp
300bp
200bp
100bp

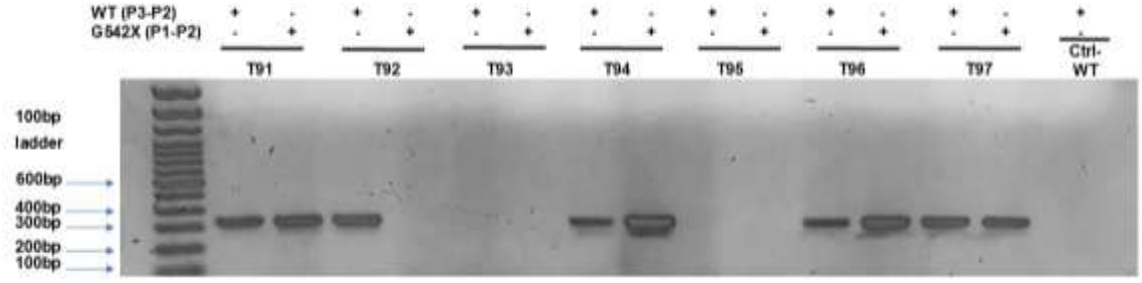
WT (P3-P2)
G542X (P1-P2)
T91
T92
T93
T94
T95
T96
T97
Ctrl-
WT
100bp
ladder
600bp
400bp
300bp
200bp
100bp

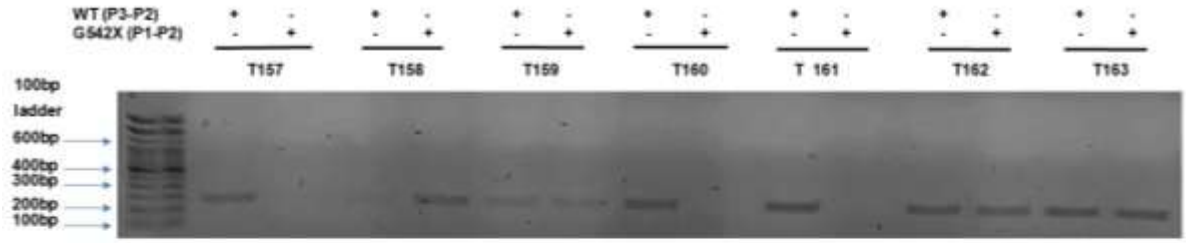
WT (P3-P2)
G542X (P1-P2)
T157
T158
T159
T160
T 161
T162
T163
100bp ladder
600bp
400bp
300bp
200bp
100bp

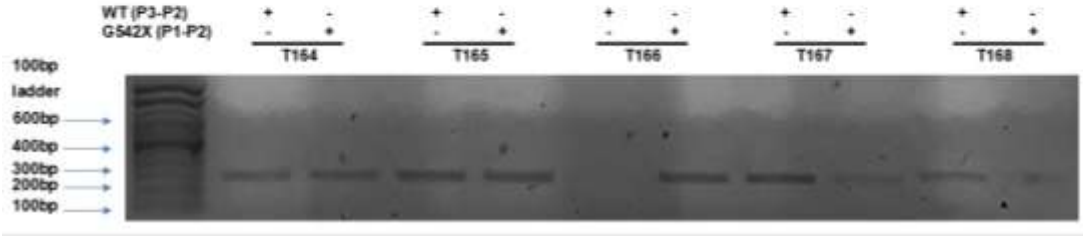
WT (P3-P2)
G542X (P1-P2)
T164
T165
T166
T167
T168
100bp ladder
600bp
400bp
300bp
200bp
100bp

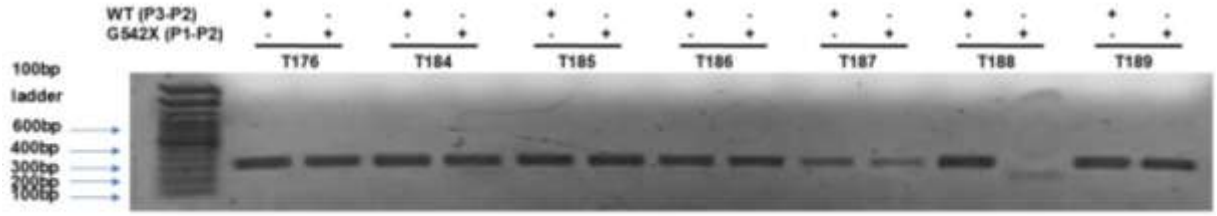
WT (P3-P2)
G542X (P1-P2)
T176
T184
T185
T186
T187
T188
T189
100bp ladder
600bp
400bp
300bp
200bp
100bp

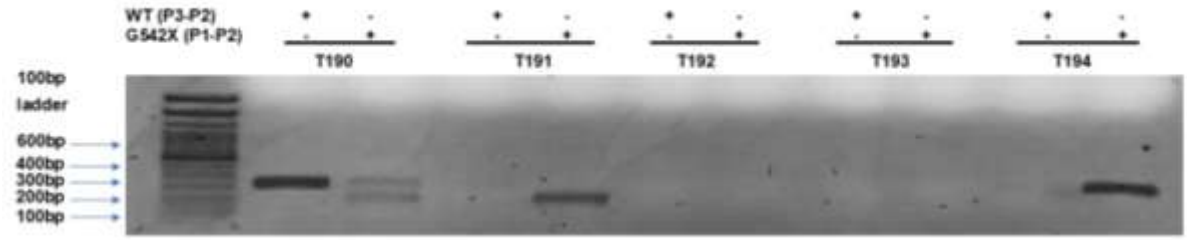
WT (P3-P2)
G542X (P1-P2)
T190
T191
T192
T193
T194
100bp ladder
600bp
400bp
300bp
200bp
100bp

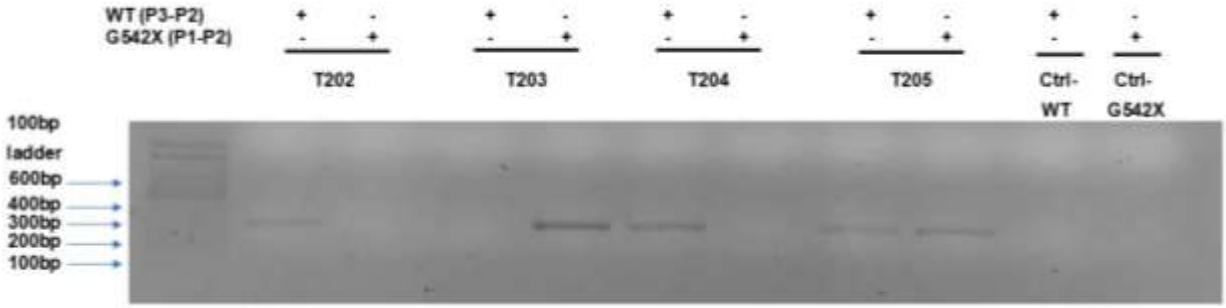
WT (P3-P2)
G542X (P1-P2)
T202
T203
T204
T205
Ctrl-WT
Ctrl-G542X
100bp ladder
600bp
400bp
300bp
200bp
100bp

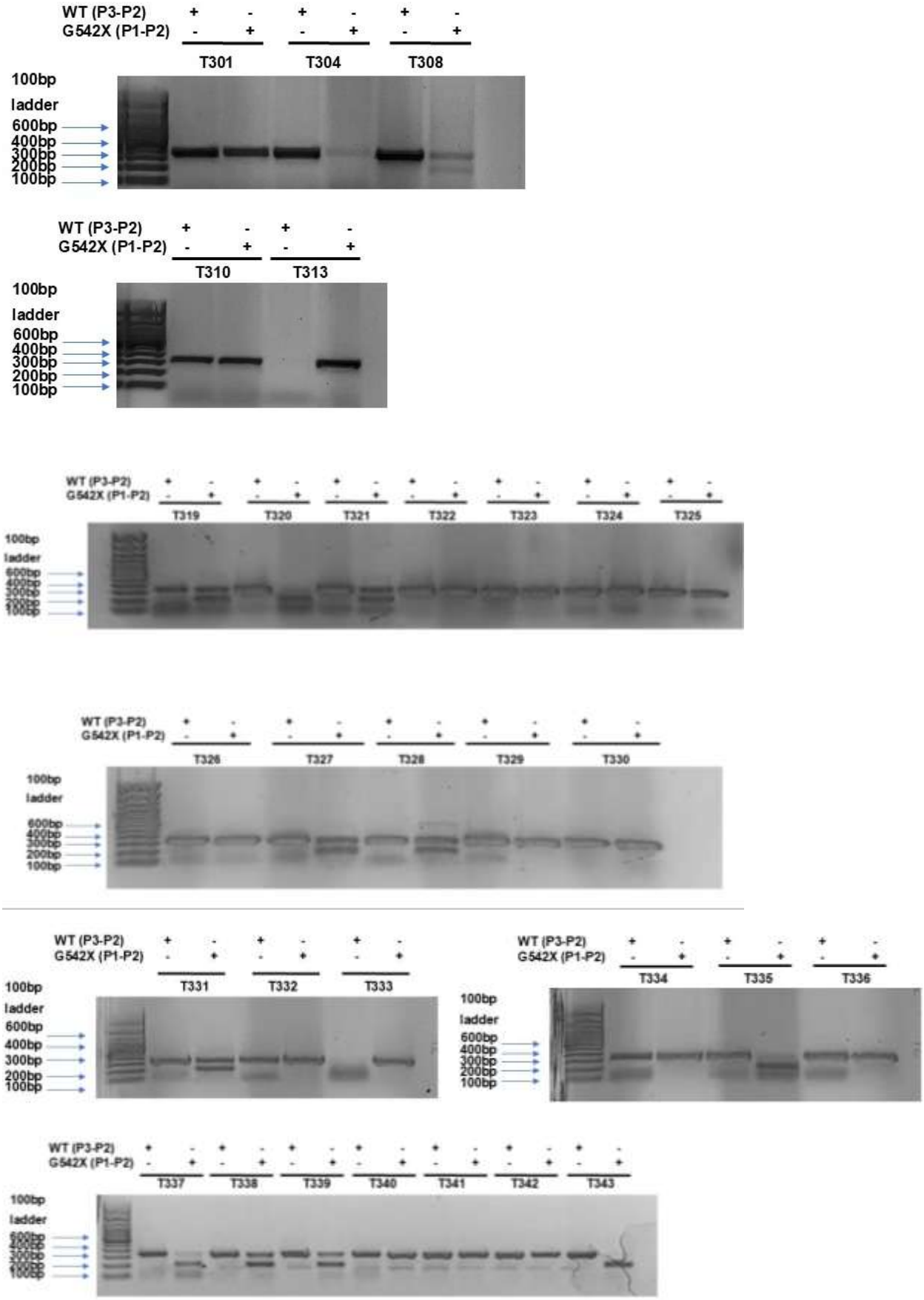

Figure S1. Electrophoresis gels showing mice genotyping*: the pictures show all the genotyping performed during the project to obtain the CFTR$^{G542X/G542X}$ mice for the experimental procedures.*

T40

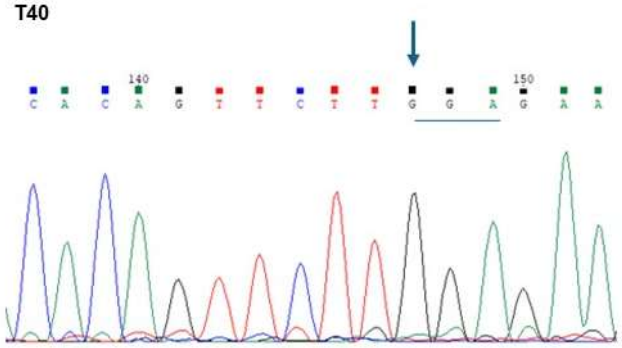

T16

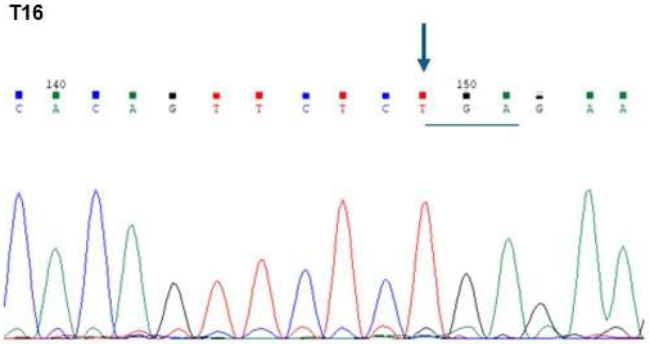

T287

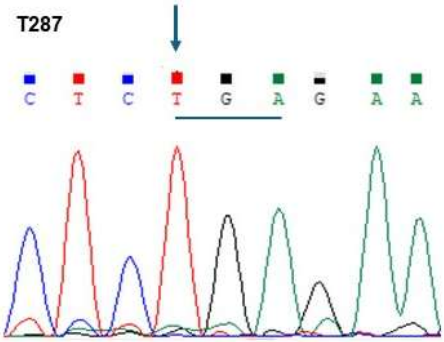

T169

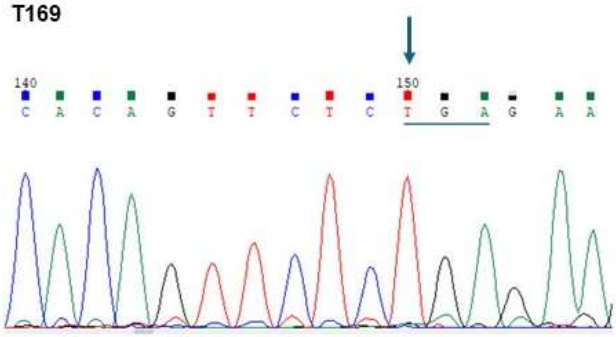

T171

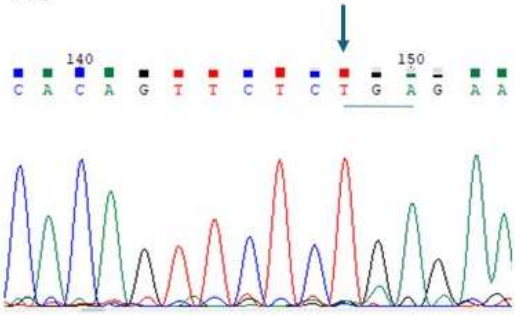

T200

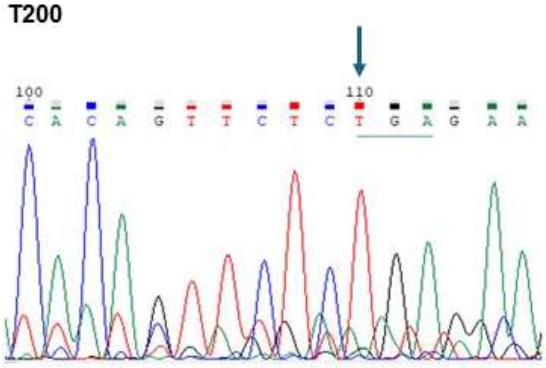

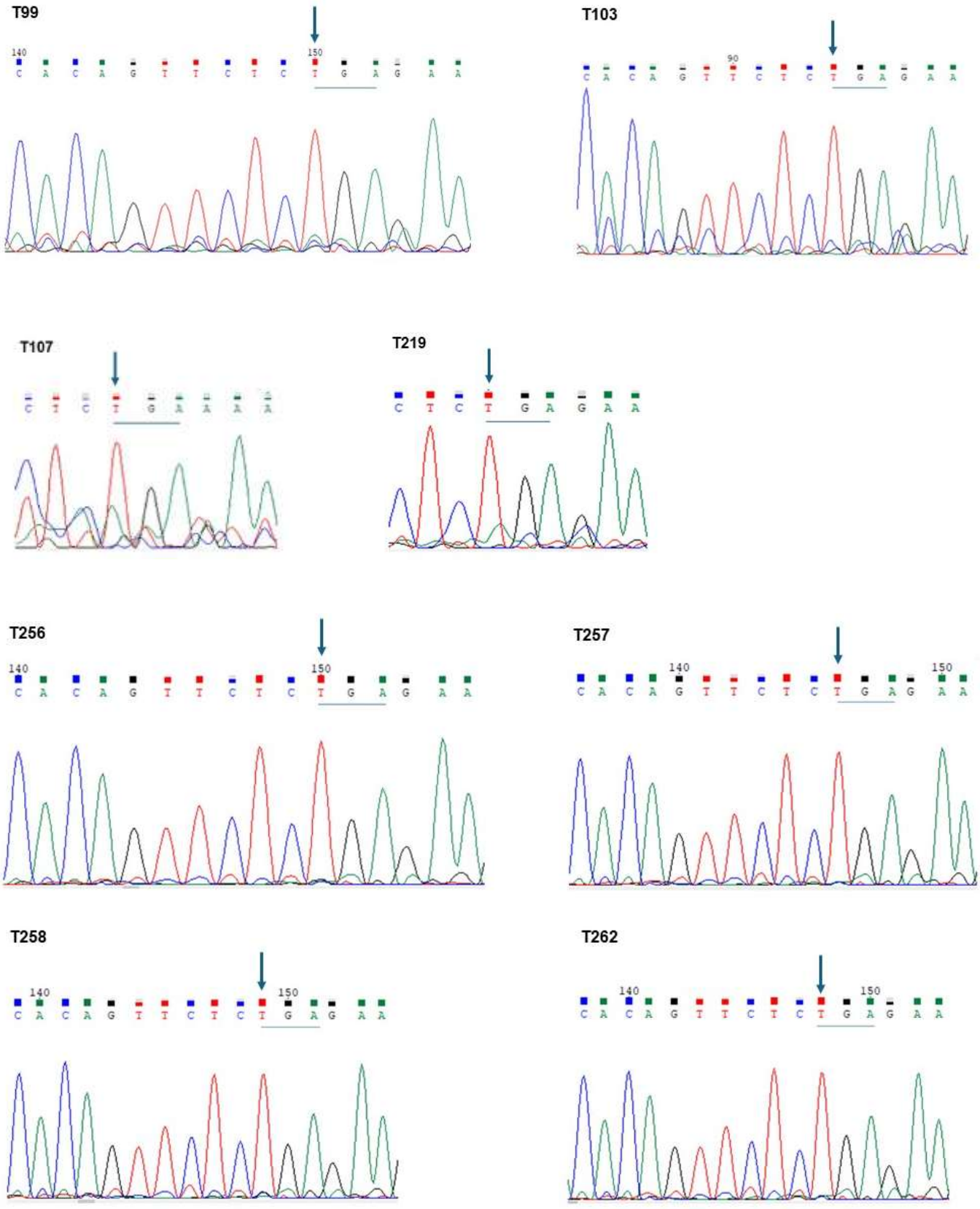

Figure S2. Sanger sequencing chromatograms: *All the sequencing have confirmed the genotypes obtained by the genotyping performed on mice involved in experimental procedures.*

8.2 Western blot analyses do not detect REP1-tGFP protein rescue in H1299 CHM^{R253X}-tGFP and CHM^{R293X}-tGFP

To assess NVs readthrough activity, a 72-hour chronic treatment was performed in the stable cell lines produced by H1299 CHM^{R253X}-tGFP or CHM^{R253X}-tGFP, separately, while the cell line H1299 CHM^{WT}-tGFP was used as a positive control. In particular, 500,000 cells were seeded in a petri dish for each condition, and after treatments with G418 (430 µM), PTC124, NV848, NV914, and NV930 (12 µM), protein extraction was performed and proteins quantified by Bradford assay. 50 µg of protein for each condition was used for western analyses, but as presented in **Figure S3**, in H1299 CHM^{R253X}-tGFP (**S3-A**) or CHM^{R293X}-tGFP (**S3-B**), no REP1-tGFP rescue has been shown for none condition.

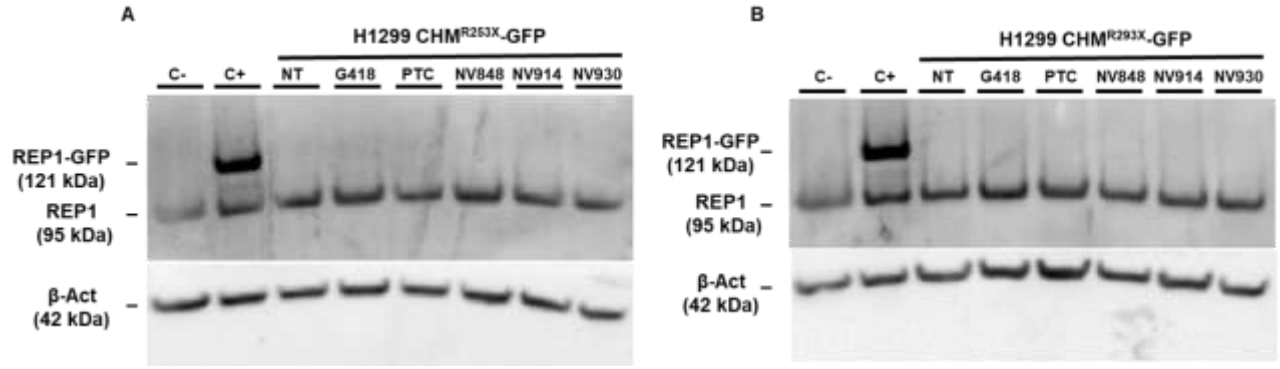

Figure S3. Western blot analyses show no REP1-GFP rescue after TRIDs treatment in H1299 CHM^{R253X}-tGFP (A) and H1299 CHM^{R293X}-tGFP (B). *Negative controls are represented by H1299 (C-), by H1299 CHM^{R253X}-tGFP and CHM^{R293X}-tGFP untreated, while positive control (C+) is represented by H1299 CHM^{WT}-tGFP.*

9. BIBLIOGRAPHY

1. Andrade EL, Bento AF, Cavalli J, Oliveira SK, Schwanke RC, Siqueira JM, Freitas CS, Marcon R, Calixto JB. Non-clinical studies in the process of new drug development - Part II: Good laboratory practice, metabolism, pharmacokinetics, safety, and dose translation to clinical studies. Braz J Med Biol Res. 2016 Dec 12;49(12):e5646. doi: 10.1590/1414-431X20165646. PMID: 27982281; PMCID: PMC5188860.
2. Aslam AA, Sinha IP, Southern KW. Ataluren and similar compounds (specific therapies for premature termination codon class I mutations) for cystic fibrosis. Cochrane Database Syst Rev. 2023 Mar 3;3(3):CD012040. doi: 10.1002/14651858.CD012040.pub3. PMID: 36866921; PMCID: PMC9983356.
3. Benslimane N, Loret C, Chazelas P, Favreau F, Faye PA, Lejeune F, Lia AS. Readthrough Activators and Nonsense-Mediated mRNA Decay Inhibitor Molecules: Real Potential in Many Genetic Diseases Harboring Premature Termination Codons. Pharmaceuticals (Basel). 2024 Feb 28;17(3):314. doi: 10.3390/ph17030314. PMID: 38543100; PMCID: PMC10975577.
4. Bezzerri V, Lentini L, Api M, Busilacchi EM, Cavalieri V, Pomilio A, Diomede F, Pegoraro A, Cesaro S, Poloni A, Pace A, Trubiani O, Lippi G, Pibiri I, Cipolli M. Novel Translational Read-through-Inducing Drugs as a Therapeutic Option for Shwachman-Diamond Syndrome. Biomedicines. 2022 Apr 12;10(4):886. doi: 10.3390/biomedicines10040886. PMID: 35453634; PMCID: PMC9024944.
5. Bezzerri, V., & Cipolli, M. (2019). Shwachman-Diamond Syndrome: Molecular Mechanisms and Current Perspectives. Molecular diagnosis & therapy, 23(2), 281–290. https://doi.org/10.1007/s40291-018-0368-2.
6. Bhat S, Bhattacharya A, Li H, Cui X, Lueck JD, Goldman YE, Cooperman BS. Mechanism-based approach in designing patient-specific combination therapies for nonsense mutation diseases. bioRxiv [Preprint]. 2024 Dec 11:2024.11.13.623453. doi: 10.1101/2024.11.13.623453. Update in: Nucleic Acids Res. 2025 Mar 20;53(6):gkaf216. doi: 10.1093/nar/gkaf216. PMID: 39605609; PMCID: PMC11601491.
7. Bidou L, Allamand V, Rousset JP, Namy O. Sense from nonsense: therapies for premature stop codon diseases. Trends Mol Med. 2012 Nov;18(11):679-88. doi: 10.1016/j.molmed.2012.09.008. Epub 2012 Oct 17. PMID: 23083810.
8. Borgatti M, Altamura E, Salvatori F, D'Aversa E, Altamura N. Screening Readthrough Compounds to Suppress Nonsense Mutations: Possible Application to β-Thalassemia. J

Clin Med. 2020 Jan 21;9(2):289. doi: 10.3390/jcm9020289. PMID: 31972957; PMCID: PMC7073686.

9. Bozkaya, D., Zou, H., Lu, C. *et al.* Bilateral visual acuity decline in males with choroideremia: a pooled, cross-sectional meta-analysis. *BMC Ophthalmol* **22**, 29 (2022). https://doi.org/10.1186/s12886-022-02250-z
10. Campofelice A, Lentini L, Di Leonardo A, Melfi R, Tutone M, Pace A, Pibiri I. Strategies against Nonsense: Oxadiazoles as Translational Readthrough-Inducing Drugs (TRIDs). Int J Mol Sci. 2019 Jul 6;20(13):3329. doi: 10.3390/ijms20133329. PMID: 31284579; PMCID: PMC6651739.
11. Carollo PS, Tutone M, Culletta G, Fiduccia I, Corrao F, Pibiri I, Di Leonardo A, Zizzo MG, Melfi R, Pace A, Almerico AM, Lentini L. Investigating the Inhibition of FTSJ1, a Tryptophan tRNA-Specific 2'-O-Methyltransferase by NV TRIDs, as a Mechanism of Readthrough in Nonsense Mutated CFTR. Int J Mol Sci. 2023 Jun 1;24(11):9609. doi: 10.3390/ijms24119609. PMID: 37298560; PMCID: PMC10253411.
12. Choi J, Kim H, Bae YK, Cheong H. REP1 Modulates Autophagy and Macropinocytosis to Enhance Cancer Cell Survival. Int J Mol Sci. 2017 Aug 28;18(9):1866. doi: 10.3390/ijms18091866. PMID: 28846638; PMCID: PMC5618515.
13. Clarke LA, Amaral MD. What Can RNA-Based Therapy Do for Monogenic Diseases? Pharmaceutics. 2023 Jan 12;15(1):260. doi: 10.3390/pharmaceutics15010260. PMID: 36678889; PMCID: PMC9863139.
14. Corrao F, Zizzo MG, Tutone M, Melfi R, Fiduccia I, Carollo PS, Leonardo AD, Caldara G, Perriera R, Pace A, Belmonte B, Sammataro S, Pibiri I, Lentini L. Nonsense codons suppression. An acute toxicity study of three optimized TRIDs in a murine model, safety and tolerability evaluation. Biomed Pharmacother. 2022 Dec;156:113886. doi: 10.1016/j.biopha.2022.113886. Epub 2022 Oct 18. PMID: 36265311.
15. Coughlan KA, Eybye M, Henderson N, DeAntonis CM, Frassetto A, Hanahoe E, Ketova T, Jacquinet E, Presnyak V, Jain R, Marshall J, Martini PGV. Improved therapeutic efficacy in two mouse models of methylmalonic acidemia (MMA) using a second-generation mRNA therapy. Mol Genet Metab. 2024 Sep-Oct;143(1-2):108560. doi: 10.1016/j.ymgme.2024.108560. Epub 2024 Aug 5. PMID: 39121792.
16. Dabrowski M, Bukowy-Bieryllo Z, Zietkiewicz E. Advances in therapeutic use of a drug-stimulated translational readthrough of premature termination codons. Mol Med. 2018 May 29;24(1):25. doi: 10.1186/s10020-018-0024-7. PMID: 30134808; PMCID: PMC6016875.

17. De Boeck K. Cystic fibrosis in the year 2020: A disease with a new face. Acta Paediatr. 2020 May;109(5):893-899. doi: 10.1111/apa.15155. Epub 2020 Jan 22. PMID: 31899933.
18. De Silva SR, Arno G, Robson AG, Fakin A, Pontikos N, Mohamed MD, Bird AC, Moore AT, Michaelides M, Webster AR, Mahroo OA. The X-linked retinopathies: Physiological insights, pathogenic mechanisms, phenotypic features, and novel therapies. Prog Retin Eye Res. 2021 May;82:100898. doi: 10.1016/j.preteyeres.2020.100898. Epub 2020 Aug 26. PMID: 32860923.
19. Dickinson KM, Collaco JM. Cystic Fibrosis. Pediatr Rev. 2021 Feb;42(2):55-67. doi: 10.1542/pir.2019-0212. PMID: 33526571; PMCID: PMC8972143.
20. Doudna JA. The promise and challenge of therapeutic genome editing. Nature. 2020 Feb;578(7794):229-236. doi: 10.1038/s41586-020-1978-5. Epub 2020 Feb 12. PMID: 32051598; PMCID: PMC8992613.
21. Du M, Liu X, Welch EM, Hirawat S, Peltz SW, Bedwell DM. PTC124 is an orally bioavailable compound that promotes suppression of the human CFTR-G542X nonsense allele in a CF mouse model. Proc Natl Acad Sci U S A. 2008 Feb 12;105(6):2064-9. doi: 10.1073/pnas 0711795105. Epub 2008 Feb 6. PMID: 18272502; PMCID: PMC2538881.
22. Fanen P, Wohlhuter-Haddad A, Hinzpeter A. Genetics of cystic fibrosis: CFTR mutation classifications toward genotype-based CF therapies. Int J Biochem Cell Biol. 2014 Jul;52:94-102. doi: 10.1016/j.biocel.2014.02.023. Epub 2014 Mar 12. PMID: 24631642.
23. Farinha CM, Callebaut I. Molecular mechanisms of cystic fibrosis - how mutations lead to misfunction and guide therapy. Biosci Rep. 2022 Jul 29;42(7):BSR20212006. doi: 10.1042/BSR20212006. PMID: 35707985; PMCID: PMC9251585.
24. Fernandez E, De Santi C, De Rose V, Greene CM. CFTR dysfunction in cystic fibrosis and chronic obstructive pulmonary disease. Expert Rev Respir Med. 2018 Jun;12(6):483-492. doi: 10.1080/17476348.2018.1475235. Epub 2018 May 23. PMID: 29750581.
25. Foote KG, Roorda A, Duncan JL. Multimodal Imaging in Choroideremia. Adv Exp Med Biol. 2019;1185:139-143. doi: 10.1007/978-3-030-27378-1_23. PMID: 31884602; PMCID: PMC9126851.
26. Freires IA, Morelo DFC, Soares LFF, Costa IS, de Araújo LP, Breseghello I, Abdalla HB, Lazarini JG, Rosalen PL, Pigossi SC, Franchin M. Correction to: Progress and promise of alternative animal and non-animal methods in biomedical research. Arch Toxicol. 2023 Nov;97(11):3021. doi: 10.1007/s00204-023-03595-0. Erratum for: Arch Toxicol. 2023 Sep;97(9):2329-2342. doi: 10.1007/s00204-023-03532-1. PMID: 37665364.

27. Fry LE, Patrício MI, Jolly JK, Xue K, MacLaren RE. Expression of Rab Prenylation Pathway Genes and Relation to Disease Progression in Choroideremia. Transl Vis Sci Technol. 2021 Jul 1;10(8):12. doi: 10.1167/tvst.10.8.12. PMID: 34254989; PMCID: PMC8287038.
28. Gao FJ, Tian GH, Hu FY, Wang DD, Li JK, Chang Q, Chen F, Xu GZ, Liu W, Wu JH. Next-generation sequencing-based clinical diagnosis of choroideremia and comprehensive mutational and clinical analyses. BMC Ophthalmol. 2020 Jun 1;20(1):212. doi: 10.1186/s12886-020-01478-x. PMID: 32487042; PMCID: PMC7268499.
29. Garattini S, Grignaschi G. Animal testing is still the best way to find new treatments for patients. Eur J Intern Med. 2017 Apr;39:32-35. doi: 10.1016/j.ejim.2016.11.013. Epub 2016 Dec 1. PMID: 27916437.
30. Geurts MH, de Poel E, Amatngalim GD, Oka R, Meijers FM, Kruisselbrink E, van Mourik P, Berkers G, de Winter-de Groot KM, Michel S, Muilwijk D, Aalbers BL, Mullenders J, Boj SF, Suen SWF, Brunsveld JE, Janssens HM, Mall MA, Graeber SY, van Boxtel R, van der Ent CK, Beekman JM, Clevers H. CRISPR-Based Adenine Editors Correct Nonsense Mutations in a Cystic Fibrosis Organoid Biobank. Cell Stem Cell. 2020 Apr 2;26(4):503-510.e7. doi: 10.1016/j.stem.2020.01.019. Epub 2020 Feb 20. PMID: 32084388.
31. Goetz LH, Schork NJ. Personalized medicine: motivation, challenges, and progress. Fertil Steril. 2018 Jun;109(6):952-963. doi: 10.1016/j.fertnstert.2018.05.006. PMID: 29935653; PMCID: PMC6366451.
32. Golkar Z. CRISPR: a journey of gene-editing based medicine. Genes Genomics. 2020 Dec;42(12):1369-1380. doi: 10.1007/s13258-020-01002-x. Epub 2020 Oct 22. PMID: 33094378; PMCID: PMC7679360.
33. Greco F, Cosentino M, Marino F. The Italian breakthrough in CRISPR trials for rare diseases: a focus on beta-thalassemia and sickle cell disease treatment. Front Med (Lausanne). 2024 Feb 15;11:1356578. doi: 10.3389/fmed.2024.1356578. PMID: 38426160; PMCID: PMC10902426.
34. Hanssens LS, Duchateau J, Casimir GJ. CFTR Protein: Not Just a Chloride Channel? Cells. 2021 Oct 22;10(11):2844. doi: 10.3390/cells10112844. PMID: 34831067; PMCID: PMC8616376.
35. Huang S, Bhattacharya A, Ghelfi MD, Li H, Fritsch C, Chenoweth DM, Goldman YE, Cooperman BS. Ataluren binds to multiple protein synthesis apparatus sites and competitively inhibits release factor-dependent termination. Nat Commun. 2022 May

6;13(1):2413. doi: 10.1038/s41467-022-30080-6. PMID: 35523781; PMCID: PMC9076611.

36. Hwang TC, Yeh JT, Zhang J, Yu YC, Yeh HI, Destefano S. Structural mechanisms of CFTR function and dysfunction. J Gen Physiol. 2018 Apr 2;150(4):539-570. doi: 10.1085/jgp.201711946. Epub 2018 Mar 26. PMID: 29581173; PMCID: PMC5881446.
37. Imani S, Ijaz I, Shasaltaneh MD, Fu S, Cheng J, Fu J. Molecular genetics characterization and homology modeling of the CHM gene mutation: A study on its association with choroideremia. Mutat Res Rev Mutat Res. 2018 Jan-Mar;775:39-50. doi: 10.1016/j.mrrev.2018.02.001. Epub 2018 Feb 18. PMID: 29555028.
38. Jiang T, Henderson JM, Coote K, Cheng Y, Valley HC, Zhang XO, Wang Q, Rhym LH, Cao Y, Newby GA, Bihler H, Mense M, Weng Z, Anderson DG, McCaffrey AP, Liu DR, Xue W. Chemical modifications of adenine base editor mRNA and guide RNA expand its application scope. Nat Commun. 2020 Apr 24;11(1):1979. doi: 10.1038/s41467-020-15892-8. PMID: 32332735; PMCID: PMC7181807.
39. Jolly JK, Groppe M, Birks J, Downes SM, MacLaren RE. Functional Defects in Color Vision in Patients With Choroideremia. Am J Ophthalmol. 2015 Oct;160(4):822-31.e3. doi: 10.1016/j.ajo.2015.06.018. Epub 2015 Jun 29. PMID: 26133251.
40. Justice MJ, Dhillon P. Using the mouse to model human disease: increasing validity and reproducibility. Dis Model Mech. 2016 Feb;9(2):101-3. doi: 10.1242/dmm.024547. PMID: 26839397; PMCID: PMC4770152.
41. Kerem E, Konstan MW, De Boeck K, Accurso FJ, Sermet-Gaudelus I, Wilschanski M, Elborn JS, Melotti P, Bronsveld I, Fajac I, Malfroot A, Rosenbluth DB, Walker PA, McColley SA, Knoop C, Quattrucci S, Rietschel E, Zeitlin PL, Barth J, Elfring GL, Welch EM, Branstrom A, Spiegel RJ, Peltz SW, Ajayi T, Rowe SM; Cystic Fibrosis Ataluren Study Group. Ataluren for the treatment of nonsense-mutation cystic fibrosis: a randomised, double-blind, placebo-controlled phase 3 trial. Lancet Respir Med. 2014 Jul;2(7):539-47. doi: 10.1016/S2213-2600(14)70100-6. Epub 2014 May 15. PMID: 24836205; PMCID: PMC4154311.
42. Kerem E. ELX-02: an investigational read-through agent for the treatment of nonsense mutation-related genetic disease. Expert Opin Investig Drugs. 2020 Dec;29(12):1347-1354. doi: 10.1080/13543784.2020.1828862. Epub 2020 Oct 12. PMID: 32972261.
43. Kim YJ, Sivetz N, Layne J, Voss DM, Yang L, Zhang Q, Krainer AR. Exon-skipping antisense oligonucleotides for cystic fibrosis therapy. Proc Natl Acad Sci U S A. 2022 Jan

18;119(3):e2114858118. doi: 10.1073/pnas.2114858118. PMID: 35017301; PMCID: PMC8784140.

44. Ko W, Porter JJ, Sipple MT, Edwards KM, Lueck JD. Efficient suppression of endogenous CFTR nonsense mutations using anticodon-engineered transfer RNAs. Mol Ther Nucleic Acids. 2022 May 4;28:685-701. doi: 10.1016/j.omtn.2022.04.033. PMID: 35664697; PMCID: PMC9126842.
45. Krishnamurthy S, Traore S, Cooney AL, Brommel CM, Kulhankova K, Sinn PL, Newby GA, Liu DR, McCray PB. Functional correction of CFTR mutations in human airway epithelial cells using adenine base editors. Nucleic Acids Res. 2021 Oct 11;49(18):10558-10572. doi: 10.1093/nar/gkab788. PMID: 34520545; PMCID: PMC8501978.
46. Lee JA, Cho A, Huang EN, Xu Y, Quach H, Hu J, Wong AP. Gene therapy for cystic fibrosis: new tools for precision medicine. J Transl Med. 2021 Oct 30;19(1):452. doi: 10.1186/s12967-021-03099-4. PMID: 34717671; PMCID: PMC8556969.
47. Lentini L, Melfi R, Di Leonardo A, Spinello A, Barone G, Pace A, Palumbo Piccionello A, Pibiri I. Toward a rationale for the PTC124 (Ataluren) promoted readthrough of premature stop codons: a computational approach and GFP-reporter cell-based assay. Mol Pharm. 2014 Mar 3;11(3):653-64. doi: 10.1021/mp400230s. Epub 2014 Feb 7. PMID: 24483936; PMCID: PMC4167060.
48. Leroy C, Spelier S, Essonghe NC, Poix V, Kong R, Gizzi P, Bourban C, Amand S, Bailly C, Guilbert R, Hannebique D, Persoons P, Arhant G, Prévotat A, Reix P, Hubert D, Gérardin M, Chamaillard M, Prevarskaya N, Rebuffat S, Shapovalov G, Beekman J, Lejeune F. Use of 2,6-diaminopurine as a potent suppressor of UGA premature stop codons in cystic fibrosis. Mol Ther. 2023 Apr 5;31(4):970-985. doi: 10.1016/j.ymthe.2023.01.014. Epub 2023 Jan 14. PMID: 36641622; PMCID: PMC10124085.
49. Li S, Li J, Shi W, Nie Z, Zhang S, Ma F, Hu J, Chen J, Li P, Xie X. Pharmaceuticals Promoting Premature Termination Codon Readthrough: Progress in Development. Biomolecules. 2023 Jun 14;13(6):988. doi: 10.3390/biom13060988. PMID: 37371567; PMCID: PMC10296333.
50. Lin TY, Glatt S. ACEing premature codon termination using anticodon-engineered sup-tRNA-based therapy. Mol Ther Nucleic Acids. 2022 Aug 6;29:368-369. doi: 10.1016/j.omtn.2022.07.019. PMID: 36035751; PMCID: PMC9386023.

51. Liu Z, Guo D, Wang D, Zhou J, Chen Q, Lai J. Prime editing: A gene precision editing tool from inception to present. FASEB J. 2024 Nov 15;38(21):e70148. doi: 10.1096/fj.202401692R. PMID: 39530600.
52. Lombardi S, Testa MF, Pinotti M, Branchini A. Molecular Insights into Determinants of Translational Readthrough and Implications for Nonsense Suppression Approaches. Int J Mol Sci. 2020 Dec 11;21(24):9449. doi: 10.3390/ijms21249449. PMID: 33322589; PMCID: PMC7764779.
53. Lopes-Pacheco M. CFTR Modulators: The Changing Face of Cystic Fibrosis in the Era of Precision Medicine. Front Pharmacol. 2020 Feb 21;10:1662. doi: 10.3389/fphar.2019.01662. PMID: 32153386; PMCID: PMC7046560.
54. Lueck JD, Yoon JS, Perales-Puchalt A, Mackey AL, Infield DT, Behlke MA, Pope MR, Weiner DB, Skach WR, McCray PB Jr, Ahern CA. Engineered transfer RNAs for suppression of premature termination codons. Nat Commun. 2019 Feb 18;10(1):822. doi: 10.1038/s41467-019-08329-4. PMID: 30778053; PMCID: PMC6379413.
55. MacArthur Clark J. The 3Rs in research: a contemporary approach to replacement, reduction and refinement. Br J Nutr. 2018 Aug;120(s1):S1-S7. doi: 10.1017/S0007114517002227. Epub 2017 Oct 30. PMID: 29081302.
56. MacDonald IM, Hume S, Zhai Y, Xu M. Choroideremia. 2003 Feb 21 [updated 2021 Mar 4]. In: Adam MP, Everman DB, Mirzaa GM, Pagon RA, Wallace SE, Bean LJH, Gripp KW, Amemiya A, editors. GeneReviews® [Internet]. Seattle (WA): University of Washington, Seattle; 1993–2023. PMID: 20301511.
57. Maule G, Arosio D, Cereseto A. Gene Therapy for Cystic Fibrosis: Progress and Challenges of Genome Editing. Int J Mol Sci. 2020 May 30;21(11):3903. doi: 10.3390/ijms21113903. PMID: 32486152; PMCID: PMC7313467.
58. McDonald EF, Meiler J, Plate L. CFTR Folding: From Structure and Proteostasis to Cystic Fibrosis Personalized Medicine. ACS Chem Biol. 2023 Oct 20;18(10):2128-2143. doi: 10.1021/acschembio.3c00310. Epub 2023 Sep 20. PMID: 37730207; PMCID: PMC10595991.
59. McHugh DR, Steele MS, Valerio DM, Miron A, Mann RJ, LePage DF, Conlon RA, Cotton CU, Drumm ML, Hodges CA. A G542X cystic fibrosis mouse model for examining nonsense mutation directed therapies. PLoS One. 2018 Jun 20;13(6):e0199573. doi: 10.1371/journal.pone.0199573. PMID: 29924856; PMCID: PMC6010256.
60. Michaels WE, Pena-Rasgado C, Kotaria R, Bridges RJ, Hastings ML. Open reading frame correction using splice-switching antisense oligonucleotides for the treatment of cystic

fibrosis. Proc Natl Acad Sci U S A. 2022 Jan 18;119(3):e2114886119. doi: 10.1073/pnas.2114886119. PMID: 35017302; PMCID: PMC8784102.

61. Michicich M, Traylor Z, McCoy C, Valerio DM, Wilson A, Schneider M, Davis S, Barabas A, Mann RJ, LePage DF, Jiang W, Drumm ML, Kelley TJ, Conlon RA, Hodges CA. A W1282X cystic fibrosis mouse allows the study of pharmacological and gene-editing therapeutics to restore CFTR function. J Cyst Fibros. 2025 Jan;24(1):164-174. doi: 10.1016/j.jcf.2024.10.008. Epub 2024 Nov 12. PMID: 39532588; PMCID: PMC11788034.
62. Michorowska S. Ataluren-Promising Therapeutic Premature Termination Codon Readthrough Frontrunner. Pharmaceuticals (Basel). 2021 Aug 9;14(8):785. doi: 10.3390/ph14080785. PMID: 34451881; PMCID: PMC8398184.
63. Mort M, Ivanov D, Cooper DN, Chuzhanova NA. A meta-analysis of nonsense mutations causing human genetic disease. Hum Mutat. 2008 Aug;29(8):1037-47. doi: 10.1002/humu.20763. PMID: 18454449.
64. Ng MY, Li H, Ghelfi MD, Goldman YE, Cooperman BS. Ataluren and aminoglycosides stimulate read-through of nonsense codons by orthogonal mechanisms. Proc Natl Acad Sci U S A. 2021 Jan 12;118(2):e2020599118. doi: 10.1073/pnas.2020599118. PMID: 33414181; PMCID: PMC7812769.
65. Ng MY, Zhang H, Weil A, Singh V, Jamiolkowski R, Baradaran-Heravi A, Roberge M, Jacobson A, Friesen W, Welch E, Goldman YE, Cooperman BS. New in Vitro Assay Measuring Direct Interaction of Nonsense Suppressors with the Eukaryotic Protein Synthesis Machinery. ACS Med Chem Lett. 2018 Nov 21;9(12):1285-1291. doi: 10.1021/acsmedchemlett.8b00472. PMID: 30613341; PMCID: PMC6295867.
66. Oren YS, Avizur-Barchad O, Ozeri-Galai E, Elgrabli R, Schirelman MR, Blinder T, Stampfer CD, Ordan M, Laselva O, Cohen-Cymberknoh M, Kerem E, Bear CE, Kerem B. Antisense oligonucleotide splicing modulation as a novel Cystic Fibrosis therapeutic approach for the W1282X nonsense mutation. J Cyst Fibros. 2022 Jul;21(4):630-636. doi: 10.1016/j.jcf.2021.12.012. Epub 2021 Dec 28. PMID: 34972649.
67. Palma M, Lejeune F. Deciphering the molecular mechanism of stop codon readthrough. Biol Rev Camb Philos Soc. 2021 Feb;96(1):310-329. doi: 10.1111/brv.12657. Epub 2020 Oct 22. PMID: 33089614.
68. Pan D, Kirillov S, Zhang CM, Hou YM, Cooperman BS. Rapid ribosomal translocation depends on the conserved 18-55 base pair in P-site transfer RNA. Nat Struct Mol Biol. 2006 Apr;13(4):354-9. doi: 10.1038/nsmb1074. Epub 2006 Mar 12. PMID: 16532005.

69. Pan D, Qin H, Cooperman BS. Synthesis and functional activity of tRNAs labeled with fluorescent hydrazides in the D-loop. RNA. 2009 Feb;15(2):346-54. doi: 10.1261/rna.1257509. Epub 2008 Dec 31. PMID: 19118261; PMCID: PMC2648706.
70. Pankonien I, Quaresma MC, Rodrigues CS, Amaral MD. CFTR, Cell Junctions and the Cytoskeleton. Int J Mol Sci. 2022 Feb 28;23(5):2688. doi: 10.3390/ijms23052688. PMID: 35269829; PMCID: PMC8910340.
71. Parmann R, Greenstein VC, Tsang SH, Sparrow JR. Choroideremia Carriers: Dark-Adapted Perimetry and Retinal Structures. Invest Ophthalmol Vis Sci. 2022 Jul 8;63(8):4. doi: 10.1167/iovs.63.8.4. PMID: 35816046; PMCID: PMC9284471.
72. Pennesi ME, Birch DG, Duncan JL, Bennett J, Girach A. CHOROIDEREMIA: Retinal Degeneration With an Unmet Need. Retina. 2019 Nov;39(11):2059-2069. doi: 10.1097/IAE.0000000000002553. PMID: 31021898; PMCID: PMC7347087.
73. Perriera R, Vitale E, Pibiri I, Carollo PS, Ricci D, Corrao F, Fiduccia I, Melfi R, Zizzo MG, Tutone M, Pace A, Lentini L. Readthrough Approach Using NV Translational Readthrough-Inducing Drugs (TRIDs): A Study of the Possible Off-Target Effects on Natural Termination Codons (NTCs) on TP53 and Housekeeping Gene Expression. Int J Mol Sci. 2023 Oct 11;24(20):15084. doi: 10.3390/ijms242015084. PMID: 37894764; PMCID: PMC10606485.
74. Pibiri I, Melfi R, Tutone M, Di Leonardo A, Pace A, Lentini L. Targeting Nonsense: Optimization of 1,2,4-Oxadiazole TRIDs to Rescue CFTR Expression and Functionality in Cystic Fibrosis Cell Model Systems. Int J Mol Sci. 2020 Sep 3;21(17):6420. doi: 10.3390/ijms21176420. PMID: 32899265; PMCID: PMC7504161.
75. Potapova NA. Nonsense Mutations in Eukaryotes. Biochemistry (Mosc). 2022 May;87(5):400-412. doi: 10.1134/S0006297922050029. PMID: 35790376.
76. Pylypenko O, Hammich H, Yu IM, Houdusse A. Rab GTPases and their interacting protein partners: Structural insights into Rab functional diversity. Small GTPases. 2018 Mar 4;9(1-2):22-48. doi: 10.1080/21541248.2017.1336191. Epub 2017 Jul 7. PMID: 28632484; PMCID: PMC5902227.
77. Pylypenko O, Rak A, Reents R, Niculae A, Sidorovitch V, Cioaca MD, Bessolitsyna E, Thomä NH, Waldmann H, Schlichting I, Goody RS, Alexandrov K. Structure of Rab escort protein-1 in complex with Rab geranylgeranyltransferase. Mol Cell. 2003 Feb;11(2):483-94. doi: 10.1016/s1097-2765(03)00044-3. PMID: 12620235.

78. Rafeeq MM, Murad HAS. Cystic fibrosis: current therapeutic targets and future approaches. J Transl Med. 2017 Apr 27;15(1):84. doi: 10.1186/s12967-017-1193-9. PMID: 28449677; PMCID: PMC5408469.
79. Regard L, Martin C, Burnet E, Da Silva J, Burgel PR. CFTR Modulators in People with Cystic Fibrosis: Real-World Evidence in France. Cells. 2022 May 28;11(11):1769. doi: 10.3390/cells11111769. PMID: 35681464; PMCID: PMC9179538.
80. Ruan J, Yu X, Xu H, Cui W, Zhang K, Liu C, Sun W, Huang X, An L, Zhang Y. Suppressor tRNA in gene therapy. Sci China Life Sci. 2024 Oct;67(10):2120-2131. doi: 10.1007/s11427-024-2613-y. Epub 2024 Jun 24. PMID: 38926247.
81. S. Spelier, E. P. M. van der Doorn, C. K. Ent, J. M. Beekman, andM. A. J. Koppens, "Readthrough Compounds for Nonsense Mutationcausesdging the Translational Gap," Trends in Molecular Medicine 29, no. 4(2023): 297–314, .
82. Sarkar H, Mitsios A, Smart M, Skinner J, Welch AA, Kalatzis V, Coffey PJ, Dubis AM, Webster AR, Moosajee M. Nonsense-mediated mRNA decay efficiency varies in choroideremia, providing a target to boost small molecule therapeutics. Hum Mol Genet. 2019 Jun 1;28(11):1865-1871. doi: 10.1093/hmg/ddz028. PMID: 30689859; PMCID: PMC6522067.
83. Sarkar H, Moosajee M. Choroideremia: molecular mechanisms and therapies. Trends Mol Med. 2022 May;28(5):378-387. doi: 10.1016/j.molmed.2022.02.011. Epub 2022 Mar 24. PMID: 35341685.
84. Sharma J, Keeling KM, Rowe SM. Pharmacological approaches for targeting cystic fibrosis nonsense mutations. Eur J Med Chem. 2020 Aug 15;200:112436. doi: 10.1016/j.ejmech.2020.112436. Epub 2020 May 21. PMID: 32512483; PMCID: PMC7384597.
85. Shen G, Liu J, Yang H, Xie N, Yang Y. mRNA therapies: Pioneering a new era in rare genetic disease treatment. J Control Release. 2024 May;369:696-721. doi: 10.1016/j.jconrel.2024.03.056. Epub 2024 Apr 13. PMID: 38580137.
86. Song KH, Woo SR, Chung JY, Lee HJ, Oh SJ, Hong SO, Shim J, Kim YN, Rho SB, Hong SM, Cho H, Hibi M, Bae DJ, Kim SY, Kim MG, Kim TW, Bae YK. REP1 inhibits FOXO3-mediated apoptosis to promote cancer cell survival. Cell Death Dis. 2017 Jan 5;8(1):e2536. doi: 10.1038/cddis.2016.462. PMID: 28055019; PMCID: PMC5386371.
87. Trzaska C, Amand S, Bailly C, Leroy C, Marchand V, Duvernois-Berthet E, Saliou JM, Benhabiles H, Werkmeister E, Chassat T, Guilbert R, Hannebique D, Mouray A, Copin MC, Moreau PA, Adriaenssens E, Kulozik A, Westhof E, Tulasne D, Motorin Y, Rebuffat

S, Lejeune F. 2,6-Diaminopurine as a highly potent corrector of UGA nonsense mutations. Nat Commun. 2020 Mar 20;11(1):1509. doi: 10.1038/s41467-020-15140-z. PMID: 32198346; PMCID: PMC7083880.

88. Vasireddy V, Mills JA, Gaddameedi R, Basner-Tschakarjan E, Kohnke M, Black AD, Alexandrov K, Zhou S, Maguire AM, Chung DC, Mac H, Sullivan L, Gadue P, Bennicelli JL, French DL, Bennett J. AAV-mediated gene therapy for choroideremia: preclinical studies in personalized models. PLoS One. 2013 May 7;8(5):e61396. doi: 10.1371/journal.pone.0061396. Erratum in: PLoS One. 2015 Jun 19;10(6):e0129982. doi: 10.1371/journal.pone.0129982. PMID: 23667438; PMCID: PMC3646845.
89. Vitale E, Ricci D, Corrao F, Fiduccia I, Cruciata I, Carollo PS, Branchini A, Lentini L, Pibiri I. Nonsense Mutations in Rare and Ultra-Rare Human Disorders: An Overview. IUBMB Life. 2025 Jun;77(6):e70031. doi: 10.1002/iub.70031. PMID: 40474765; PMCID: PMC12142302.
90. Welch EM, Barton ER, Zhuo J, Tomizawa Y, Friesen WJ, Trifillis P, Paushkin S, Patel M, Trotta CR, Hwang S, Wilde RG, Karp G, Takasugi J, Chen G, Jones S, Ren H, Moon YC, Corson D, Turpoff AA, Campbell JA, Conn MM, Khan A, Almstead NG, Hedrick J, Mollin A, Risher N, Weetall M, Yeh S, Branstrom AA, Colacino JM, Babiak J, Ju WD, Hirawat S, Northcutt VJ, Miller LL, Spatrick P, He F, Kawana M, Feng H, Jacobson A, Peltz SW, Sweeney HL. PTC124 targets genetic disorders caused by nonsense mutations. Nature. 2007 May 3;447(7140):87-91. doi: 10.1038/nature05756. Epub 2007 Apr 22. PMID: 17450125.
91. Wittenstein A, Caspi M, Rippin I, Elroy-Stein O, Eldar-Finkelman H, Thoms S, Rosin-Arbesfeld R. Nonsense mutation suppression is enhanced by targeting different stages of the protein synthesis process. PLoS Biol. 2023 Nov 9;21(11):e3002355. doi: 10.1371/journal.pbio.3002355. Erratum in: PLoS Biol. 2024 Feb 14;22(2):e3002524. doi: 10.1371/journal.pbio.3002524. PMID: 37943958; PMCID: PMC10684085.
92. Yun UJ, Sung JY, Park SY, Ye SK, Shim J, Lee JS, Hibi M, Bae YK, Kim YN. Oncogenic role of rab escort protein 1 through EGFR and STAT3 pathway. Cell Death Dis. 2017 Feb 23;8(2):e2621. doi: 10.1038/cddis.2017.50. PMID: 28230863; PMCID: PMC5386492.
93. Zhang H, Ng MY, Chen Y, Cooperman BS. Kinetics of initiating polypeptide elongation in an IRES-dependent system. Elife. 2016 Jun 2;5:e13429. doi: 10.7554/eLife.13429. PMID: 27253065; PMCID: PMC4963199.

94. Zinkernagel MS, MacLaren RE. Recent advances and prospects in choroideremia. Clin Ophthalmol. 2015 Nov 23;9:2195-200. doi: 10.2147/OPTH.S65732. PMID: 26648685; PMCID: PMC4664510.

10. ACKNOWLEDGEMENTS

I wish to express my deepest gratitude to Professor Laura Lentini, my supervisor, who over these three years has been much more than a simple tutor. Her passion for research, tireless dedication to scholarships, and constant availability and patience have made her a true academic mentor. These rare qualities have been fundamental in the completion of this journey.

My sincere thanks go to Professor Maria Grazia Zizzo, my co-supervisor, an extraordinary and empathetic researcher. I am truly grateful to her for the constant support in the *in vivo* studies and for teaching me everything concerning animal facility and animal welfare, no one has ever approached this with as much love and dedication as she did.

I would also like to thank Professors Aldo Di Leonardo, Raffaella Melfi, and Ivana Pibiri for their valuable contribution to my research, their insightful advice, and the techniques they taught me. Their suggestions have been a great source of encouragement and inspiration throughout my doctoral studies.

My heartfelt gratitude goes to Dr. Viviana Barra and Dr. Pietro Salvatore Carollo, two researchers who have turned their profession into a true passion. Their ideas, availability, and helpful insights over the years have been of great support and inspiration for my work and research.

I am deeply thankful to Professor Barry S. Cooperman for welcoming me into his laboratory at the University of Pennsylvania in Philadelphia during my research stay abroad, and for all the valuable lessons I learned there. To his research group Saleem, Adam, Arpan, and Hong, I extend my warmest thanks for making me feel at home and for welcoming me as part of the team.

A special thanks to my current lab colleagues Ilenia, Michele, Riccardo, Serena, Ignazio, Davide Sefora, Elisa, and Claudia to former members Federica, Riccardo and Simona, for their collaboration, support, and patience throughout my research activities.

To all my fellow Ph.D. colleagues, and especially Salvatore, Sara, and Emanuela, thank you for sharing your ideas with me, stimulating my curiosity, and accompanying me through this journey, both academically and personally.

My deepest gratitude goes to my family, and especially to my parents, who have devoted themselves tirelessly to their children, making sacrifices that have allowed me to achieve the highest level of education and personal growth.

To my dearest friends from Palermo and Caltavuturo, thank you for your unwavering emotional support and encouragement throughout this endeavour.

Finally, thanks to M.S.S., without whom this journey could not have reached its completion.